In Vitro to *In Vivo* Translation of Complex Drug-Drug Interactions Involving Retinoic Acid

Faith M. Stevison

A dissertation

submitted in partial fulfillment of the

requirements for the degree of

Doctor of Philosophy

University of Washington

2018

Reading Committee:

Nina Isoherranen, Chair

Kenneth E. Thummel

Yvonne S. Lin

Program Authorized to Offer Degree:

Pharmaceutics

University of Washington

Abstract

In Vitro to *In Vivo* Translation of Complex Drug-Drug Interactions Involving Retinoic Acid

Faith M. Stevison

Chair of the Supervisory Committee:

Professor and Vice Chair, Nina Isoherranen

Pharmaceutics

all-trans-retinoic acid (*at*RA), the active metabolite of vitamin A, is a ligand for several nuclear receptors and acts as a critical regulator of many physiological processes. The cytochrome P450 26 (CYP26) enzymes are responsible for *at*RA clearance and are potential drug targets to increase concentrations of endogenous *at*RA in a tissue-specific manner. The first project of this thesis aimed to establish the relationship between CYP26 inhibition, by the potent CYP26A1 and B1 inhibitor talarozole, and altered *at*RA concentrations in tissues, and to quantify the increase in endogenous *at*RA concentrations necessary to alter *at*RA signaling in target organs. The second part of this thesis focused on evaluating exogenous *at*RA and retinoid dosing on gene regulation. Several in vitro and preclinical studies have suggested that *at*RA down-regulates CYP2D6 expression and activity. Both *at*RA and its stereoisomer 13-*cis* retinoic acid (13*cis*RA) are used clinically, and steady state exposures of *at*RA are similar after dosing

with *at*RA or 13*cis*RA. The second aim of this thesis was to determine whether 13-*cis* retinoic acid (13*cis*RA) or its active metabolites, *at*RA and 4-oxo-13*cis*RA, cause a drug-drug interaction (DDI) with CYP2D6, decreasing the clearance of the CYP2D6 probe dextromethorphan. Further, the effects of 13*cis*RA and its metabolites (i.e., *at*RA and 4-oxo-13*cis*RA) on CYP2D6 and CYP3A4 in human hepatocytes were determined and used to predict whether the in vivo results could be correctly predicted from in vitro.

Following a single 2.5-mg/kg dose of talarozole to mice, *at*RA concentrations increased up to 5.7-, 2.7-, and 2.5-fold in serum, liver, and testis, respectively, resulting in induction of Cyp26a1 in the liver and testis and Rarβ and Pgc1β in liver. The increase in *at*RA concentrations was well-predicted from talarozole pharmacokinetics and in vitro data of CYP26 inhibition. After multiple doses of talarozole, a significant increase in *at*RA concentrations was observed in serum but not in liver or testis. This lack of increase in tissue *at*RA concentrations correlated with increase in CYP26A1 expression in liver and testis. The increased *at*RA concentrations in serum without a change in liver suggest that CYP26B1 in extrahepatic sites plays a key role in regulating systemic *at*RA exposure.

The putative DDI between 13*cis*RA and dextromethorphan was studied in clinical study in eight healthy volunteers. The geometric mean ratio (GMR; 90% CI) of dextromethorphan area under the curve from time zero to infinity ($AUC_{0-\infty}$) prior to and after 13*cis*RA treatment was 0.822 (0.677 – 0.998) indicating that dextromethorphan clearance and CYP2D6 activity was increased following 13*cis*RA treatment. The dextrorphan-to-dextromethorphan $AUC_{0-\infty}$ ratio and dextrorphan formation clearance (Cl_f) were also increased consistent with CYP2D6 induction. In addition, the Cl_f of 3-methoxymorphinan, a CYP3A4-specific metabolite of dextromethorphan,

and the Cl_f of 6β-hydroxycortisol, an endogenous marker of CYP3A4 activity, were also increased suggesting that CYP3A4 expression was also induced by 13*cis*RA.

Quantitative DDI predictions were made with data for *CYP2D6* mRNA down-regulation in human hepatocytes assuming that 13*cis*RA and its metabolites competitively bind to the same receptor to elicit CYP2D6 down-regulation. An ~50% decrease in CYP2D6 activity and 2-fold increase in dextromethorphan AUC were predicted to be observed in vivo after dosing with 13*cis*RA. These data demonstrate a clear disconnect between in vitro and in vivo CYP2D6 down-regulation. In contrast to data with CYP2D6, data from hepatocytes support the induction of CYP3A4 observed in the clinical study. This is the first study to fully characterize the concentration-response effect of retinoids on CYP2D6 activity and highlights the difficulty in translating in vitro observations of CYP down-regulation to the clinic.

TABLE OF CONTENTS

LIST OF FIGURES

LIST OF TABLES

ACKNOWLEDGEMENTS

I would like to thank my advisor, Dr. Nina Isoherranen, for her mentorship during my PhD training. Nina is an exemplary scientist who holds herself and her students to the highest standards, and she is also a passionate teacher. I am grateful for the rigorous training she has provided me, which includes not only a strong foundation in pharmacokinetic principles but also the ability to generate knowledge from data. Nina's integrity and commitment to follow where the data leads have been instrumental in my development as a scientist.

I would also like to thank my lab-mates and classmates. Graduate school is incredibly challenging, and I have been fortunate to be surrounded by insightful and encouraging peers during my time in Pharmaceutics.

Additionally, I would like to acknowledge all of the collaborators I have been fortunate to work with over the last five years. Without their hard work and thoughtful input, the work presented in this dissertation would not have been possible.

Finally, I would like to thank my committee members Dr. Ken Thummel, Dr. Yvonne Lin, Dr. Jash Unadkat, Dr. John Amory, and Dr. Edith Wang. Their feedback on my projects helped to broaden my perspective for my research. I am especially appreciative for the countless hours of mentorship from John. His endless enthusiasm and passion for science is contagious. I am grateful for his support and encouragement throughout my PhD training.

DEDICATION

I would like to dedicate this dissertation to my husband Jim. Thank you for always encouraging me to follow my dreams.

Chapter 1. INTRODUCTION

Portions of this chapter have been published in:

James Hardwick, editor: Cytochrome P450 function and pharmacological roles in inflammation and cancer, Vol 74, APHA, UK: Academic Press, 2015, pp. 373-412

1.1 RETINOIC ACID ISOMERS AS IMPORTANT ENDOGENOUS SIGNALING MOLECULES AND THERAPEUTIC AGENTS

Retinoic acid (RA), the active metabolite of the fat-soluble vitamin A, has been shown to be important in various biological processes and in treatment of several diseases (Wolbach and Howe, 1925; Cantorna et al., 1995; Fenaux et al., 2007; Ross, 2012; Matthay, 2013). The biological activity of RA is predominantly mediated by binding to the family of nuclear retinoic acid receptors (RARα, RARβ and RARγ), but all-trans-RA (*at*RA) has also been shown to bind to peroxisome proliferator-activated receptors (PPARβ/δ) (Schug et al., 2007). Binding of retinoids to either RARs or PPARs results in increased transcription of respective target genes, generally promoting apoptosis through RAR signaling and cell proliferation through PPARβ/δ signaling (Noy, 2010; Gudas, 2012). The importance of the RAR signaling and RAR binding of *at*RA is illustrated in the pro-apoptotic effects of *at*RA in the treatment of acute promyelocytic leukemia (APL). APL is definitively marked by a chromosomal translocation affecting the RARα gene (Martens et al., 2010). The translocation ultimately results in a promyelocytic leukemia (PML)-RARα fusion protein (Kakizuka et al., 1991; Pandolfi et al., 1991; Guidez et al., 1998), which binds, with its heterodimer partner retinoid X receptor (RXR), to the retinoic acid response element of target genes (Martens et al., 2010) ultimately blocking myeloid differentiation and leading to leukemogenesis (Guidez et al., 1998; Collins, 2002). With wild type RARα, physiological levels of *at*RA are sufficient to dissociate negative co-repressors, but PML-RARα fusion proteins are less sensitive to *at*RA and pharmacological levels of *at*RA are required to dissociate negative co-repressors from the fusion protein for gene transcription and terminal myeloid differentiation (Guidez et al., 1998).

Retinoic acid has five chemical isomers (*at*RA, 9*cis*RA, 13*cis*RA, 11*cis*RA and 9,13-*dicis*RA). Of these isomers *at*RA (Figure 1.1) is considered to be the biologically active isomer because of its high affinity (1 – 24 nM EC_{50}) for RARs compared to its endogenous levels (ranging from 3 nM in serum to 7 – 40 nM in mouse tissues) (Aström et al., 1990; Idres et al., 2002; Kane et al., 2008; Topletz et al., 2015). However, in various species including humans, the 9*cis*RA, 13*cis*RA, and 9,13-*dicis*RA isomers have also been detected in different organs and in circulation (Kane et al., 2008; Arnold et al., 2012). 9*cis*RA binds to RXRs and this isomer may be important in tissues such as the pancreas where it has been detected (Kane et al., 2010). Yet, 9*cis*RA concentrations in tissues and in circulation are typically very low or undetectable, and the biological role of this isomer has not been confirmed. In contrast, 13*cis*RA has been detected in several tissues in mice and humans (Kane et al., 2008; Arnold et al., 2012; Nya-Ngatchou et al., 2013). However, 13*cis*RA has historically been considered to be devoid of biological activity due to its relatively low affinity to RARs (43 – 365 nM EC_{50}) compared to *at*RA and low endogenous 13*cis*RA concentrations (generally $\leq$ 6 nM in mouse tissues and 4 – 5 nM in human serum) (Aström et al., 1990; Idres et al., 2002; Kane et al., 2008; Arnold et al., 2012). The major primary metabolite of *at*RA, 4-OH-*at*RA, and its subsequent oxidation product 4-oxo-*at*RA, also bind RARs, but with lower affinity than the parent molecule (45 – 800 nM and 8 – 90 nM EC_{50} for 4-OH-*at*RA and 4-oxo-*at*RA, respectively) (Idres et al., 2002; Topletz et al., 2015). Both 4-OH-*at*RA and 4-oxo-*at*RA have been shown to induce expression of the RARα-responsive genes RARβ and CYP26A1 in vitro (Topletz et al., 2015). 13*cis*RA is also extensively metabolized to 4-OH-13*cis*RA and then to 4-oxo-13*cis*RA, but no data are available for binding of these metabolites to RARs. However, *at*RA, 13*cis*RA and their 4-oxo metabolites exhibit transcriptional activity in

in vitro cultures of keratinocytes and fibroblasts (Baron *et al.*, 2005), and 4-oxo-13*cis*RA activity has been demonstrated in neuroblastoma cell lines (Sonawane et al., 2014).

Although several RA isomers and metabolites exhibit affinity to RARs and have activity in vitro, the importance of endogenous *at*RA signaling is apparent in several organ systems. For example, endogenous *at*RA is critical in the maintenance of healthy skin, epithelia and the immune system (Napoli, 2012), in regulation of bone growth and homeostasis, and in regulating continuous, asynchronous spermatogenesis (Chung and Wolgemuth, 2004; Hogarth and Griswold, 2013b). In addition, *at*RA is a classic morphogen that regulates embryonic development (Duester, 2008), organogenesis, stem cell differentiation (Gudas and Wagner, 2011) and body patterning in all chordates. In addition, retinoid signaling has been linked to regulation of insulin stimulated glucose secretion (Chung and Wolgemuth, 2004; Kane et al., 2008, 2010) and to lipid homeostasis and adiposity (Bonet et al., 2012).

Exogenous *at*RA and 13*cis*RA have been shown to be beneficial in the treatment of chronic hand eczema (Ruzicka et al., 2004) and in a variety of cancers including APL (Tang and Gudas, 2011), neuroblastoma in children (Veal et al., 2007), and Kaposi's sarcoma (Altucci et al., 2007). Whether exogenous *at*RA or 13*cis*RA function via similar pathways and receptors as endogenous *at*RA is not well defined especially given that circulating concentrations of retinoids after therapeutic dosing are much higher than endogenous levels. For example, steady state concentrations for a typical dosing regimen of 13*cis*RA range from 500 – 1000 nM (Muindi et al., 2008a; Amory et al., 2017), concentrations considerably higher than the EC_{50} for RARs. Thus, it is plausible that exogenous 13*cis*RA could exert signaling effects through this pathway. Throughout this text the terms *at*RA and 13*cis*RA are used when a specific isomer has been

identified in the research, and the generic term RA is employed when the identity of the isomer has not been specified.

1.2 SYNTHESIS, ELIMINATION, AND PHARMACOKINETICS OF *AT*RA AND 13*CIS*RA

The main dietary forms of vitamin A, the precursor to RA, are retinol and retinyl esters (Figure 1.1), typically obtained from animal products (Schoeff, 1983; Sklan, 1987). However, retinol and retinyl esters are not biologically active but require oxidation by several enzymes to generate retinaldehyde and ultimately RA (D'Ambrosio *et al.*, 2011; Kedishvili, 2013). While the oxidation of retinol to retinaldehyde by alcohol dehydrogenase enzymes is reversible, oxidation of retinaldehyde to RA is irreversible. Aldehyde dehydrogenase (ALDH1A1, 1A2, and 1A3) enzymes and aldehyde and xanthine oxidases have been reported to catalyze the oxidation of retinaldehyde to RA (D'Ambrosio *et al.*, 2011; Kedishvili, 2013). The clearance of *at*RA has been studied extensively and is mediated predominantly by the cytochrome P450 family 26 enzymes (CYP26) in all chordates, although many other CYP enzymes including human CYP3A4 and CYP2C8 and rat Cyp2c22 also oxidize *at*RA (Nadin and Murray, 1999; Marill *et al.*, 2000; McSorley and Daly, 2000) (Figure 1.1).

The effects of endogenous *at*RA on gene transcription are dependent on the cellular concentrations of *at*RA as well as the expression levels of RAR and PPAR nuclear receptors. Endogenous *at*RA concentrations in various tissues are tightly controlled by the expression and activity of the *at*RA synthesizing and eliminating enzymes. For example, ALDH1A1 appears to be responsible for *at*RA synthesis in the mouse liver while ALDH1A2 and ALDH1A1 make the main contributions to *at*RA synthesis in both mouse and human testes (Arnold *et al.*, 2015a; Arnold *et al.*, 2015b). Similarly, extrahepatic expression of CYP26 enzymes has been demonstrated (Topletz *et al.*, 2012) and likely plays a role in tissue specific clearance and

regulation of *at*RA concentrations. CYP26 enzymes are proposed to constitute a tissue barrier for *at*RA distribution from circulation to specific organs. This hypothesis originated from the observation that uptake of administered *at*RA was limited in some tissues, such as the testes, pancreas and spleen, (Smith *et al.*, 1973; Ahluwalia *et al.*, 1975; McCormick *et al.*, 1983; Kurlandsky *et al.*, 1995), and that CYP26 enzymes were detected in keratinocytes and epithelial cells of the testes and embryonic uterus (Heise *et al.*, 2006; Vernet *et al.*, 2006; Xia *et al.*, 2010). The metabolic barrier provided by CYP26 enzymes in some tissues, such as the testes, likely ensures that tissue *at*RA concentrations are regulated by enzyme expression and activity within the tissue and not by circulating concentrations. Therefore, understanding the activity and expression of CYP26 enzymes in individual tissues and cell types is critically important for defining the relationship between *at*RA concentrations and biological outcomes within a tissue.

The CYP26 family consists of three highly conserved enzymes CYP26A1, CYP26B1 and CYP26C1. Despite the fact that *at*RA appears to be the primary substrate of all three CYP26 enzymes, these enzymes share only 40-50% sequence similarity in a given species (Thatcher and Isoherranen, 2009). Yet, the individual isoforms are highly conserved across chordates which all have three CYP26 enzymes. Overall, the affinity of *at*RA to each of the CYP26 enzymes is high, but the CYP26 isozymes metabolize *at*RA in a stereoselective manner (Topletz *et al.*, 2012; Zhong *et al.*, 2018), further supporting the spatiotemporal importance of the three CYP26 enzymes in regulating *at*RA concentrations. The K_m values for CYP26A1, CYP26B1, and CYP26C1 are <100 nM for *at*RA (Topletz *et al.*, 2012; Zhong *et al.*, 2018), and are near the concentrations of *at*RA in various tissues (Topletz *et al.*, 2012). While the affinity of the substrate is high, the k_{cat} values for *at*RA with CYP26 enzymes are similar to other mammalian P450 enzymes (approximately 1-10 pmol/min/pmol) (Thatcher *et al.*, 2010; Topletz *et al.*, 2012). Since the

affinity of *at*RA to CYP26 is approximately 1000-fold higher than that to other CYP enzymes, the overall intrinsic clearance of *at*RA by CYP26 enzymes is 1,000- to 10,000-fold higher than other CYP enzymes such as CYP3A4 and CYP2C8 (Thatcher *et al.*, 2010). Therefore, even in tissues such as the human liver which have high expression of CYP3A4 and CYP2C8, the CYP26s are expected to be the main contributors to *at*RA clearance even if they are expressed at lower levels (Thatcher and Isoherranen, 2009; Thatcher *et al.*, 2010, 2011). Indeed, in a study of individual donors in a human liver bank, CYP26A1 was shown to be the main enzyme contributing to hepatic *at*RA clearance, although the expression of CYP26A1 was subject to considerable inter-individual variability (Thatcher, Zelter, & Isoherranen, 2010). Interestingly, in the human liver, CYP26B1 protein was completely absent pointing to tissue- and cell-type specific roles of the CYP26 enzymes in adult tissues and during fetal development.

Based on tissue specific expression and activity of CYP26 enzymes, it can be hypothesized that tissue specific alterations in CYP26 activity will alter *at*RA concentrations in a given tissue and result in altered *at*RA signaling. For example, inhibition of CYP26s or genetic polymorphisms that decrease CYP26 activity would be expected to increase *at*RA concentrations within the tissue. Yet a direct effect of decreased CYP26 activity and increased *at*RA concentrations in a tissue has never been demonstrated, even though P450 inhibitors such as ketoconazole and CYP26-specific inhibitors talarozole and liarozole increase RA concentrations in various tissues and plasma (Van Wauwe *et al.*, 1990; Stoppie *et al.*, 2000; Nelson *et al.*, 2013). Likewise, specific effects of inhibition of CYP26A1 or CYP26B1 have not been shown to have different effects in different tissues.

The products of metabolism of *at*RA by CYP26 have been characterized in vitro, and it is widely believed that oxidation of *at*RA in the 4-position of the β-ionone ring to generate 4-OH-

*at*RA (Figure 1.2) is the predominant route of elimination of *at*RA but no unequivocal mass balance studies confirm this (Lutz *et al.*, 2009; Thatcher *et al.*, 2011). Determining the major route of *at*RA elimination in humans or animal species is challenging, as 4-OH-*at*RA is extensively metabolized both in vitro and in vivo. 4-OH-*at*RA is glucuronidated predominantly by UGT2B7 and oxidized by CYP26s and microsomal alcohol dehydrogenases to 4-oxo-*at*RA and other products (Samokyszyn *et al.*, 2000; Topletz *et al.*, 2015). The CYP26s and other CYP enzymes also generate several other hydroxylation products from *at*RA (Thatcher *et al.*, 2011). The best characterized of these additional hydroxylation products is the 18-OH-*at*RA which has been synthesized (Rosenberger and Neukom, 1982) and shown to be a metabolite formed by CYP26A1, CYP26B1, CYP26C1, and other CYPs (Topletz *et al.*, 2012; Zhong *et al.*, 2018). In addition, 16-OH-*at*RA has been proposed as a metabolite of *at*RA, but this metabolite has never been synthesized, and therefore the identification of the metabolite is based on interpretation of mass spectrometry fragmentation patterns (Thatcher *et al.*, 2011).

Similar to *at*RA, 13*cis*RA is extensively metabolized, but elimination of 13*cis*RA has been attributed primarily to CYP2C8, CYP2C19 and CYP3A4 (Marill *et al.*, 2002; Sonawane *et al.*, 2014) rather than CYP26s. We have observed that CYP26A1, CYP26B1, and CYP26C1 in addition to CYP2C8, CYP2C19, and CYP3A4 can all catalyze the formation of 4-OH-13*cis*RA (Figure 1.3), but the rate of metabolite formation by CYP26s is only ~5-fold higher than the rate of formation by CYP3A4. Thus, given the low expression levels of CYP26s compared to CYP3A4, it is unlikely that CYP26s are the predominant route of 4-OH-13*cis*RA formation in vivo. While 4-OH-13*cis*RA appears to be the primary 13*cis*RA metabolite formed by CYPs, several other metabolites of 13*cis*RA have also been identified. Following oral administration of 13*cis*RA in humans, metabolites including 4-OH-13*cis*RA, 4-oxo-13*cis*RA, *at*RA, 4-oxo-*at*RA and their

glucuronides as well as glucuronide conjugates of 13*cis*RA, 16-OH-13*cis*RA and 18-OH-13*cis*RA (Figure 1.2) have been detected in either blood, urine or feces (Vane and Buggé, 1981; Khoo *et al.*, 1982; Lucek and Colburn, 1985; Vane *et al.*, 1990). The predominant circulating metabolite of 13*cis*RA is 4-oxo-13*cis*RA (Brazzell and Colburn, 1982; Colburn *et al.*, 1983) (Figure 1.2). As is the case for 4-oxo-*at*RA, 4-oxo-13*cis*RA is a secondary metabolite generated from oxidation of 4-OH-13*cis*RA although the enzyme primarily responsible for formation of 4-oxo-13*cis*RA from 4-OH-13*cis*RA is unknown. In addition, the pathway for elimination of 4-oxo-13*cis*RA is unclear, but several UGT1A isoforms have been shown to form 13*cis*RA and 4-oxo-13*cis*RA glucuronide conjugates in vitro (Rowbotham *et al.*, 2010; Sonawane *et al.*, 2014).

While the metabolite profiles for *at*RA and 13*cis*RA are similar, the pharmacokinetics of the two isomers as therapeutic agents are quite different. *at*RA is used in the treatment of APL, and pharmacologically administered *at*RA has a short ~1-hour half-life (Ozpolat *et al.*, 2003a; Thudi *et al.*, 2011). *at*RA exhibits non-linear kinetics with dose-dependent decreases in oral clearance (Jing *et al.*, 2017). In addition, upon multiple dosing, *at*RA also induces its own clearance (Ozpolat *et al.*, 2003b). In fact, auto-induction of *at*RA metabolism and resulting resistance to *at*RA is the best characterized mechanism of APL relapse. In clinical pharmacokinetic studies in APL patients, exposure to *at*RA was significantly decreased at relapse when compared to exposure after the first dose (Muindi *et al.*, 1992). Doubling the clinical dose of *at*RA at relapse was insufficient to match initial *at*RA exposures. To overcome this auto-induction and maintain exposure in APL patients, *at*RA is dosed on an intermittent schedule of one week on *at*RA treatment and one week off *at*RA treatment. In contrast, although 13*cis*RA is also extensively metabolized, it exhibits linear kinetics with an oral clearance ranging from 240 – 900 mL/min, a ~20-hour half-life, and does not induce its own clearance (Khoo *et al.*, 1982; Brazzell *et al.*, 1983;

Colburn *et al.*, 1983). The predominant circulating metabolite of 13*cis*RA, 4-oxo-13*cis*RA, circulates at concentrations 3 - 5-fold higher than the parent drug and exhibits elimination rate-limited kinetics with a longer half-life than the parent drug (Brazzell and Colburn, 1982; Colburn *et al.*, 1983).

Another important metabolite of 13*cis*RA is *at*RA, which is formed by isomerization. In vitro, 13*cis*RA and *at*RA have been shown to interconvert, although 13*cis*RA conversion to *at*RA occurs to a greater extent than the reverse (Sass *et al.*, 1994; Chen and Juchau, 1997; Tsukada *et al.*, 2000). For example, incubation with 13*cis*RA alone in neuroblastoma cell lines resulted in *at*RA accounting for 15–31% of total RA. In contrast, after incubation with *at*RA, 13*cis*RA accounted for <10% of total RA (Armstrong *et al.*, 2007). Isomerization has been observed both via glutathione-S-transferase-mediated and thermodynamic processes (Sass *et al.*, 1994; Chen and Juchau, 1997). Because of the differences in RAR affinity for the two isomers, the activity of 13*cis*RA is widely believed to be a result of isomerization to *at*RA. Further, because of the longer half-life of 13*cis*RA compared to *at*RA, *at*RA as a metabolite of 13*cis*RA exhibits formation rate-limited kinetics resulting in a much longer *at*RA half-life with much less fluctuation in *at*RA concentrations after dosing with 13*cis*RA (Muindi *et al.*, 2008b). As a result, exposure to *at*RA is similar after dosing of either 13*cis*RA or *at*RA. At present, it is not possible to differentiate the pharmacodynamic effects caused by 13*cis*RA versus *at*RA following 13*cis*RA dosing and the clinical advantages are largely due to pharmacokinetic effects. For example, in neuroblastoma cell lines, 13*cis*RA and *at*RA have similar potency on cellular differentiation and growth arrest (Reynolds *et al.*, 1994), but 13*cis*RA is superior to *at*RA in the treatment of neuroblastoma due to its favorable pharmacokinetic and toxicological properties (Reynolds *et al.*, 2003).

1.3 CYP DOWN-REGULATION AND DRUG-DRUG INTERACTIONS WITH RETINOIDS

In addition to classically recognized roles for RA signaling, RA isomers have also been shown to regulate expression of CYPs. Induction of CYP3A4 by *at*RA, 13*cis*RA, and 9*cis*RA has been shown in vitro and proposed to be mediated by RXR/CAR (constitutive androstane receptor) and RXR/VDR (vitamin D receptor) pathways (Wang *et al.*, 2008; Chen *et al.*, 2010). Between 1.5- and 2.5-fold induction of CYP3A4 and CYP2C19 has also been observed in human hepatocytes treated with 5 μM of 13*cis*RA (Sonawane *et al.*, 2014). Much of the CYP regulatory activity of RA isomers has been associated with activation of RXR, the obligate heterodimer partner of many nuclear receptors including RARs, PPARs, VDR, the thyroid hormone receptor (TR), liver X receptor (LXR), farsenoid X receptor (FXR), pregnane X receptor (PXR), and CAR (Wang *et al.*, 2008; Yang *et al.*, 2014). While 9*cis*RA is considered the endogenous ligand for RXR due to its 40-fold higher affinity for RXR compared to other retinoids, both *at*RA and 13*cis*RA can bind RXR as well (Heyman *et al.*, 1992; Allenby *et al.*, 1993). Thus, pharmacologic dosing of *at*RA or 13*cis*RA could result in induction of CYP3A4 in vivo.

*at*RA has also been implicated in down-regulation of CYPs, but whether down-regulation of CYPs observed in vitro translates to clinical DDIs is uncertain. The best example of DDIs involving decreases in CYP expression stems from the effects of pro-inflammatory cytokines like interleukin -6 (IL-6) decreasing transcriptional regulation and increasing proteolytic degradation of CYPs in inflammatory diseases (Lee *et al.*, 2009; Dickmann *et al.*, 2011; Schmitt *et al.*, 2011; Evers *et al.*, 2013). Clinical therapeutic protein-drug interactions have been observed following treatment of rheumatoid arthritis patients with anti-IL-6 monoclonal antibodies tocilizumab and sirukumab where exposures of substrates of CYP2C9, CYP2C19, and CYP3A4 were decreased after treatment compared to baseline (Schmitt *et al.*, 2011; Zhuang *et al.*, 2015). These decreases

in exposure were presumably due to increased CYP expression following treatment with anti-IL-6 monoclonal antibodies, which reversed the suppressive effects of IL-6 on CYP expression. Examples of in vitro CYP down-regulation by small molecule perpetrators have also been presented in the literature (Gibson *et al.*, 2005; Zamek-Gliszczynski *et al.*, 2014; Sager *et al.*, 2017). However, due to a lack of in vitro-to-in vivo translation of CYP down-regulation in preclinical species (Gibson *et al.*, 2005) and insufficient exposure of perpetrators to predict a clinical DDI (Zamek-Gliszczynski *et al.*, 2014), no study of a DDI resulting solely from CYP down-regulation has been reported. In the case of bupropion, the effects of bupropion and its metabolites to down-regulate and reversibly inhibit CYP2D6 were combined to correctly predict the magnitude of the decrease in CYP2D6 activity observed clinically (Sager *et al.*, 2017), but at present it is impossible to differentiate between CYP down-regulation and reversible inhibition based on the clinical data. As such, CYP down-regulation by a drug resulting in a clinical DDI remains to be shown.

A classic example of the importance of CYP down-regulation in vivo is homeostatic regulation of bile acids. Bile acids are critical endogenous signaling molecules and are formed from metabolic break-down of cholesterol by several enzymes including CYP7A1 and CYP8B1 (Goodwin *et al.*, 2000). Bile acids are also cytotoxic and endogenous concentrations are tightly regulated (Kim *et al.*, 2007). Activation of the nuclear receptor FXR by excess bile acids induces expression of small heterodimer partner (SHP). SHP is a classic FXR target gene and a co-repressor protein that is recruited to the promoter of target genes to prevent transcription (Goodwin *et al.*, 2000; Cai *et al.*, 2010). Upon bile acid activation of FXR and SHP induction, SHP inhibits hepatocyte nuclear receptor 4α (HNF4α)-activated transcription of CYP7A1 and CYP8B1, resulting in enzyme down-regulation to decrease bile acid formation (Shimamoto *et al.*, 2004;

Boulias *et al.*, 2005). *at*RA has also been shown to induce SHP and down-regulate CYP7A1 and CYP8B1 in in vitro models of human liver and in vivo in the mouse (Cai *et al.*, 2010; Yang *et al.*, 2014). Treatment of HepG2 cells with *at*RA caused rapid induction of SHP mRNA and down-regulation of CYP7A1 that was linked to RXR activation (Cai *et al.*, 2010). After 12 or 24 hours of *at*RA treatment in both HepG2 cells and primary human hepatocytes at least 2-fold SHP induction resulted in greater than 50% decreases in CYP7A1 and CYP8B1 mRNA (Cai *et al.*, 2010; Yang *et al.*, 2014). Signaling effects of *at*RA on bile acid homeostasis have also been demonstrated in vivo where an approximate 2-fold increase in SHP and 50% decrease in CYP7A1 and CYP8B1 was observed in livers of mice treated with *at*RA (Yang *et al.*, 2014).

A similar mechanism of SHP- and HNF4α-mediated regulation of CYP2D6 has been proposed (Koh *et al.*, 2014; Pan and Jeong, 2015; Pan *et al.*, 2015). In CYP2D6-humanized (Tg-CYP2D6) mice when SHP levels were decreased (during pregnancy or with the introduction of siRNA targeting SHP), increased HNF4α and CYP2D6 were observed (Koh *et al.*, 2014). Conversely, activation of FXR or treatment with *at*RA in Tg-CYP2D6 mice demonstrated approximately 2-fold increases in SHP, which resulted in 50% decreases in CYP2D6 (Koh *et al.*, 2014; Pan and Jeong, 2015; Pan *et al.*, 2015). These data provide strong evidence that increased levels of *at*RA lead to induction of SHP and that multiple enzymes including CYP2D6 are down-regulated as a result of SHP induction. This suggests that patients who take *at*RA therapeutically may be at risk for DDIs resulting from down-regulation of CYP2D6. However, the pharmacokinetic profile (short half-life and auto-induction of clearance with multiple doses) makes *at*RA a poor model compound to test whether down-regulation of CYP2D6 observed in vitro and in preclinical species translates to a clinical DDI. In contrast, after dosing with 13*cis*RA, *at*RA has a much longer half-life and steady state concentrations of *at*RA are similar to those

achieved after dosing with *at*RA (Muindi *et al.*, 2008a). Thus, a greater risk for a DDI involving CYP2D6 may be expected with 13*cis*RA as compared to *at*RA. In addition, activity of 13*cis*RA and 4-oxo-13*cis*RA has been demonstrated in a variety of in vitro systems, and it is plausible that these retinoids could also contribute to CYP2D6 down-regulation. In fact, decreased expression of CYP2B6, CYP2C8, and CYP2C9 has been observed in human hepatocytes following treatment with 13*cis*RA (changes in CYP2D6 were not studied) (Sonawane *et al.*, 2014). Therefore, dosing of 13*cis*RA provides a unique model to assess the potential for a clinical DDI involving CYP2D6 down-regulation.

1.4 HYPOTHESIS AND AIMS

Retinoic acid, specifically *at*RA, is a critical endogenous signaling molecule that regulates a variety of physiological processes. The enzymes of the CYP26 family are important regulators of tissue-specific concentrations of endogenous *at*RA, and pharmacological-targeted inhibition of CYP26 enzymes has been proposed to increase endogenous *at*RA levels in certain diseases. In addition, *at*RA and its stereoisomer 13*cis*RA are used as therapeutic agents in treatment of psoriasis, acne, and cancers (e.g., APL and neuroblastoma). For APL, CYP26 is also an attractive drug target to overcome the auto-induction of *at*RA metabolism that occurs with multiple dosing of *at*RA. In vitro and preclinically, *at*RA has also been shown to down-regulate CYP2D6 and *at*RA and 13*cis*RA have been shown to induce CYP3A4, but whether *at*RA and 13*cis*RA cause DDIs has not been tested in humans. The overall hypothesis for this thesis is that in vitro characterization of the inhibition by the panCYP26 inhibitor talarozole, and induction and down-regulation caused by retinoids can be used to predict the magnitude of CYP interactions in vivo. This hypothesis was tested with three aims:

Aim 1. Quantify the increase in endogenous *at*RA in serum, liver, and testis after administration of the panCYP26 inhibitor, talarozole, and correlate *at*RA concentration changes to *at*RA signaling changes via the RAR and PPAR nuclear receptors in these tissues.

Aim 2. Determine whether CYP2D6 down-regulation by *at*RA translates to decreased CYP2D6 activity in humans after *at*RA exposure using 13*cis*RA with its circulating metabolites *at*RA and 4-oxo-13*cis*RA as precipitants.

Aim 3. Quantitatively predict the magnitude of DDIs involving CYP2D6 down-regulation and CYP3A4 induction perpetrated by 13*cis*RA and its metabolites, *at*RA and 4-oxo-13*cis*RA, by characterizing the effects of each retinoid in human hepatocytes.

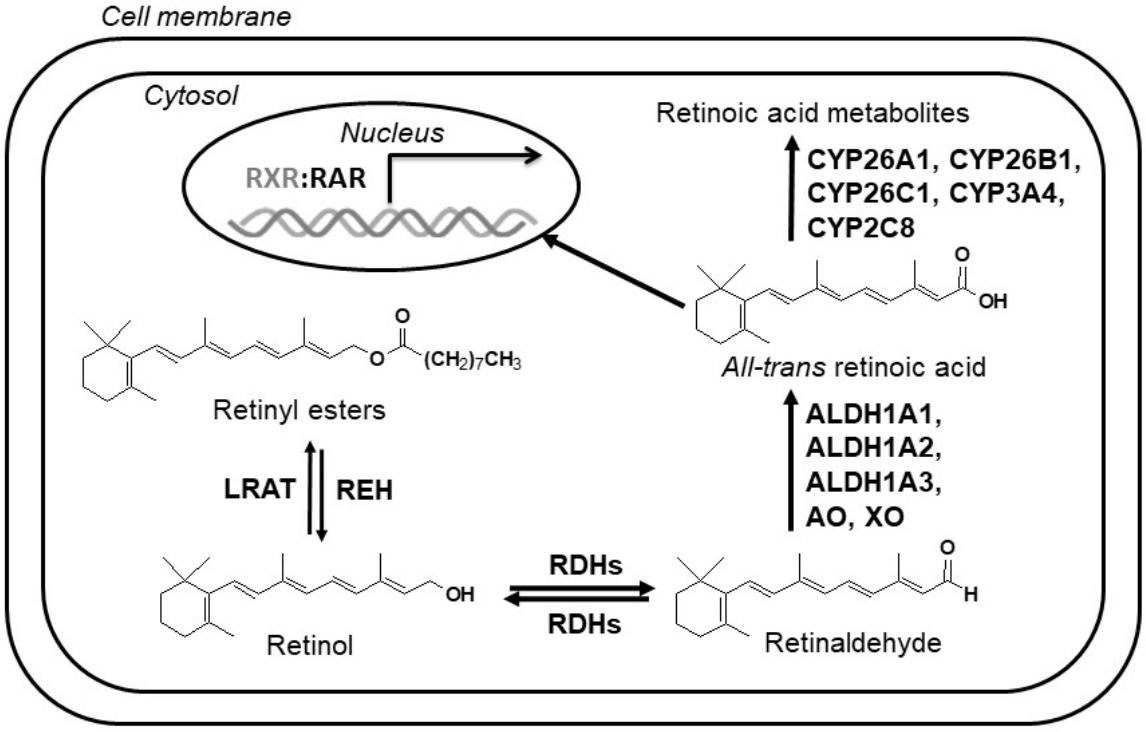

Figure 1.1. Enzymatic processes that regulate endogenous *at*RA homeostasis in humans. Retinyl ester hydrolase (REH) hydrolyzes retinyl esters, acquired as vitamin A from the diet, to retinol, and lecithin retinol acyltransferase (LRAT) esterifies retinol to retinyl esters for storage. Retinol is reversibly converted to retinaldehyde by retinol dehydrogenases (RDHs), and then retinaldehyde is irreversibly oxidized to the active metabolite *at*RA by ALDH1A isoforms, aldehyde oxidase (AO) and xanthine oxidase (XO). In the cell, *at*RA will localize to the nucleus and bind to RXR:RAR heterodimers to induce gene transcription. *at*RA is cleared through oxidation to polar metabolites by several P450 enzymes, including predominantly the CYP26 family. Figure adapted from *Cytochrome P450 function and pharmacological roles in inflammation and cancer*, Vol 74, APHA, UK: Academic Press, 2015, pp. 373-412.

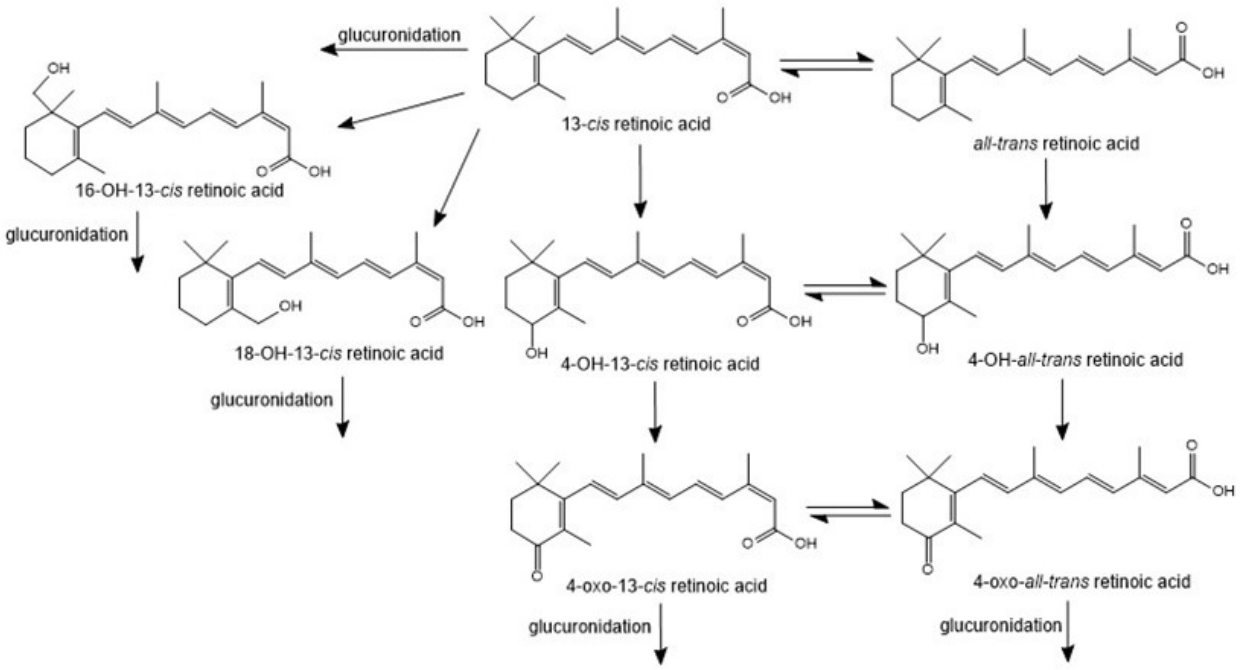

Figure 1.2. Metabolic scheme for 13-*cis*-retinoic acid (13*cis*RA) and *all-trans*-retinoic acid (*at*RA). *at*RA is metabolized primarily to 4-OH-*at*RA and subsequently to 4-oxo-*at*RA. Interconversion between 13*cis*RA and *at*RA favors conversion from 13*cis*RA to *at*RA. 13*cis*RA is extensively metabolized and 4-OH-13*cis*RA, 4-oxo-13*cis*RA, and the glucuronide conjugates of 13*cis*RA, 4-OH-13*cis*RA, 4-oxo-13*cis*RA, 16-OH-13*cis*RA and 18-OH-13*cis*RA have been detected following dosing of 13*cis*RA to human subjects.

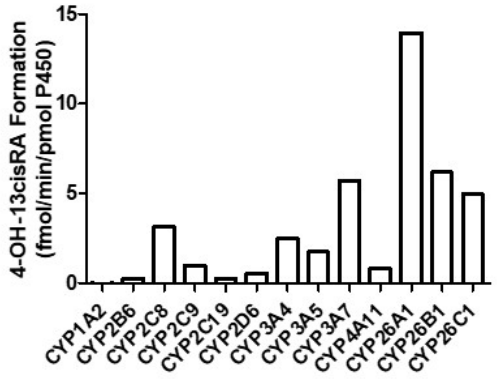

Figure 1.3. Formation of 4-OH-13*cis*RA from incubation of 13*cis*RA. Recombinantly expressed CYPs (10 pmol protein/mL) were incubated with 10 μM 13*cis*RA for 20 min and formation of 4-OH-13*cis*RA was measured.

Chapter 2. INHIBITION OF THE *ALL TRANS*-RETINOIC ACID (*AT*RA) HYDROXYLASES CYP26A1 AND CYP26B1 RESULTS IN DYNAMIC, TISSUE-SPECIFIC CHANGES IN ENDOGENOUS *AT*RA SIGNALING

This chapter was published in: *Drug Metabolism and Disposition* (2017) **45**:1 - 9

2.1 INTRODUCTION

The active metabolite of vitamin A, *all-trans* retinoic acid (*at*RA), is essential in the regulation of many physiological processes including embryonic development, immune system function, reproduction, and epithelial integrity, among others (Wolbach and Howe, 1925; Cantorna *et al.*, 1995; Ross, 2012). Due to its many endogenous roles, control of *at*RA concentrations in various tissues is of critical importance. Decreased levels of retinoic acid have been found in a variety of diseases such as cancer, diabetes and non-alcoholic fatty liver disease (Moulas *et al.*, 2006; Chang *et al.*, 2008; Liu *et al.*, 2015). In the liver, *at*RA has been proposed to regulate lipid homoeostasis and mitochondrial function via activation of the nuclear retinoic acid receptors (RARs) and peroxisome proliferator activated receptor (PPAR) β/δ (Berry and Noy, 2009; Tripathy *et al.*, 2016). In healthy testes, *at*RA signaling through RARs has been shown to control sex-specific timing of meiotic initiation and asynchronous spermatogenesis (Griswold, 2016). Importantly, studies in mouse testis containing synchronized germ cell development have shown that spermatogonial differentiation is associated with a 2- to 5-fold change in intratesticular *at*RA concentrations (Hogarth *et al.*, 2015a). However, it is not known what magnitude of change in *at*RA concentrations in different tissues is required to alter *at*RA signaling.

Maintenance of *at*RA homeostasis is complex and involves several enzymes. Vitamin A is stored as retinyl esters mainly in the liver, lungs and adipose, and upon demand, the esters are hydrolyzed to retinol. Retinol is oxidized to *at*RA via a two-step enzymatic process involving retinol dehydrogenase (RDH) enzymes and the aldehyde dehydrogenase 1A family (ALDH1A) (Napoli, 2012). *at*RA is eliminated from the body via metabolism to polar metabolites predominantly by the cytochrome P450 26 (CYP26) enzymes CYP26A1 and CYP26B1(Lutz *et al.*, 2009; Thatcher and Isoherranen, 2009; Thatcher *et al.*, 2010). CYP26A1 and CYP26B1 appear

to have functional redundancy as *at*RA hydroxylases, but have distinct tissue- and cell-type specific expression (Topletz *et al.*, 2012). For example, CYP26A1 is the predominant CYP26 enzyme in adult human and mouse liver while CYP26B1 protein is not detectable in the liver (Thatcher *et al.*, 2010; Peng *et al.*, 2012). Similarly, cell-type specific knock outs of CYP26B1 have a distinct phenotype (Li *et al.*, 2009; Hogarth *et al.*, 2015b). Both CYP26A1 and CYP26B1 are expressed in the adult testis and play a role in the onset and maintenance of spermatogenesis (Hogarth *et al.*, 2015a). Yet, it is not known what effect CYP26 inhibition may have on tissue-specific retinoid signaling. In humans, several variant alleles of CYP26A1 and CYP26B1 have been associated with increased risk of oral cancer, increased size in atherosclerotic lesions and decreased risk of Crohn's disease (Krivospitskaya *et al.*, 2012; Fransén *et al.*, 2013; Wu *et al.*, 2015), but at present it is not known whether these variants alter *at*RA concentrations or signaling in target tissues.

CYP26 enzymes appear to play a critical role in the control of tissue *at*RA concentrations, and their expression is believed to be regulated via an auto-feedback of *at*RA concentrations. When *at*RA levels are increased, such as in pharmacologic dosing of *at*RA, *at*RA clearance is significantly increased, likely via induction of CYP26 expression leading to *at*RA therapy resistance and relapse (Ozpolat *et al.*, 2002; Ross *et al.*, 2011). Upregulation of CYP26 has also been noted in many cancers. suggesting potential changes in *at*RA concentrations (Shelton *et al.*, 2006; Brown *et al.*, 2014; Wu *et al.*, 2015). Overall, the changes in CYP26 expression suggest that altered *at*RA signaling contributes to disease development and progression. However, whether endogenous *at*RA concentrations are altered as a result of, or lead to increased CYP26 expression, is not known.

Inhibition of CYP26s has been proposed as an attractive drug target both to increase endogenous *at*RA concentrations and to prevent *at*RA therapy resistance. Yet, at present it is not known what magnitude of change in endogenous *at*RA concentrations is needed to alter *at*RA signaling in target tissues. In addition, it is not known whether inhibition of CYP26 enzymes increases *at*RA concentrations in vivo in a manner that can be predicted from in vitro data. The aim of this study was to quantify the increase in endogenous *at*RA in serum, liver and testis after single and multiple dose administration of the panCYP26 inhibitor, talarozole, and to correlate concentration changes to *at*RA signaling changes via the RAR and PPAR nuclear receptors in these tissues.

2.2 MATERIALS AND METHODS

2.2.1 Chemicals and reagents

all-trans retinoic acid, itraconazole, and mass spectrometry grade formic acid were purchased from Sigma-Aldrich (St. Louis, MO). *at*RA-d_5 was obtained from Santa Cruz Biotechnology (Santa Cruz, CA). Talarozole was purchased from Active Biochem (Maplewood, NJ). Hexanes, water, acetonitrile and methanol were Optima LC/MS grade from Thermo Fisher Scientific (Waltham, MA). Ethanol, xylene, and Histoplast paraffin used in preparation of slides for immunohistochemistry were from Thermo Fisher Scientific (Waltham, MA), and HARLECO® Bouin fixative fluid from EMD Millipore (Darmstadt, Germany).

2.2.2 Animal care and talarozole treatments

All animal experiments were approved by the Washington State University Animal Care and Use Committee. Male C57BL/6X129 mice were housed in a temperature- and humidity-controlled environment and food and water were available *ad libitum.* Two separate talarozole treatment

studies were conducted. In the first study, male mice (n=24) were treated with a single oral dose of 2.5 mg/kg talarozole dissolved in PEG 300 (Sigma-Aldrich, St. Louis, MO) or PEG 300 alone as a vehicle control (n=3). Talarozole-treated mice (n=3 per time point) were euthanized via CO_2 asphyxiation followed by cervical dislocation at 0.25, 0.5, 1, 2, 4, 8, 12, and 24 h after the single dose of talarozole while vehicle controls were euthanized at 24 h. In the second study, male mice (n=5) were treated with multiple oral doses of 2.5 mg/kg talarozole dissolved in PEG 300 twice daily for three days or with PEG 300 alone as a vehicle control group (n=5). Talarozole-treated mice were fasted overnight and euthanized 4 h following a final dose of talarozole in the morning of the fourth day of treatment. Vehicle control mice (n=5) were similarly fasted and euthanized at the same time to serve as a baseline control. In both studies, the mice were exsanguinated, and all of the blood was collected into 1.5 ml Eppendorf tubes and serum isolated from blood by centrifugation at 1,100 x g for 10 min at 4°C. Liver and testis were collected for *at*RA concentration measurements and for mRNA analysis. All samples were collected in a light-protected environment, snap frozen on dry ice and stored at -80°C until use. In the multiple dose study, one testis from three mice was processed to be analyzed via immunohistochemistry (IHC). For IHC analysis, testes were fixed in HARLECO® Bouin fixative fluid for 5 h, dehydrated through a graded ethanol series, washed with xylene, embedded in Histoplast LP paraffin wax and sectioned (4 µm sections) onto charged glass slides.

2.2.3 Determination of talarozole pharmacokinetic parameters in the mouse

To prepare mouse serum samples for analysis of talarozole by liquid chromatography-tandem mass spectrometry (LC-MS/MS), 80 µL of 1:3 methanol:acetonitrile with 10 nM of itraconazole as internal standard was added to 40 µL of serum, the samples were centrifuged at 3,000 x g for 20 min at 4°C, and supernatant was collected for quantification. Concentrations of

talarozole and internal standard were measured using an AB Sciex (Framingham, MA) API 4500 triple quadrupole mass spectrometer. Analytes were separated using a 100 x 2.1mm, 1.9-µm C18 Hypersil Gold column (Thermo Fisher Scientific, Waltham, MA) coupled to a Shimadzu (Kyoto, Japan) LC-20AD liquid chromatography system. Ten microliters of sample was injected and the mobile phase flow was 500 µL/min. LC solvents were A: 0.1% formic acid in water and B: acetonitrile. The following gradient was used: 0 → 0.5 min 5% B, 0.5 → 3.5 min gradient to 90% B, 3.5 → 5 min 90% B, then returned to initial conditions over 0.1 min and equilibrated at 5% B until 7 min. Analytes were monitored using positive ion electrospray ionization and *m/z* transitions of 378.1 → 239.0 for talarozole and 705.2 → 392.2 for itraconazole. For mass spectrometry parameters, a declustering potential of 16, collision energy of 33, and collision exit potential of 4 for talarozole and declustering potential of 76, collision energy of 43, and collision exit potential of 6 for itraconazole were used, and the source temperature was 450ºC. Data were analyzed using Analyst software (AB Sciex, Foster City, CA) and talarozole concentrations were quantified with a standard curve ranging from 0.5 – 50 nM.

A one compartment model with first-order absorption and elimination (equation 2.1) was fit to data collected from the single 2.5 mg/kg dose of talarozole in Phoenix WinNonlin v6.3 (Pharsight, St. Louis, MO) using sparse sampling fitting methods:

$$C = \frac{F \times D \times k_a}{V\left(k_a - k\right)} \times \left(e^{-k(t)} - e^{-k_a(t)}\right) \tag{2.1}$$

where F is bioavailability, D is the dose, k_a is the rate of absorption, k is the rate of elimination, and V is the volume of distribution of talarozole.

2.2.4 Talarozole protein binding

The unbound fraction of talarozole in mouse serum was determined by ultracentrifugation as previously described (Shirasaka *et al.*, 2013). Serum from mice treated with oral 2.5 mg/kg talarozole as a single dose or twice daily for three days was pooled into three groups (n=7 per group), which was then aliquoted into ultracentrifuge tubes. Samples (n=2 per group) were incubated for 90 min at 37°C or centrifuged at 435,000 x g at 37°C for 90 min in a Sorval Discovery M150 SE ultracentrifuge with a Thermo Scientific (Waltham, MA) S100-AT3 rotor. Supernatant or incubated sample (40 µL) was added to 80 µL of 1:3 methanol:acetonitrile with 10 nM of itraconazole as internal standard and centrifuged at 3,000 x g at 4°C for 20 min. The supernatant was transferred and talarozole concentrations were analyzed by LC-MS/MS as described above. For each group, the fraction unbound was calculated as the ratio between mean talarozole concentrations with (unbound concentration) and without (total concentration) ultracentrifugation. The final fraction unbound is reported as the mean ± standard deviation of the three groups.

2.2.5 Prediction of CYP26 inhibition following single or multiple doses of talarozole

The change in CYP26A1 and CYP26B1 activity following a single dose of talarozole was predicted according to equation 2.2:

$$CYP26\ Activity\ Remaining\left(\%\right) = 100 \times \frac{1}{\left(1 + \frac{I_u}{K_i}\right)} \tag{2.2}$$

in which I_u is the unbound talarozole concentration and K_i is the reported inhibition constant for CYP26A1 or CYP26B1 (Diaz *et al.*, 2016).

Induction of CYP26A1 protein in the liver was incorporated to predict the change in CYP26A1 activity following multiple doses of talarozole using equation 2.3:

$$CYP26\ Activity\ Remaining\left(\%\right)=100\times\frac{1}{\left(1+\frac{I_u}{K_i}\right)}\times E_{ind} \quad (2.3)$$

where E_{ind} is the observed fold-increase in CYP26A1 protein in the liver measured by Western blot following the final dose of 2.5 mg/kg talarozole administered twice daily for three days.

2.2.6 Quantitation of *at*RA in mouse serum and tissues

*at*RA was quantified in serum, liver and testis as previously described (Arnold *et al.*, 2015a; Arnold *et al.*, 2015b). In brief, liver (68 – 84 mg) or testis (65 – 126 mg) tissue samples were homogenized with a 1:1 volume of saline and 10 µL of 1.5 µM *at*RA-d_5 as internal standard was added. Each homogenate or serum (50 µL serum plus 10 µL of 1.5 µM *at*RA-d_5) sample was transferred to a 15 mL glass culture tube and extracted in a 2:1 volume of acetonitrile + 1% formic acid and 10 mL of hexanes. The organic layer was separated by centrifugation, dried under nitrogen flow and reconstituted in 60:40 acetonitrile:water for LC-MS/MS analysis. All extractions were performed on ice and under red light to ensure *at*RA stability.

The concentrations of *at*RA with *at*RA-d_5 as an internal standard in serum and tissue homogenates were measured using an AB Sciex (Framingham, MA) qTrap 5500 mass spectrometer equipped with an Agilent Technologies (Santa Clara, CA) 1290 Infinity ultrahigh pressure liquid chromatography system as previously described (Arnold *et al.*, 2012; Arnold *et al.*, 2015b). Briefly, *at*RA was separated with an Ascentis® Express RP-Amide 15 cm x 2.1 mm, 2.7 µm column (Sigma-Aldrich, St. Louis, MO) with an Ascentis Express RP-Amide 2.7 µm guard column with a mobile phase flow of 500 µL/min and solvents A: 0.1 % formic acid in water and B: 60:40 acetonitrile:methanol plus 0.1% formic acid. The gradient was 0→2 min 40% B, 2 → 10 min increase to 95% B, 10 → 15 min hold at 95% B before return to initial conditions. For detection, positive mode atmospheric pressure chemical ionization was used and *m/z* transitions of

301.2→205.3 and 306.2→116.0 were monitored for *at*RA and *at*RA-d_5 quantification, respectively. Data was analyzed using Analyst software (AB Sciex, Foster City, CA).

2.2.7 Quantification of mRNA and protein changes in mouse liver and testis

Mouse liver and testis mRNA was extracted as previously published (Tripathy *et al.*, 2016). In brief, 1 mL of TRI reagent (Invitrogen, Grand Island, NY) was added to approximately 100 mg of liver or testis tissue and mRNA was extracted according to the manufacturer's recommendations. Total mRNA was quantified using a Nanodrop 2000c Spectrophotometer (Thermo Fischer Scientific, Waltham, MA), cDNA was generated using 1 µg RNA and TaqMan Reverse Transcription Reagents (catalog number N8080243, Applied Biosystems, Carlsbad, CA). Changes in *Rdh1, Rdh11, Aldh1a1, Aldh1a2, Cyp26a1, Cyp26b1, Rarβ*, small heterodimer partner (*Shp*), peroxisome proliferator activated receptor gamma coactivator 1α (*Pgc1α*), *Pgc1β*, nuclear respiratory factor (*Nrf1*), and stimulated by retinoic acid 8 (*Stra8*) mRNA were measured by quantitative reverse-transcriptase polymerase chain reaction (q-rtPCR) using a StepOnePlus (Applied Biosystems) instrument with TaqMan real-time gene expression master mix and PCR primers and probes as described previously (Tripathy *et al.*, 2016). The primer probe pairs were obtained from Applied Biosystems and included *Rdh1* (Mm00650636_m1), *Rdh11* (Mm00458129_m1), *Aldh1a1* (Mm00657317_m1), *Aldh1a2* (Mm00501306_m1), *Cyp26a1* (Mm00514486_m1, FAM), *Cyp26b1* (Mm00558507_m1), *Rarβ* (Mm01319677_m1, FAM), *Shp* (Mm0044278_m1), *Pgc1α* (Mm01208835_m1, FAM), *Pgc1β* (Mm00504730_m1, FAM), *Nrf1* (Mm01135606_m1, FAM), *Stra8* (Mm00486473_m1), β-glucuronidase (*Gusb*; Mm00446953_m1), and β-actin (*Actb*; Mm00607939_s1, FAM). Both *Gusb* and *Actb* were evaluated as housekeeping genes for liver and testis, and based on the data, *Gusb* was used as a housekeeping gene in the liver and *Actb* in the testis. All samples were analyzed in duplicate and

any undetermined C_T values were assigned a C_T value of 40 (the maximum number of cycles). Changes in target mRNA were measured using relative quantification (fold-difference) and the ΔΔ cycle threshold method.

The amount of CYP26A1 protein in livers from mice treated with either vehicle or 2.5 mg/kg talarozole twice daily for three days was measured by Western blot as described previously (Tripathy *et al.*, 2016). The expression of CYP26A1 protein following a single dose of talarozole was not measured, as previous data suggested a delay of CYP26A1 protein synthesis following mRNA induction (Topletz *et al.*, 2015). In brief, livers were homogenized and proteins were extracted using whole liver lysis buffer in the presence of protease (Roche Applied Science, Indianapolis, IN) and phosphatase inhibitors (1 mM β-glycerol phosphate, 2.5 mM Na-pyrophosphate, 1 mM Na_3VO_4). Protein concentrations were measured by BCA protein assay (Thermo Fisher Scientific, Waltham, MA). Whole liver protein extracts were separated by SDS-polyacrylamide gel electrophoresis (NuPAGE-Novex 4–12% polyacrylamide Bis-Tris, Life Science Technologies, Carlsbad, CA) and transferred to nitrocellulose membranes. Blots were incubated with primary antibodies against CYP26A1 and β-Actin overnight at 4°C, and on the next day, blots were washed and incubated with secondary antibody for 1 hour at room temperature. The CYP26A1 antibody was made in-house as previously described (Thatcher *et al.*, 2010), and the β-Actin antibody (product # AC-15) was purchased from Abcam (Cambridge, MA). The secondary antibodies, IRDye 680 (anti-mouse) and IRDye 800 (anti-rabbit), were obtained from LiCor Inc (Lincoln, NE). Antigen-antibody reactions were detected and quantified using LiCor Odyssey scanner and software (Licor Inc., Lincoln, NE). All Western blots were conducted as technical duplicates.

2.2.8 Immunohistochemistry of Stra8 in mouse testis

IHC was performed as previously described (Hogarth and Griswold, 2013a). In brief, the tissue sections were first immersed in xylene, rehydrated using a graded series of ethanol and then antigen retrieval was achieved using 0.01 M citrate buffer (2.94 mg/mL sodium citrate dihydrate in double distilled water; pH 6) at a rolling boil for ~5 min. Non-specific binding of the secondary antibody was blocked via incubation of the tissue sections in a commercially available blocking solution (Histostain Kit, #956143B, Invitrogen, Carlsbad, CA) for 20 min at room temperature. To detect Stra8, sections were incubated at room temperature overnight (~16 h) in 1:1000 dilution of Stra8 primary antibody in blocking solution. The Stra8 antibody was made in-house as described previously (Hogarth *et al.,* 2015a). Control sections were incubated in blocking solution alone. Biotinylated goat-anti-rabbit secondary antibody (Histostain Kit) was applied for 1 hour at room temperature following the manufacturer's instructions. Strepdavidin-conjugated horseradish peroxidase (Histostain Kit) was then applied for 1 hour at room temperature. Primary antibody binding was visualized by a brown precipitate formed by HRP activity in the presence of 3,3′-diaminobenzidine tetrahydrochloride (DAB, Invitrogen, Carlsbad, CA). Tissue sections were then counterstained with a 1:3 dilution Harris Hematoxylin (Sigma-Aldrich, St. Louis, MO) and dehydrated via a graded ethanol series to xylene. Tissue sections were mounted under glass coverslips using DPX mounting media (VWR International, Radnor, PA) or DAPI. Cell types were determined using nuclear morphology and location within the tubules (Russell *et al.*, 1993).

2.2.9 Statistical analysis

Results are presented as mean ± standard deviation. To determine time-dependent changes in *at*RA tissue concentration or mRNA levels, log transformed concentration or q-rtPCR data was analyzed by ANOVA with a Dunnett's test as a post-hoc analysis using Prism (GraphPad, La Jolla,

CA). Differences between vehicle control and treated mice in the multiple dose study were assessed by t-tests on log-transformed data. In all analyses, $p<0.05$ was considered significant.

2.3 RESULTS

2.3.1 Effect of single dose talarozole on CYP26 activity and endogenous *at*RA concentrations

Following a single 2.5 mg/kg oral dose of talarozole in mice, the absorption of talarozole was rapid with a peak concentration (80.3 nM) observed at 30 min post dose (Figure 2.1). The observed talarozole $AUC_{0-\infty}$ was 190 h*nM resulting in a relatively high oral clearance of 590 mL/min/kg. Talarozole had a short half-life in mice, 2.2 h, leading to low to undetectable concentrations of talarozole 12 h after dosing. The unbound fraction of talarozole in plasma was 5.8 ± 2.5%.

Based on the reported inhibitory constants for talarozole (5.1 nM for CYP26A1 and 0.46 nM for CYP26B1) (Diaz *et al.*, 2016), talarozole concentrations in mice were above the CYP26A1 K_i for 8 h and above the CYP26B1 K_i for 12 h. Using the observed concentrations of talarozole, talarozole unbound fraction, and the K_i for each CYP26 isoform, a maximum 48% decrease in CYP26A1 activity and 79% decrease in CYP26B1 activity was predicted at 30 min post-dose (Figure 2.1). In agreement with the time above K_i and the short half-life of talarozole, at least 80% of enzyme activity was predicted to return by 4 h post-dose for CYP26A1 and 12 h post-dose for CYP26B1. These results suggest that talarozole is a transient inhibitor of both CYP26 enzymes.

Observed serum, liver, and testis concentrations of *at*RA as a function of time after a single dose of talarozole are presented in Figure 2.2. Baseline concentrations of *at*RA in vehicle-treated mice were 1.0 ± 0.61 nM in serum, 21 ± 0.48 pmol/g tissue in liver, and 11 ± 2.5 pmol/g tissue in

testis. Following talarozole dosing, endogenous *at*RA concentrations increased transiently with a maximum increase in *at*RA 4 h after talarozole dosing. The maximum *at*RA concentrations were 5.7 ± 3.7 nM, 56 ± 20 pmol/g tissue, and 27 ± 13 pmol/g tissue in serum, liver, and testis, respectively, representing a 5.7-, 2.7-, and 2.5-fold increase over concentrations measured in vehicle control mice. In all matrices, concentrations of *at*RA returned to baseline by 12 h after the talarozole dose.

To determine whether the 2.5- and 2.7-fold increases in testis and liver *at*RA concentrations resulted in increased *at*RA signaling in these organs, changes in the mRNA of *Cyp26a1, Rarβ, Shp, Pgc1α, Pgc1β,* and *Nrf1* in the liver and *Cyp26a1*, *Cyp26b1*, *Rarβ*, and *Stra8* in the testis were measured by q-rtPCR. *Cyp26a1* mRNA was increased in both the liver and testis, and similar to *at*RA concentrations, the induction was transient and peaked at 8 h. A significant increase in *Cyp26a1* was observed in the liver at 4, 8, and 12 h (Figure 2.3, $p<0.05$) and at 4 and 8 h in the testis (Figure 2.3, $p<0.05$) There was no change in *Cyp26b1* in the testis (Figure 2.3). Of the RAR target genes, *Rarβ* was significantly increased in the liver at 4 and 8 h, while *Shp* was unchanged. In contrast, in the testis, no changes in *Rarβ* or *Stra8* mRNA expression were observed (Figure 2.3). In the liver, a significant increase in the PPARδ target gene *Pgc1β* was observed at 2, 4, 8, and 12 h (Figure 2.3, $p<0.05$), while *Pgc1α, and Nrf1* were unchanged. In addition, no changes were detected over 24 h following a single dose of talarozole in the mRNA levels of genes that are involved in *at*RA formation (i.e., *Rdh1*, *Rdh11*, *Aldh1a1*, or *Aldh1a2*), in the liver or testis (Figure 2.3). Despite previous reports, no *Rdh1* was detected in the liver.

2.3.2 Effects of multiple doses of talarozole on CYP26 activity and endogenous *at*RA concentrations

Multiple doses of talarozole (2.5 mg/kg BID for 3 days) were administered to mice to assess the effect of prolonged inhibition of Cyp26 on *at*RA concentrations and signaling. The disposition of talarozole following a single dose was used to simulate the concentrations of talarozole in mice during the 2.5 mg/kg BID dosing for 3 days (Figure 2.4). Due to the short half-life of talarozole, no accumulation was expected with multiple dosing. Concentrations of talarozole in serum were measured at 4 h following the last dose, and the observed concentrations were similar (11.3 ± 4.9 nM) to those observed at 4 h in the single dose study (12.9 ± 3.5 nM). As in single dose inhibition predictions, a transient inhibition of Cyp26a1 and Cyp26b1 was expected during each dosing interval with greatest inhibition predicted at 30 min post-talarozole dose and complete return of Cyp26a1 and Cyp26b1 activity by 12 h following talarozole dosing (Figure 2.4).

Based on the inhibition data and simulated and observed talarozole concentrations, *at*RA serum and tissue concentrations were expected to be increased following multiple doses of 2.5 mg/kg talarozole BID. Indeed, serum *at*RA concentrations were significantly higher in talarozole-treated compared to vehicle-treated mice (Figure 2.4, $p<0.05$). However, there was no significant increase in endogenous *at*RA in livers or testes of mice treated with multiple doses of talarozole (Figure 2.4). Based on the transient increase in *Cyp26a1* mRNA following the single dose of talarozole, and the lack of increase in tissue *at*RA concentrations despite similar inhibitor exposure as measured after a single dose of talarozole, it was hypothesized that the lack of increase in *at*RA following multiple doses of talarozole was due to Cyp26 induction in target tissues. Therefore, the *Cyp26a1* and *Cyp26b1* mRNA expression in liver and testis were measured. Liver *Cyp26a1* mRNA was significantly higher in talarozole-treated mice compared to control mice (Figure 2.5, $p<0.05$). In the testis, no significant increase in *Cyp26a1* or *Cyp26b1* mRNA was observed in

talarozole-treated mice compared to control mice, though a trend of increased *Cyp26a1* was observed (Figure 2.5).

To determine whether changes in *Cyp26a1* mRNA in the liver translated to increased CYP26A1 protein expression, hepatic CYP26A1 protein was measured by Western blot. On average, an 11-fold increase in CYP26A1 protein in livers from talarozole-treated versus vehicle-treated mice was observed (Figure 2.5). When the 11-fold induction was included with the transient CYP26A1 inhibition in the prediction of changes in CYP26A1 activity, a net 5-fold increase in hepatic CYP26A1 activity was predicted. Thus, in the liver, which expresses CYP26A1 but not CYP26B1, accounting for transient inhibition, as well as induction of CYP26A1 protein, predicted a potential decrease in *at*RA concentrations. To explore potential reasons for the discrepancy between predicted and observed liver *at*RA concentrations, the changes in the mRNA of enzymes involved in vitamin A homeostasis (*Rdh11* and *Aldh1a1* in the liver and *Rdh1*, *Rdh11*, *Aldh1a1*, and *Aldh1a2* in the testis) were measured. Consistent with results from the single dose talarozole study, no significant changes in the expression of any of these genes were observed in the liver or testis (Figure 2.5).

2.3.3 Effect of CYP26 inhibition on *at*RA signaling in mouse liver and testis

The effect of multiple doses of talarozole on genes that are transcriptionally regulated by *at*RA in the liver was investigated to further assess *at*RA signaling. No differences were observed in *Rarβ, Shp, Pgc1α* or *Nrf1* mRNA in the liver (Figure 2.6) while *Pgc1β* mRNA was decreased in talarozole-treated mice compared to vehicle-treated mice (Figure 2.6, $p<0.05$). The impact of CYP26 inhibition on *at*RA signaling in the testis was assessed by immunohistochemical staining for STRA8, a marker of response to *at*RA in testicular germ cells (Hogarth *et al.*, 2015a). In agreement with the lack of significant increase in *at*RA concentrations in the testis, there was no

increase in STRA8 expression 4 h following the last dose of multiple doses of talarozole (Figure 2.6).

2.4 DISCUSSION

The aim of this study was to determine whether changes in endogenous *at*RA concentrations will alter retinoid signaling in two target organs, liver, and testis, following administration of talarozole, a potent inhibitor of the *at*RA hydroxylase enzymes CYP26A1 and CYP26B1 according to the model shown in Figure 2.7. In addition, this study aimed to determine whether the magnitude and time-course of changes in the concentrations of an endogenous signaling molecule upon inhibition of its main clearance pathway could be predicted from *in vitro* data. *at*RA clearance by CYP26 and the inhibition of CYP26 by talarozole were used as a model system. Inhibition of *at*RA clearance has been an attractive drug target due to the many tissue-specific roles of *at*RA and the potential therapeutic benefits of increasing *at*RA concentrations in various tissues, including the liver and the testis (Njar *et al.*, 2006; Nelson *et al.*, 2013). However, inhibition of *at*RA clearance could also lead to unwanted side effects due to excessive *at*RA exposure. As such, better understanding of the effects of xenobiotic CYP inhibitors on endogenous compound homeostasis is needed to aid in design of more effective inhibitors of key enzymes for therapeutic purposes and in assessing potential toxicity of CYP inhibition.

Talarozole has previously been used as a CYP26 inhibitor to increase *at*RA levels and signaling in mice, rats and humans but no data are available for talarozole disposition in these species (Stoppie *et al.*, 2000; Verfaille *et al.*, 2007a; Verfaille *et al.*, 2007b). Increased concentrations of *at*RA have been observed following talarozole dosing, but effects of inhibitor potency and disposition, and tissue-specific expression of CYP26 enzymes on *at*RA concentrations in specific organs, has not been reported. This study showed that talarozole dosing

caused the greatest changes in serum *at*RA concentrations, a finding in good agreement with previously reported data in rats showing the greatest increase in retinoic acid concentrations in plasma and skin and the smallest increase in the liver (Stoppie *et al.*, 2000). However, the increase in *at*RA concentrations in this study was modest in light of the inhibitory potency of talarozole (K_i 0.46 nM for CYP26B1 and 5.1 nM for CYP26A1) (Diaz *et al.*, 2016). The data presented here suggest that the limiting factor in the efficacy of talarozole is its short half-life, as the inhibition of CYP26 enzymes lasts only a few hours. In addition, the lower potency of talarozole towards CYP26A1 compared to CYP26B1 suggests that talarozole will inhibit predominantly CYP26B1 in vivo with smaller effects on CYP26A1. As a result, it is likely that talarozole will more effectively increase *at*RA concentrations in tissues that have high CYP26B1 expression. This is in agreement with the reported expression of CYP26B1 in the skin and the efficacy of talarozole in disorders of the skin such as acne and psoriasis (Topletz *et al.*, 2012; Verfaille *et al.*, 2007a; Verfaille *et al.*, 2007b).

Of the two CYP26 enzymes, CYP26A1 has been shown to be the predominant *at*RA metabolizing enzyme in the human liver with CYP26B1 being either absent or below limit of detection (Thatcher *et al.*, 2010). Hence, altered *at*RA concentrations in the liver are expected to mainly reflect CYP26A1 inhibition. Both *Cyp26a1* and *Cyp26b1* mRNA have been detected in mouse testis (Hogarth *et al.*, 2015b), thus inhibition of both enzymes is likely needed to alter intratesticular *at*RA concentrations significantly. The predicted maximum 50% decrease in CYP26A1 activity by talarozole after the single dose used in this study is expected to result in an up to 2-fold increase in *at*RA concentrations in tissues mainly expressing CYP26A1. The maximum observed 2.7- and 2.5-fold increases in liver and testis *at*RA concentrations after single dose talarozole, respectively, are in excellent agreement with this prediction and support a major

role of CYP26A1 in regulating liver and testis *at*RA concentrations. However, the 5.7-fold increase in *at*RA in serum after a single talarozole dose cannot be explained by inhibition of CYP26A1 and likely reflects inhibition of CYP26B1 in extrahepatic tissues. The predicted 80% decrease in CYP26B1 activity by talarozole is predicted to result in up to 5-fold increase in *at*RA concentrations in tissues mainly expressing CYP26B1. Taken together, these data suggest that circulating *at*RA levels are largely controlled by CYP26B1 expression at extrahepatic sites and indicate that CYP26B1 inhibition by talarozole contributes significantly to the increase in circulating *at*RA. Although CYP26 inhibition and subsequent increases in *at*RA concentrations were well-predicted after a single dose of talarozole, the lack of any change in liver or testis *at*RA concentrations following multiple talarozole doses was unexpected. When multiple-dose predictions included CYP26A1 induction, the magnitude of CYP26A1 induction was expected to result in net induction of *at*RA clearance despite talarozole inhibition and an overall decrease in *at*RA concentrations in the liver. Yet no decrease in *at*RA concentrations was observed in the liver. This discrepancy is unlikely to be due to altered *at*RA synthesis, as *Rdh* and *Aldh1a* mRNA were unchanged. The lack of decrease in liver *at*RA concentrations is more likely due to inhibition of CYP26B1 in extrahepatic tissues (Topletz *et al.*, 2012) and the role of CYP26B1 in regulating retinoic acid homeostasis. Serum *at*RA concentrations, which were elevated despite CYP26A1 induction, may contribute significantly to liver *at*RA concentrations. Thus, to establish whether therapeutic CYP26 inhibition will alter *at*RA concentrations in a target tissues, a better understanding of the relative contributions of individual organs and CYP26A1 and CYP26B1 to *at*RA clearance is needed. These data also suggest that, in the liver and testis, > 90% inhibition of CYP26s must be achieved to overcome autoinduction of CYP26A1 to increase *at*RA concentrations.

The brief inhibition of CYP26A1 and CYP26B1 activity in the single dose study was sufficient to increase *at*RA concentrations in the serum, liver and testis of mice, although the increase in *at*RA concentrations was transient. The time-course of the observed increase in endogenous *at*RA following a single dose of talarozole is in good agreement with the previously published *at*RA half-life ranging from 30 minutes in mouse liver to 1.3 hours in mouse testis (Arnold *et al.,* 2015a). Based on the maximum predicted inhibition of CYP26A1 and CYP26B1 by talarozole at 30 minutes post-dose, peak concentrations of *at*RA would be predicted to occur four *at*RA half-lives later or between 2.5 and 5.7 hours following talarozole administration. This predicted time-course of the peak effect is in good agreement with the observed peak concentrations at 4 hours.

The transient and modest ~2-fold increase in *at*RA concentrations in the liver and testis following a single dose of talarozole was nevertheless sufficient to induce *Cyp26a1* in both organs. This demonstrates that even small changes in the concentrations of endogenous signaling molecules can cause major changes in specific signaling pathways. This is also in excellent agreement with the observed 2- to 5-fold changes in testis *at*RA concentrations and altered *at*RA signaling across the spermatogenic cycle (Hogarth *et al.*, 2015a). The rapid time course of change in *Cyp26a1* induction suggests that *Cyp26a1* mRNA half-life is only 2-3 hours in the liver and testis, which is much shorter than the 7 hour half-life determined for *CYP26A1* mRNA in HepG2 cells (Tay *et al.*, 2010). This short half-life is biologically plausible as it allows rapid dynamic changes in CYP26 expression in response to environmental factors and *at*RA concentrations (Topletz *et al.*, 2015). Several other genes, including the RAR target gene *Rarβ* and the PPARδ target gene *Pgc1β*, which have previously been shown to be inducible by *at*RA, were also responsive to the observed increase in endogenous *at*RA following a single dose of talarozole. In

contrast, *Shp, Pgc1α, Nrf1, Cyp26b1* and *Stra8*, which also have been shown to be inducible by *at*RA, were not altered by single dose talarozole treatment in the liver or testis, possibly due to the small changes in *at*RA concentrations in those tissues. These differences in gene responses are likely due to diversity in inherent responses to *at*RA and other regulatory elements for these genes. Multiple doses of exogenous *at*RA have previously been shown to induce *Shp* mRNA in mouse liver (Koh *et al.*, 2014). Although the magnitude of increase in *at*RA concentrations was not measured in that study, it is likely to have been much greater than 2-fold, as therapeutic *at*RA concentrations can exceed endogenous concentrations by 100-fold (Ozpolat *et al.*, 2003a). Similarly, administration of *at*RA to mice led to signaling changes in *at*RA-responsive mitochondrial biogenesis genes *Pgc1α, Pgc1β,* and *Nrf1* in the liver (Tripathy *et al.*, 2016) and STRA8 in the testis (Hogarth *et al.*, 2015a). Yet in the current study, no effect in these genes was observed following the 3-day dosing of talarozole, likely due to the lack of change in liver and testis *at*RA concentrations.

In conclusion, inhibition of CYP26A1 and CYP26B1 with a single dose of talarozole led to a modest and transient increase in endogenous *at*RA and increased *at*RA-mediated signaling in the liver and testis. However, induction of CYP26A1 upon multiple dosing with talarozole was sufficient to overcome the effect of CYP26A1 inhibition in these tissues. Inhibition of CYP26B1 by talarozole appears to drive the change in *at*RA concentrations observed in serum and specific inhibition of CYP26B1 may be sufficient to promote tissue-specific changes in *at*RA concentrations.

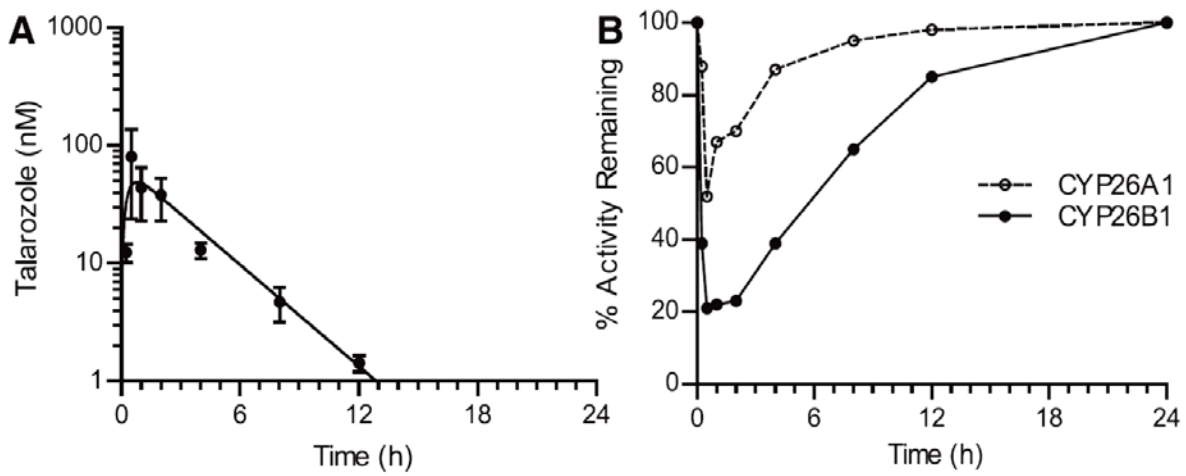

Figure 2.1. Talarozole pharmacokinetics and predicted inhibition of CYP26A1 and CYP26B1 by talarozole. (A) Serum concentration versus time profile of talarozole after oral dosing of 2.5-mg/kg to mice. Data are shown as mean ± SD (n=3). (B) Predicted change in CYP26A1 and CYP26B1 activity as a function of time following a single dose of 2.5-mg/kg talarozole to mice.

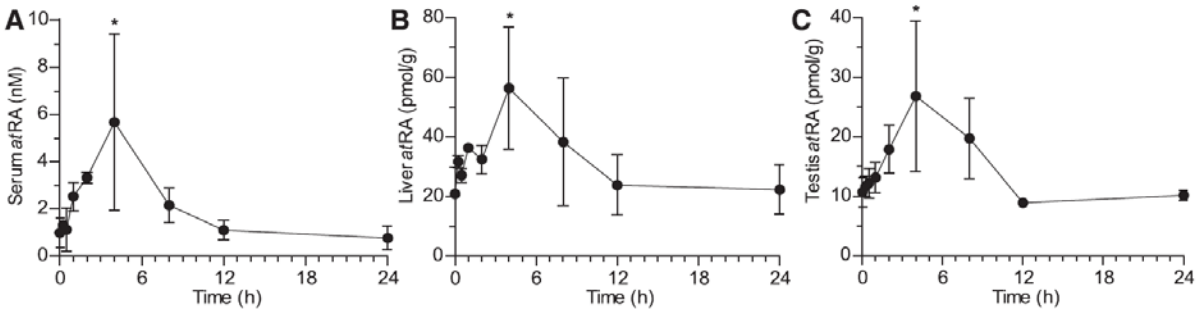

Figure 2.2. Time course of endogenous *at*RA changes following a single oral dose of 2.5 mg/kg talarozole to mice. Concentrations of endogenous *at*RA in serum (A), liver (B), and testis (C) as a function of time after a single 2.5 mg/kg oral dose of talarozole to mice. Data are presented as mean ± SD (n=3). *$p<0.05$ compared to pre-dose *at*RA.

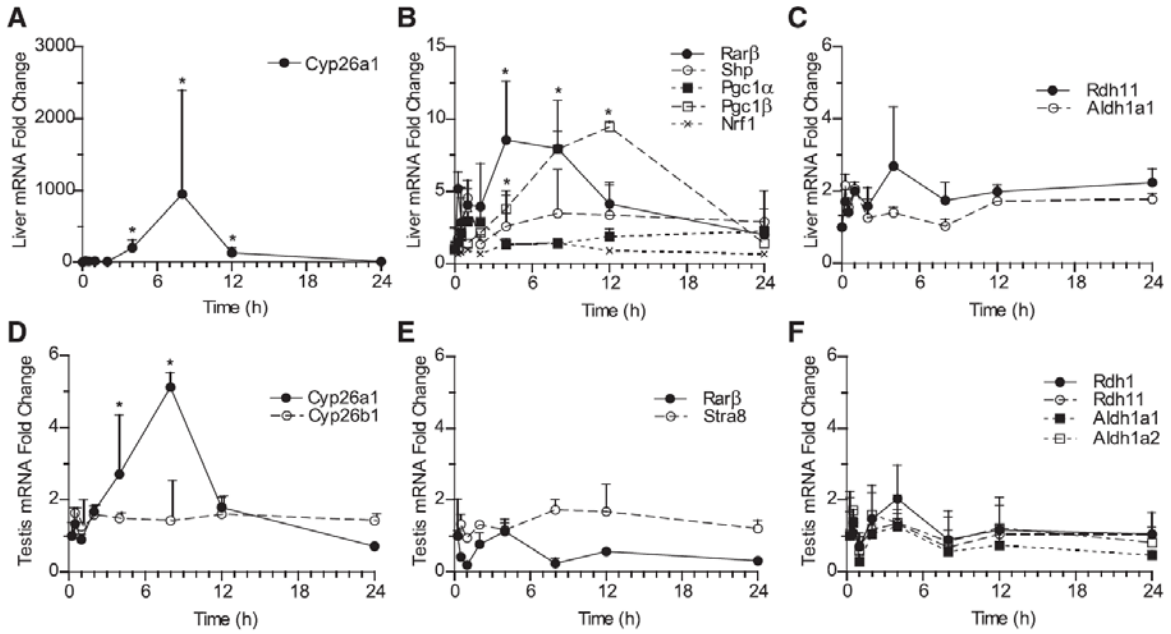

Figure 2.3. **Time-course of mRNA changes for genes involved in *at*RA formation and elimination and *at*RA target genes following a single oral dose of 2.5 mg/kg talarozole to mice.** The fold change in *Cyp26a1* (A); *Rarβ* (solid circle and solid line), *Shp* (open circle and hashed line), *Pgc1α* (closed square and dotted line), *Pgc1β* (open square and hashed line), *Nrf1* (cross and dotted line) (B); *Rdh11* (solid circle and solid line), and *Aldh1a1* (open circle and hashed line) (C) mRNA in the liver in talarozole-treated mice versus vehicle-treated mice as a function of time after talarozole dosing. The fold-change in *Cyp26a1* (solid circle and solid line), *Cyp26b1* (open circle and hashed line) (D); *Rarβ* (solid circle and solid line), *Stra8* (open circle and hashed line) (E); *Rdh1* (solid circle and solid line), *Rdh11* (open circle and hashed line), *Aldh1a1* (solid square and solid line), and *Aldh1a2* (open square and hashed line) (F) mRNA in the testis of talarozole-treated mice as a function of time after the earliest treatment timepoint (0.25 hour). Data are presented as mean ± SD (n=3). *$p<0.05$ compared to predose mRNA

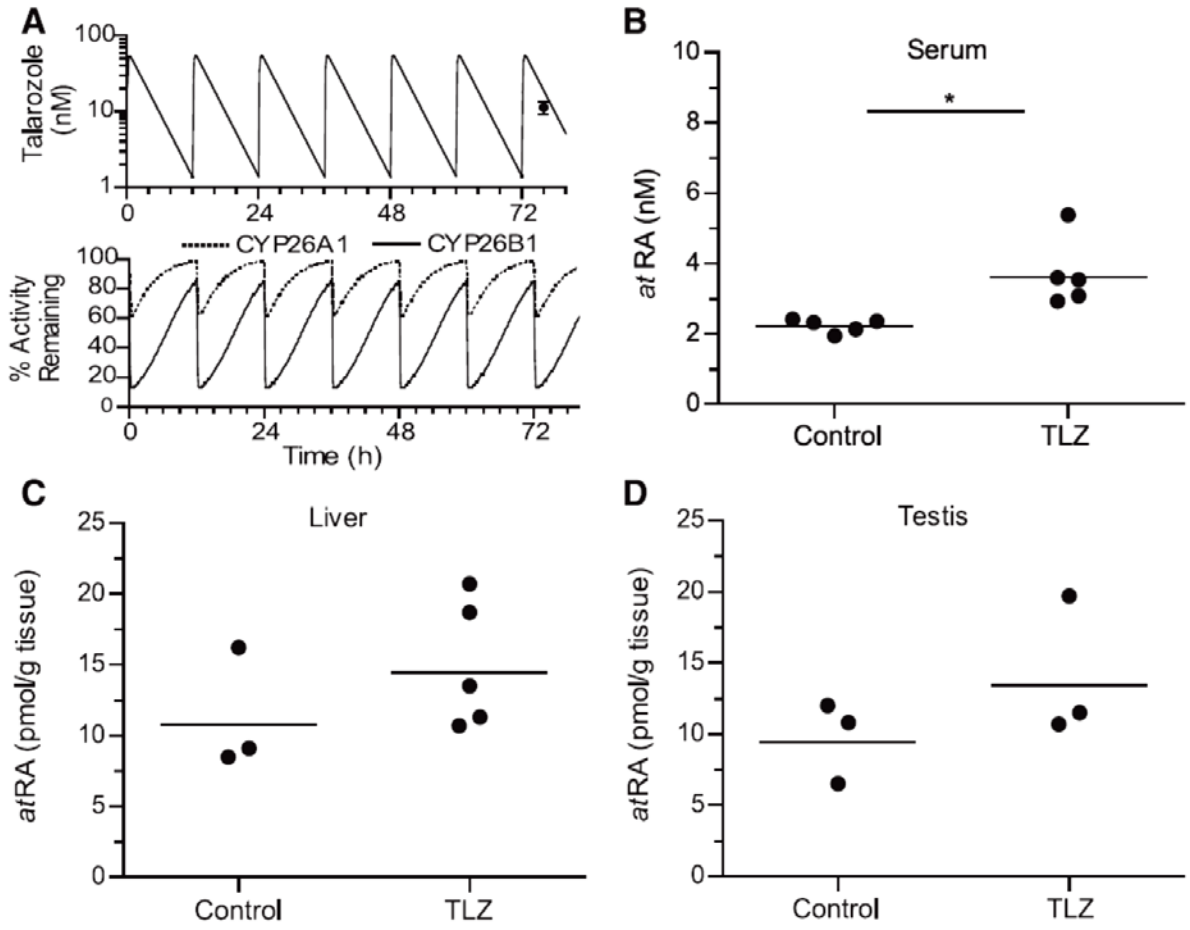

Figure 2.4. **Predicted change in CYP26 activity and concentrations of endogenous *at*RA following 2.5 mg/kg talarozole dosed twice a day for 3 days.** (A, top) Simulated concentrations of talarozole administered as 2.5 mg/kg twice a day for 3 days (solid line). A final dose was administered on the fourth day after overnight fast. Observed talarozole concentrations 4 hours following the last 2.5 mg/kg dose are presented as mean ± SD (n=5). (A, bottom) Static predictions of CYP26A1 (hashed line) and CYP26B1 (solid line) inhibition following 2.5 mg/kg talarozole BID for 3 days. Concentrations of *at*RA in vehicle-treated and talarozole-treated mice in serum (B), liver (C), and testis (D). Each data point represents an individual animal, and mean value is shown as a solid line. *$p<0.05$. TLZ, talarozole.

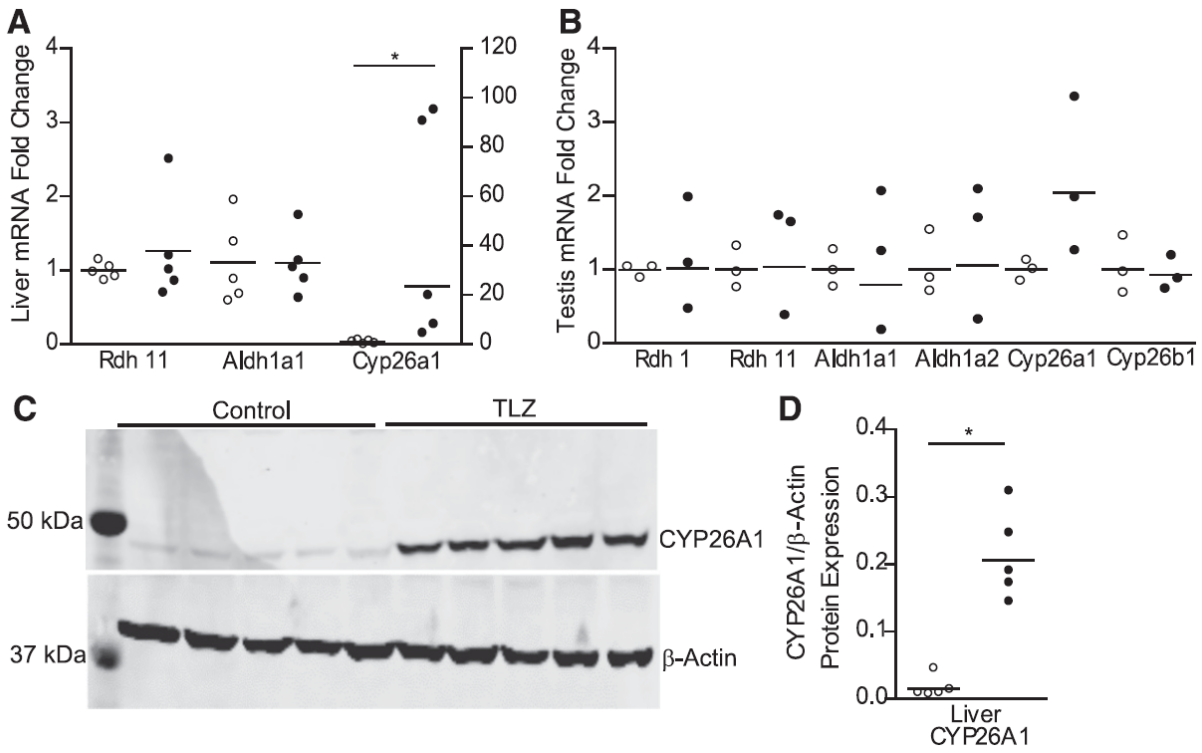

Figure 2.5. Fold change in mRNA of enzymes involved in *at*RA formation and elimination and Cyp26a1 protein following dosing of 2.5 mg/kg talarozole twice a day for 3 days. (A) The fold change in *Rdh11* and *Aldh1a1* (left axis) and *Cyp26a1* (right axis) mRNA in the liver in talarozole-treated mice (closed circles) compared with vehicle-treated mice (open circles). (B) The fold-change in *Rdh1*, *Rdh11*, *Aldh1a1*, *Aldh1a2*, *Cyp26a1*, and *Cyp26b1* mRNA in the testis in talarozole-treated mice (closed circles) compared with vehicle-treated mice (open circles). (C) Representative Western blot image of CYP26A1 and β-actin in vehicle control mice (lanes 1 – 5) and talarozole-treated mice (lanes 6 – 10). (D) The quantification of signal intensity from Western blot of CYP26A1 protein relative to β-actin protein in the livers of vehicle control mice (open circles) and talarozole-treated mice (closed circles). Each data point represents an individual animal and the mean is shown as a solid line. *$p<0.05$

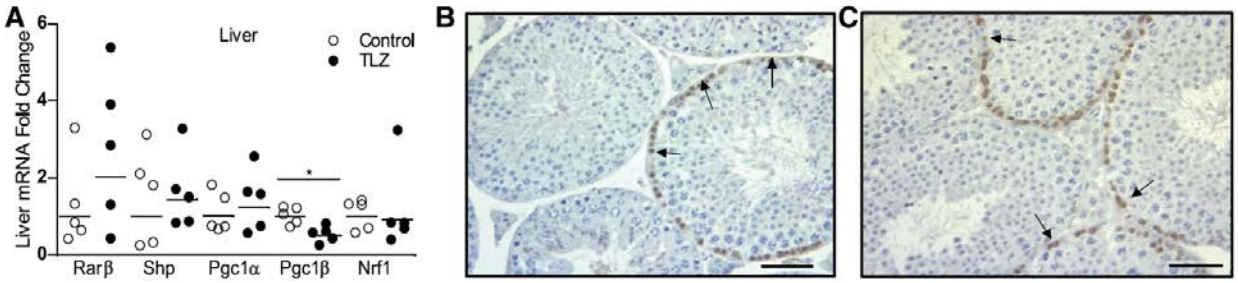

Figure 2.6. Changes in the expression of *at*RA target genes in the liver and testis following dosing of mice with 2.5 mg/kg talarozole (TLZ) twice a day for 3 days. (A) Fold change in mRNA of genes responsive to *at*RA signaling in the liver (*Rarβ, Shp, Pgc1α, Pgc1β*, and *Nrf1*) in talarozole-treated mice compared with control. Each data point represents an individual animal, and the mean is shown as a solid line. Representative cross-sections of testis collected from adult male mice treated twice a day with 2.5 mg/kg talarozole (C) or vehicle (B) for 3 days. Cross-sections were stained via immunohistochemistry to detect STRA8 protein as a means of assessing *at*RA response. Black arrows indicate STRA8-positive cells. Scale bar = 50 µm.

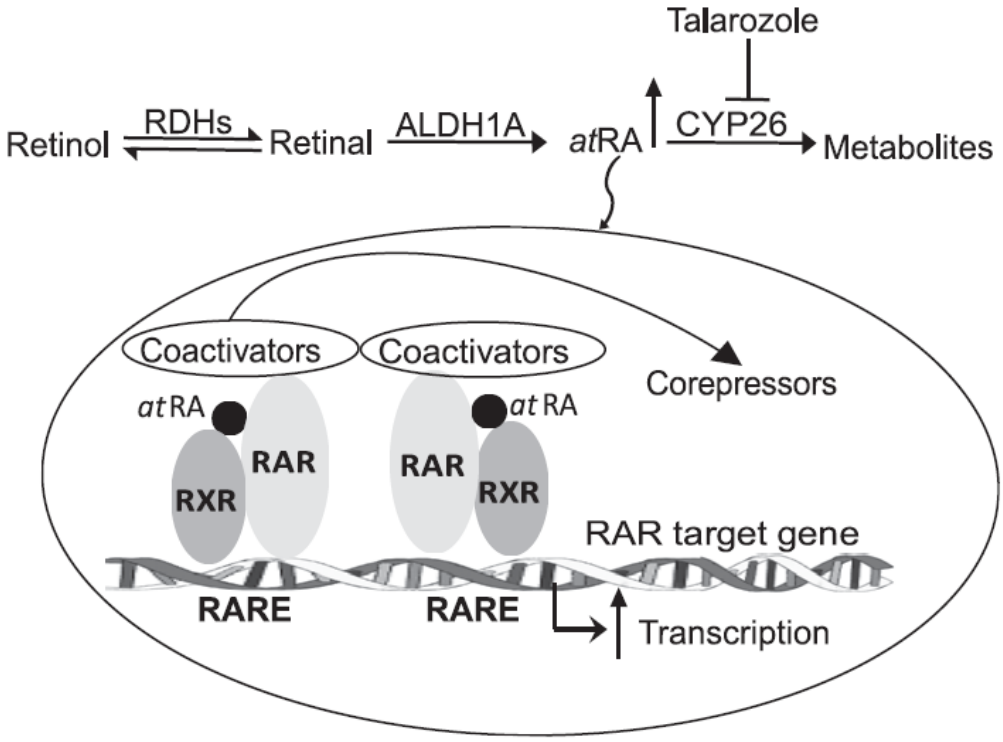

Figure 2.7. A proposed schematic of increased RAR-responsive gene transcription in response to CYP26 inhibition by talarozole. Synthesis of *at*RA from retinol occurs via a two-step enzymatic process involving RDH and ALDH1A enzymes, and CYP26 enzymes are responsible for *at*RA elimination. Decreased metabolism via CYP26 increases *at*RA levels, which promotes *at*RA binding at retinoic acid receptor/retinoid X receptor (RAR/RXR) heterodimers on retinoic acid response elements (RAREs). Binding of *at*RA causes dissociation of corepressors to promote gene transcription.

Chapter 3. INVESTIGATION OF CLINICAL DRUG-DRUG INTERACTIONS INVOLVING 13-*CIS* RETINOIC ACID AND CYTOCHROME P450S

3.1 INTRODUCTION

Drug-drug interactions (DDIs) can have severe consequences such as adverse events resulting from unanticipated increased exposure of a victim drug or diminished efficacy due to decreased exposure of the victim drug. Thus, to minimize the risk of unanticipated DDIs, regulatory agencies require screening of new drug candidates for potential DDIs involving inhibition or induction of drug metabolizing enzymes and transporters (EMA, 2012; Food and Drug Administration, 2017b). Guidance from the European Medicines Agency (EMA) also recommends investigation of possible DDIs resulting from transcriptional down-regulation of enzymes in hepatocytes. In a recent survey of Innovation and Quality Consortium member companies, more than half of survey respondents reported observing mRNA down-regulation in at least 10% of routine induction studies (Hariparsad *et al.*, 2017). When down-regulation of mRNA was observed, maximal decreases of at least 50% were reported for approximately 14% of studies, which would trigger follow-up investigations per EMA guidance. While in some cases, the decreased mRNA may be due to cytotoxicity, these findings suggest CYP down-regulation may occur relatively frequently in vitro.

Recently, two small molecule drugs (bupropion and LY2090314) that caused in vitro down-regulation of a cytochrome P450 (CYP) were proposed to cause in vivo DDIs (Zamek-Gliszczynski *et al.*, 2014; Sager *et al.*, 2017). However, neither of these in vitro examples could be unequivocally associated with in vivo CYP down-regulation due to confounding reversible inhibition and/or lack of clinical DDI data. The active metabolite of vitamin A, *all-trans* retinoic acid (*at*RA), has been shown to cause transcriptional down-regulation of CYPs and is not known to be a reversible inhibitor of CYPs. Administration of *at*RA to CYP2D6-humanized mice was shown to down-regulate CYP2D6 activity and expression (Koh *et al.*, 2014). Moreover, liver

concentrations *at*RA are negatively correlated with *CYP2D6* mRNA in human liver biopsies (Ning, M., et al., *in revision*). This down-regulation is believed to be a result of *at*RA inducing the expression of the transcriptional corepressor small heterodimer partner (SHP) (Mamoon *et al.*, 2008; Cai *et al.*, 2010; Yang *et al.*, 2014), which represses hepatocyte nuclear receptor 4α (HNF4α) activity and consequently CYP2D6 transcription (Koh *et al.*, 2014). Whether down-regulation of CYP2D6 occurs in humans is unknown, but *at*RA presents an intriguing opportunity to study a DDI resulting from transcriptional down-regulation, in the absence of reversible CYP inhibition. In addition, *at*RA has been shown to induce expression of CYP3A4 in vitro as CYP3A4 has been shown to be regulated by the retinoid X receptor α (RXRα) (Wang *et al.*, 2008; Chen *et al.*, 2010). Thus, interactions involving *at*RA may result in down-regulation of CYP2D6, induction of CYP3A4, or alterations in the activity of both enzymes.

Both *at*RA and its isomer 13-*cis* retinoic acid (13*cis*RA) are used clinically. 13*cis*RA has a more favorable pharmacokinetic profile than *at*RA in humans (Muindi *et al.*, 1992, 2008a; Adamson *et al.*, 1995) including a much longer half-life (~20 hours for 13*cis*RA compared to ~1 hour for *at*RA) and linear kinetics (Khoo *et al.*, 1982; Brazzell *et al.*, 1983). *at*RA is a major metabolite of 13*cis*RA, and dosing with 13*cis*RA was expected to mimic *at*RA exposures given that steady state concentrations of *at*RA have been shown to be similar following dosing of either *at*RA or 13*cis*RA (Muindi *et al.*, 2008a). 13*cis*RA dosing provides a prolonged exposure to *at*RA due to formation rate-limited kinetics of *at*RA from 13*cis*RA. The two isomers also likely share mechanisms of CYP regulation as both are ligands for the same nuclear receptors (Aström *et al.*, 1990; Idres *et al.*, 2002).

The aim of our current study was to determine whether in vitro CYP2D6 down-regulation by *at*RA translates to decreased in vivo CYP2D6 activity as assessed by dextromethorphan

clearance following administration of 13*cis*RA (with its circulating metabolites *at*RA and 4-oxo-13*cis*RA) in healthy male volunteers. In addition, CYP3A4 induction was also assessed using the formation of 3-methoxymorphinan and 6β-hydroxycortisol. Further work was done in mice to confirm the effect of *at*RA, 13*cis*RA, and 4-oxo-13*cis*RA on mouse *Shp* and *Cyp2d* expression in vivo.

3.2 MATERIALS AND METHODS

3.2.1 Chemicals and reagents

Reference standards for dextromethorphan, dextrorphan, dextromethorphan-d_3, 13*cis*RA, *at*RA, cortisol, 6β-hydroxycortisol, 6α-methylprednisolone, 3-methoxymorphinan, 3-hydroxymorphinan, ethyl acetate, and mass spectrometry grade formic acid were purchased from Sigma-Aldrich (St. Louis, MO). 13*cis*RA-d_5 and *at*RA-d_5 were obtained from Toronto Research Chemicals (Toronto, ON). 4-oxo-13*cis*RA, 4-oxo-*at*RA-d_3, and dextrorphan-*O*-glucuronide were obtained from Santa Cruz Biotechnology (Dallas, TX). Water and acetonitrile were Optima LC/MS grade from Thermo Fisher Scientific (Waltham, MA).

3.2.2 Clinical study protocol

This study was approved by the University of Washington Institutional Review Board, and signed informed consent was obtained from all subjects prior to participation in any study activities. Based on prior observations of the variability in dextromethorphan kinetics, this study was designed to have 80% power to detect a 50% change in dextromethorphan exposure with an α of 0.05. Eight healthy male volunteers were enrolled in the study. All subjects had normal hepatic and renal function and no history of allergy to either study medication. Tobacco users or subjects with a pregnant partner were excluded from the study. Subjects agreed to abstain from

over the counter and prescription medications and dietary supplements for the duration of the study. Subjects were administered a PHQ9 questionnaire at the beginning and end of the study to monitor for symptoms of depression, and no subject with a history of severe mental health problems was enrolled in the study. Subjects were genotyped for common CYP2D6 variants. Subjects with the CYP2D6 poor metabolizer alleles (*CYP2D6*3* or *CYP2D6*4*) or with multiple copies of CYP2D6 were excluded from the study.

On study day 1, subjects received a 30 mg dose of dextromethorphan and blood samples were collected prior to and 30 min, and 1, 2, 4, 6, 8, and 24 h after drug administration. Urine was collected from 0 – 8 and 8 – 24 h. On study day 2, subjects were given 13*cis*RA to be taken as 40 mg twice a day (BID) with food for 13 days (study days 2 – 14). 13*cis*RA capsules were purchased (as Isotretinoin) by the University of Washington Investigational Pharmacy, which dispensed all study medications. On study day 15, subjects returned to clinic and had a blood draw taken before administration of another 30 mg dose of dextromethorphan and a final 40 mg dose of 13*cis*RA. Blood samples were collected prior to and 30 min, and 1, 2, 4, 6, 8, 24, and 48 h after drug administration. Urine was collected from 0 – 8 and 8 – 24 h. Blood samples were collected in foil-wrapped serum separator tubes, allowed to clot for a minimum of 30 min and centrifuged at 1,000 x g for 10 min. Serum was collected for storage in -80°C. Serum sample handling was conducted under yellow light to protect light-sensitive retinoids from degradation.

3.2.3 Quantitation of study drugs and metabolites in serum

To measure 13*cis*RA and its metabolites *at*RA and 4-oxo-13*cis*RA in serum collected from study day 15, serum was diluted 20-fold in water prior to addition of 100 µL of acetonitrile with 13*cis*RA-d_5 (250 nM), *at*RA-d_5 (100 nM), and 4-oxo-*at*RA-d_3 (500 nM) as internal standards. Samples were centrifuged at 16,000 x g for 10 min at 4°C, chilled at 4°C for 10 min, and

centrifuged again at 16,000 x g for 10 min. Analytes were quantified on an Agilent Technologies (Santa Clara, CA) 1290 Infinity ultrahigh-pressure liquid chromatography system coupled to an AB Sciex (Framingham, MA) qTrap 5500 mass spectrometer as previously described (Arnold *et al.*, 2012). The percentage coefficient of variation (%CV) for all analytes was ≤ 11% and the lower limit of quantification (LLOQ) in serum was 2.5 nM for 13*cis*RA and *at*RA, and 50 nM for 4-oxo-13*cis*RA. Quality control samples were included in all analytical runs and had to meet standard assay validation criteria for run acceptance.

To prepare serum and urine samples for analysis of dextromethorphan and metabolites, 100 µL of serum or urine was added to 100 µL of acetonitrile with 10 nM dextromethorphan-d_3 as internal standard. The samples were centrifuged at 16,000 x g for 10 min at 4°C, chilled at 4°C for 10 min, and centrifuged again at 16,000 x g for 10 min. Supernatant was collected and concentrations of dextromethorphan, dextrorphan, dextrorphan-*O*-glucuronide, 3-hydroxymorphinan, and 3-methoxymorphinan were measured with an Agilent Technologies (Santa Clara, CA) 1290 Infinity ultrahigh-pressure liquid chromatography system coupled to an AB Sciex (Framingham, MA) qTrap 5500 mass spectrometer as previously described with minor modifications (Sager *et al.*, 2014). Briefly, analytes were separated with a Kinetex® 100 x 2.1 mm 2.6 µm EVO C18 column (Phenomenex, Torrance, CA) with a mobile phase of A) water with 0.1% formic acid and B) acetonitrile with 0.1% formic acid and a gradient elution of 10% B for 0.5 min, increased to 90% B for 2 min and held for 1.5 min before returning to initial conditions and held for 2 min. Analyte detection was performed with electrospray ionization operated in positive ion mode, with the exception of dextrorphan-*O*-glucuronide which was detected in negative ion mode, with *m/z* transitions 272→128 for dextromethorphan, 258→157 for dextrorphan, 432→256 for dextrorphan-*O*-glucuronide, 244→157 for 3-hydroxymorphinan,

258→171 for 3-methoxymorphinan, and 275→128 for dextromethorphan-d_3. Standard curves in serum ranged from 0.3 – 30 nM for dextromethorphan and dextrorphan with quality control sample %CV ≤ 8% and ≤ 17%, respectively. In urine, all analytes had LLOQs of less than 7.8 nM except for dextrorphan-*O*-glucuronide which had a LLOQ of 78.1 nM. The %CV for analytes in urine was ≤ 7% except for dextrorphan-*O*-glucuronide that had a %CV of ≤ 17%. Urine samples initially quantified above the standard curve ranges were diluted with blank urine and reanalyzed.

Concentrations of cortisol and 6β-hydroxycortisol were measured in serum and urine samples, respectively, using liquid-liquid extraction and monitored by liquid chromatography tandem mass spectrometry (LC-MS/MS) as described previously (Peng *et al.*, 2011; Sager *et al.*, 2014). Serum samples (250 µL) were diluted with 750 µL water and urine samples (1 mL) were spiked with 100 nM 6α-methylprednisolone as internal standard and then extracted twice with 3 mL of ethyl acetate. After each extraction, samples were centrifuged and the organic phase was collected. The combined ethyl acetate layers were evaporated under nitrogen and reconstituted in 100 µL 1:1 methanol:water for analysis by LC-MS/MS with an Agilent Technologies (Santa Clara, CA) 1290 Infinity ultrahigh-pressure liquid chromatography system coupled to an AB Sciex (Framingham, MA) qTrap 5500 mass spectrometer. A Thermo Hypersil Gold C18 100 x 2.1mm, 1.9 µm column (Waltham, MA) was used for analyte separation with a mobile phase of A) water plus 0.1% formic acid and B) acetonitrile. A gradient elution of 10% B for 0.5 min, increased to 90% B over 3 min and held for 1.5 min before returning to initial conditions and held for 2 min was used. Cortisol detection was performed with electrospray ionization operated in positive ion mode with *m/z* transition of 363→121 and 6β-hydroxycortisol and 6α-methylprednisolone were detected in negative ion mode with *m/z* transitions of 423→347 for 6β-hydroxycortisol and

421→345 for 6α-methylprednisolone. The LLOQ was 3.1 nM for cortisol in serum and 1.6 nM for both cortisol and 6β-hydroxycortisol in urine with CV% of ≤ 15% for all analytes.

3.2.4 Pharmacokinetic analysis

Serum pharmacokinetic parameters for dextromethorphan and its CYP2D6-generated metabolite dextrorphan were determined by noncompartmental analysis in Phoenix WinNonlin v6.3 (Pharsight, St. Louis, MO). For each analyte, the maximum concentration (C_{max}) was reported from the observed concentration versus time profiles and the area under the serum concentration-time curve from time 0 to infinity ($AUC_{0-\infty}$) was determined using the linear up-log down trapezoidal rule. The half-life ($t_{1/2}$) was calculated as ln2 divided by the slope of the terminal linear phase. The oral clearance (CL/F) for dextromethorphan was calculated as dose divided by $AUC_{0-\infty}$. The formation clearance (Cl_f) of dextrorphan was determined by dividing the sum of the molar equivalents of dextrorphan and its metabolite dextrorphan-*O*-glucuronide recovered in urine over 24 hours by the AUC_{0-24h} of dextromethorphan. The serum metabolite-to-parent AUC ratio was calculated as the ratio of the $AUC_{0-\infty}$ of dextrorphan to the $AUC_{0-\infty}$ of dextromethorphan. The urinary metabolite-to-parent ratios were determined by recovery of dextrorphan and dextrorphan-*O*-glucuronide divided by the recovery of dextromethorphan in 24 hours. The relative fraction of dextromethorphan and each of its metabolites recovered in urine was determined by dividing the molar amount of each analyte recovered in urine by the total molar amounts of all analytes recovered in urine. The formation clearance (Cl_f) of the CYP3A4-specific metabolite, 3-methoxymorphinan, was determined by dividing the molar equivalents of 3-methoxymorphinan and its metabolite 3-hydroxymorphinan recovered in urine over 24 hours by the AUC_{0-24h} of dextromethorphan. The Cl_f of 6β-hydroxycortisol was determined by dividing the molar amount of 6β-hydroxycortisol recovered in urine over 8 hours following dosing of dextromethorphan by

the $AUC_{0\text{-}8h}$ of cortisol. The average steady state concentrations (C_{ss}) for 13*cis*RA, 4-oxo-13*cis*RA, and *at*RA following two weeks of 13*cis*RA dosing were determined by dividing the $AUC_{0\text{-}12h}$ calculated for each analyte by 12 h.

3.2.5 Animal care and retinoid treatments

Experiments in mice were approved by the Washington State University Animal Care and Use Committee. Male C57BL/6X129 mice were housed in a temperature- and humidity-controlled environment, and food and water were available ad libitum. Two separate studies were conducted. In the first study, mice were treated once daily for three days with intraperitoneal (ip) injection of 5 mg/kg 13*cis*RA (n=6), 5 mg/kg *at*RA (n=6) or vehicle (10% dimethyl sulfoxide with 90% sesame oil) (n=5). In the second study, mice were treated IP once daily for three days with 5 mg/kg 4-oxo-13*cis*RA (n=6) or vehicle control (n=6). On the evening of the third day mice were fasted overnight (12 h), and then food was replaced in the morning of the fourth day and a final dose of retinoid or vehicle was administered. At 4 h following the last dose, mice were euthanized by CO_2 asphyxiation followed by cervical dislocation, and livers were collected for mRNA analysis. All samples were collected in a light-protected environment and stored at -80˚C until use.

3.2.6 Quantification of mRNA in mouse liver

Preparation and analysis of mRNA in mouse liver samples was performed as previously described (Stevison *et al.*, 2017). Briefly, approximately 100 mg of mouse liver was homogenized with 1mL of TRI reagent (Invitrogen, Grand Island, NY). Then, total mRNA from mouse liver homogenates was extracted with TRIzol Reagent (Invitrogen, Carlsbad, CA) and quantified on a Nanodrop 2000c Spectrophotometer (Thermo Fischer Scientific, Waltham, MA). cDNA was generated using 1 µg RNA and TaqMan Reverse Transcription Reagents (catalog number

N8080243, Applied Biosystems, Carlsbad, CA). Changes in *Shp, Cyp7a1, Cyp8b1, Cyp2d9, Cyp2d10, Cyp2d11, Cyp2d22, Cyp2d40, Cyp26a1*, and *Gapdh* mRNA were measured by q-rtPCR using a StepOnePlus (Applied Biosystems) instrument with TaqMan real-time gene expression master mix and PCR primers and probes as described previously (Tay *et al.*, 2010; Stevison *et al.*, 2017). The primer probe pairs were obtained from Applied Biosystems and included mouse *Shp* (Nrob2; Mm0044278_m1), *Cyp7a1* (Mm00484150_m1), *Cyp8b1* (Mm00501637_s1), *Cyp2d9* (Mm00651731_m1), *Cyp2d10* (Mm00731648_m1), *Cyp2d11* (Mm04205381_gH), *Cyp2d22* (Mm00530542_m1), *Cyp2d40* (Mm01303815_m1), *Cyp26a1* (Mm00514486_m1), and *Gapdh* (Mm99999915_g1). *Gapdh* was used as a housekeeping gene. All samples were analyzed in duplicate. Changes in target mRNA were measured using relative quantification (fold-difference) and the ΔΔ cycle threshold method.

3.2.7 Statistical analysis

Statistical analyses were performed in Prism version 5.03 for Windows (GraphPad Software, La Jolla, CA). The geometric mean and %CV are reported for all pharmacokinetic parameters. A D'Agostino-Pearson omnibus normality test was used to determine whether pharmacokinetic parameters had Gaussian distributions, and Grubbs' test was used to identify any outliers in the data. Differences in pharmacokinetic parameters on study day 15 compared to study day 1 were assessed by comparing the geometric mean ratio (GMR) and the 90% confidence interval to bioequivalence bounds of 0.8 – 1.25 according to FDA guidance on DDI studies (Food and Drug Administration, 2017a). Differences in mRNA levels between vehicle control and retinoid treated mice were assessed on log-transformed q-rtPCR data by ANOVA for the first study dosing 13*cis*RA, *at*RA, or vehicle control or by *t*-tests for the second study dosing 4-oxo-13*cis*RA and vehicle control. For all analyses, $p<0.05$ was considered significant.

3.3 RESULTS

3.3.1 Clinical study

The mean (± SD) age of study subjects was 33 ± 10 years and the mean height and weight were 177 ± 7.53 cm and 79.1 ± 11.0 kg, respectively. Five of the study subjects were Caucasian (four non-Hispanic and one Hispanic) and three were Asian. Compliance with 13*cis*RA dosing as determined by self-reported drug logs and counts of returned 13*cis*RA capsules was on average 95%. All subjects complained of anticipated adverse events related to 13*cis*RA dosing including chapped lips and dry skin around the mouth. After 13 days of 40 mg 13*cis*RA BID, concentrations of 13*cis*RA, 4-oxo-13*cis*RA, and *at*RA were relatively stable over 24 h after the final dose (Figure 3.1). The mean (CV%) C_{ss} values for 13*cis*RA, 4-oxo-13*cis*RA, and *at*RA were 0.88 µM (46%), 4.2 µM (59%), and 0.069 µM (22%), respectively.

The concentration-time profiles for dextromethorphan and dextrorphan before and after dosing of 13*cis*RA are shown in Figure 3.2 and the calculated PK parameters are listed in Table 3.1. Despite the anticipated CYP2D6 down-regulation, no increase in dextromethorphan or decrease in dextrorphan $AUC_{0-\infty}$ was observed following 13*cis*RA treatment (Figure 3.2). In contrast, based on the bioequivalence bounds of 0.8 – 1.25, the geometric mean ratio (GMR) and the 90% confidence interval for dextromethorphan C_{max} and $AUC_{0-\infty}$ indicated a decrease in dextromethorphan exposure following 13*cis*RA dosing, corresponding to increased dextromethorphan oral clearance and CYP2D6 induction (Table 3.1). In support of increased CYP2D6 activity, the urinary dextrorphan-to-dextromethorphan GMR was 1.13 following 13*cis*RA treatment (Table 3.1). The fraction of total urinary recovery as dextromethorphan and each of its metabolites (3-methoxymorphinan, 3-hydroxymorphinan, dextrorphan, and dextrorphan-*O*-glucuronide) are presented in Table 3.2. The mean (CV%) percent of the total dose

of dextromethorphan recovered in urine prior to 13*cis*RA dosing was 44% (39%) and after dosing with 13*cis*RA was 42% (36%). Dextromethorphan was recovered in urine primarily as dextrorphan-*O*-glucuronide (93% of the recovered dose) both prior to and following treatment with 13*cis*RA (Table 3.2). To further explore the potential increase in CYP2D6 activity, the metabolite-to-parent AUC ratio for dextrorphan was calculated prior to and following 13*cis*RA treatment. The dextrorphan-to-dextromethorphan AUC ratio increased after 13*cis*RA treatment (GMR 1.25, 90% CI: 0.998 – 1.57), consistent with an increase in dextrorphan formation clearance and CYP2D6 induction (Table 3.1). Finally, the dextrorphan Cl_f GMR was 1.29, consistent with increased CYP2D6 mediated clearance.

To evaluate whether 13*cis*RA also affected CYP3A4 activity, the Cl_f of 3-methoxymorphinan and 6β-hydroxycortisol were determined (Table 3.1). Formation of 3-methoxymorphinan from dextromethorphan and 6β-hydroxycortisol from cortisol are CYP3A4 marker reactions (Peng *et al.*, 2011; Shin *et al.*, 2013). The mean (range) Cl_f of 3-methoxymorphinan increased from 22.1 L/h (2.90 – 137) prior to 13*cis*RA dosing to 30.7 L/h (3.40 - 274), with a GMR of 1.39 (90% CI 1.05 – 1.84) (Table 3.1). Similarly, the mean (range) of the Cl_f of 6β-hydroxycortisol was 35.6 mL/h (24 - 52) prior to and 52.8 mL/h (42 - 67) following 13*cis*RA dosing, resulting in a GMR (90% CI) of 1.49 (0.993 – 2.24). Large inter-subject variability was observed in Cl_f of 3-methoxymorphinan and 6β-hydroxycortisol (Fig 3).

3.3.2 Changes in mRNA in mouse liver

To evaluate whether the apparent CYP2D6 induction or the predicted CYP2D down-regulation could be observed in mice, changes in mouse *Cyp2d* ortholog mRNAs were measured following dosing of 13*cis*RA, *at*RA, or 4-oxo-13*cis*RA. Genes known to be down-regulated in response to Shp induction, *Cyp7a1* and *Cyp8b1*, and a positive control for retinoic acid signaling,

Cyp26a1, were also evaluated. Changes in mouse *Cyp3a* mRNAs were not considered due to the known differences in *Cyp3a* regulation between mice and humans. As expected, dosing with *at*RA resulted in decreases in *Cyp8b1*, *Cyp2d9*, and *Cyp2d10* mRNA, but only *Cyp8b1* mRNA was significantly decreased in response to 13*cis*RA (Fig 4). In contrast to effects of *at*RA and 13*cis*RA dosing, administration of 4-oxo-13*cis*RA to mice resulted in induction of *Shp*, *Cyp2d9*, *Cyp2d10*, *Cyp2d22*, and *Cyp2d40* (Fig 4). All retinoids tested induced expression of *Cyp26a1* with the greatest magnitude of induction resulting from administration of 4-oxo-13*cis*RA.

3.4 DISCUSSION

There are several examples in the literature of in vitro down-regulation of CYPs (Zamek-Gliszczynski *et al.*, 2014; Hariparsad *et al.*, 2017; Sager *et al.*, 2017). However, minimal evidence exists of in vivo DDIs resulting solely from CYP down-regulation, and existing data on extrapolation of in vitro down-regulation by small molecule drugs is ambiguous. For example, a small molecule inhibitor of the human kinase insert domain-containing receptor caused down-regulation of CYP1A in beagle hepatocytes, but induction of CYP1A was seen in vivo (Gibson *et al.*, 2005). Another compound, LY2090314 decreased CYP2B6 in human hepatocytes in a concentration-dependent manner, but simulations based on human hepatocyte data and human circulating concentrations suggested that in vivo LY2090314 would only decrease hydroxybupropion exposure and CYP2B6 activity by <1% (Zamek-Gliszczynski *et al.*, 2014). At present, the best established DDIs resulting from CYP down-regulation are related to the suppressive effects of pro-inflammatory cytokines on CYPs (Dickmann *et al.*, 2011; Schmitt *et al.*, 2011; MacHavaram *et al.*, 2013; Xu *et al.*, 2015; Jiang *et al.*, 2016). Pro-inflammatory cytokines such as interleukin -6 (IL-6) and IL-1β are elevated in diseases like rheumatoid arthritis. Increased levels of inflammatory cytokines are associated with decreased CYP expression and

activity likely due to transcriptional down-regulation and increased proteosomal degradation of CYPs (Lee *et al.*, 2009; Dickmann *et al.*, 2011; J. Dickmann *et al.*, 2012). When therapeutic proteins are administered to ameliorate inflammation, cytokine-mediated CYP suppression can be reversed. For example, treatment with the anti-IL-6 monoclonal antibodies, tocilizumab and sirukumab, increased the clearance of CYP2C9, CYP2C19, and CYP3A4 substrates in rheumatoid arthritis patients (Schmitt *et al.*, 2011; Zhuang *et al.*, 2015). However, therapeutic protein-drug interactions are challenging to predict from in vitro data due to the complex nature of the interactions.

In terms of selecting a compound to demonstrate in vitro and in vivo CYP down-regulation, LY2090314 is not a good model due to the predicted minimal change in CYP2B6 activity. Bupropion has been shown to down-regulate CYP2D6 in vitro, but the simultaneous reversible CYP2D6 inhibition by bupropion and its metabolites (Sager *et al.*, 2017) may confound in vitro-to-in vivo extrapolation. Therefore, a bupropion-CYP2D6 DDI does not allow unequivocal translation of in vitro CYP down-regulation to in vivo DDIs. Overall, due to the lack of good model compounds, the translation of in vitro CYP downregulation to in vivo DDIs has not been established. This study sought to determine whether down-regulation of CYP2D6 observed in preclinical studies can be translated to clinical DDIs using retinoic acid as a model compound. Retinoic acid was chosen as it does not inhibit any CYP enzymes but decreases CYP2D6 expression in several model systems.

The downregulation of CYP2D6 by *at*RA is believed to be a result of induction of the transcriptional corepressor SHP. *at*RA induces SHP in various mouse models and in vitro systems (Mamoon *et al.*, 2008, 2014; Cai *et al.*, 2010; Yang *et al.*, 2014). In the in vitro studies, dose-response relationships were not characterized and the nominal *at*RA concentrations tested (1 – 10

μM) were higher than circulating concentrations of *at*RA after dosing to humans, preventing systematic in vitro-to-in vivo predictions. Nevertheless, *at*RA has been shown to induce *Shp* mRNA and decrease the mRNA of *Cyp8b1*, a SHP target gene, in mice (Mamoon *et al.*, 2014; Yang *et al.*, 2014). While this study reproduced the *Cyp8b1* downregulation by *at*RA and 13*cis*RA, neither retinoid induced *Shp* mRNA. The lack of *Shp* induction in this study is similar to the observed lack of *Shp* induction in mice with increased endogenous *at*RA concentrations after treatment with talarozole, an inhibitor of *at*RA metabolism (Stevison *et al.*, 2017). The lack of *Shp* induction may be attributed to differences in dosing regimens between the current study (5 mg/kg IP daily for four days) and the previous studies (150 mg/kg *at*RA in chow for 7 days), likely resulting in different *at*RA exposure and potentially different receptor activation. The *at*RA dosing in the current study is consistent with typical pharmacologically-active doses of *at*RA in mice that result in activation of retinoic acid receptors (RARs) (Snyder *et al.*, 2011; Davis *et al.*, 2013; Busada *et al.*, 2014). The RAR activation in the mice was confirmed by robust *Cyp26a1* induction. *Shp* induction may require activation of other nuclear receptors such as farsenoid X receptor (FXR) or RXR. In vivo evidence of *at*RA-mediated regulation of SHP and CYP2D6 comes from induction of *Shp* and down-regulation of CYP2D6 observed following *at*RA treatment in a CYP2D6 humanized mouse model (Koh *et al.*, 2014). Further, decreased *at*RA concentrations during mouse pregnancy were linked to decreased *Shp* expression and consequently increased CYP2D6 expression (Koh *et al.*, 2014). Similarly, several studies have shown that FXR/RXR agonists induce SHP and down-regulate CYP2D6 in CYP2D6-humanized mice (Pan and Jeong, 2015; Pan *et al.*, 2015). In contrast, FXR activation by cholic acid was shown to induce both SHP and CYP2D6 in the same mouse model (Pan *et al.*, 2017a). Nevertheless, collectively the existing data suggest that CYP2D6 is regulated in vivo by *at*RA and via SHP.

We explored the regulation of CYP2D6 in humans in this study using 13*cis*RA as the precipitant. Administration of 13*cis*RA, which isomerizes to *at*RA (Tsukada *et al.*, 2000; Veal *et al.*, 2002; Armstrong *et al.*, 2005), avoids issues specific to *at*RA pharmacokinetics, such as large fluctuations in *at*RA concentrations due to a short 1 hour half-life and *at*RA induction of its own clearance by greater than 2-fold (Muindi *et al.*, 1992, 2008a; Adamson *et al.*, 1995). *at*RA as a metabolite of 13*cis*RA exhibits formation rate-limited kinetics. As 13*cis*RA has an ~20 hour half-life, *at*RA concentrations after 13*cis*RA dosing have little fluctuation and average steady-state concentrations are similar to those observed after *at*RA dosing (Muindi *et al.*, 2008a). As expected from the previous studies, steady-state *at*RA concentrations of ~70 nM were observed following 13*cis*RA dosing. Based on the side effects observed in all study subjects, adequate and pharmacologically active exposure to retinoids was achieved during 13*cis*RA dosing. However, in contrast to the expected decrease in CYP2D6 activity, all the measures of CYP2D6 activity (i.e., dextromethorphan AUC, urinary dextrorphan-to-dextromethorphan ratio, formation clearance of dextrorphan, and dextrorphan-to-dextromethorphan AUC ratio) indicated that CYP2D6 was induced following 13*cis*RA treatment. The change in urinary dextrorphan-to-dextromethorphan ratio was the smallest of all PK parameters assessed (GMR 1.13, Table 3.1). This ratio depends on renal clearance of both dextrorphan and dextromethorphan, which can be affected by urine pH, and has been shown to be an unreliable method of detecting small changes in CYP2D6 activity (Özdemir *et al.*, 2004; Borges *et al.*, 2005). However, the change in dextrorphan formation clearance is independent of changes in renal clearance, and in the absence of changes in the clearance of dextrorphan, any change in formation clearance is indicative of altered metabolite formation. While these findings are inconsistent with the expected decrease in CYP2D6 activity, they are in agreement with the observations in pregnant mice; namely, increased *Cyp2d11*,

Cyp2d22, Cyp2d26, and *Cyp2d40* mRNA and activity, the positive correlation between the *Cyp2d* isoforms and *Rar* mRNA, as well as increased retinoic acid signaling in the maternal liver during pregnancy (Topletz *et al.*, 2013).

It is possible that the results of this study that were inconsistent with previous findings of CYP2D6 down-regulation by *at*RA were influenced by 13*cis*RA and 4-oxo-13*cis*RA exposure. While both *at*RA and 13*cis*RA can bind to RARs and activate transcription (Aström *et al.*, 1990; Idres *et al.*, 2002; Wang *et al.*, 2008; Chen *et al.*, 2010), the transcriptional regulation of RAR target genes by 4-oxo-13*cis*RA has not been previously evaluated. To further investigate the potential impact of 13*cis*RA and 4-oxo-13*cis*RA, mice were treated with either 13*cis*RA, 4-oxo-13*cis*RA, or *at*RA and the changes in hepatic mRNA of *Cyp2d* orthologs, *Shp,* and SHP target genes *Cyp7a1* and *Cyp8b1* were assessed. Surprisingly, while both 13*cis*RA and *at*RA decreased *Cyp8b1*, 13*cis*RA had no effect on *Cyp2d* in the mice and *at*RA decreased expression of *Cyp2d9* and *Cyp2d10*. In contrast, 4-oxo-13*cis*RA significantly induced *Shp, Cyp2d9, Cyp2d10, Cyp2d22* and *Cyp2d40*. Taken together, these data suggest a lack of linkage between SHP and CYP2D regulation and indicate that in the clinical study, 4oxo-13*cis*RA may be responsible for the apparent CYP2D6 induction. It is noteworthy that in mice, unlike in humans, 4-oxo-13*cis*RA is not the primary circulating metabolite of 13*cis*RA and therefore the effects of dosing 13*cis*RA to mice are likely to be independent of the effects of the metabolite (Nau, 2001). 4-oxo-13*cis*RA was also found to be the strongest inducer of *Cyp26a1*, a classic RAR target gene, in mice with increases of approximately 30-fold by 4-oxo-13*cis*RA, but less than 10-fold by *at*RA and 13*cis*RA. This higher in vivo potency would be expected to translate to humans as 4-oxo-13*cis*RA circulates at 10-100-fold higher concentrations than 13*cis*RA or *at*RA following dosing of 13*cis*RA. Based

on these data, the effect of the 13*cis*RA metabolites must be accounted for in in vitro-to-in vivo predictions of changes in CYP2D6 expression.

In addition to CYP2D6 induction, our results suggest that CYP3A4 induction occurs in vivo upon 13*cis*RA dosing. The Cl_f of the CYP3A4-specific metabolite of dextromethorphan, 3-methoxymorphinan, as well as the endogenous CYP3A4-probe 6β-hydroxycortisol increased approximately 1.3-fold, indicating that CYP3A4 was induced by treatment with 13*cis*RA. Both *at*RA and 13*cis*RA have been shown to induce *CYP3A4* in vitro (Wang *et al.*, 2008; Chen *et al.*, 2010). Prospective studies with CYP3A4 probe substrates are needed to confirm this induction and to define the magnitude of CYP3A4 induction by 13*cis*RA and/or *at*RA in vivo.

The variability in CYP2D6 activity in vivo is believed to be mainly due to genetic polymorphisms and variability in CYP2D6 genotypes (Gaedigk *et al.*, 2017). In general, CYP2D6 is not considered to be inducible by xenobiotics although constitutive expression of CYP2D6 is believed to be transcriptionally regulated by factors such as SHP and HNF4α (Lee *et al.*, 2008; Pan *et al.*, 2017b). Further studies are required to determine whether treatment with retinoids induces CYP2D6 as suggested by this study, as the current study was not adequately powered to determine low level induction of CYP2D6.

In conclusion, the findings presented here suggest that 13*cis*RA, likely via the activity of its major circulating metabolite 4-oxo-13*cis*RA, induces both CYP2D6 and CYP3A4 in vivo. These data demonstrate the difficulty in translating observations of enzyme down-regulation to clinical DDIs and show that further work is necessary to elucidate the mechanisms of down-regulation observed in pre-clinical studies.

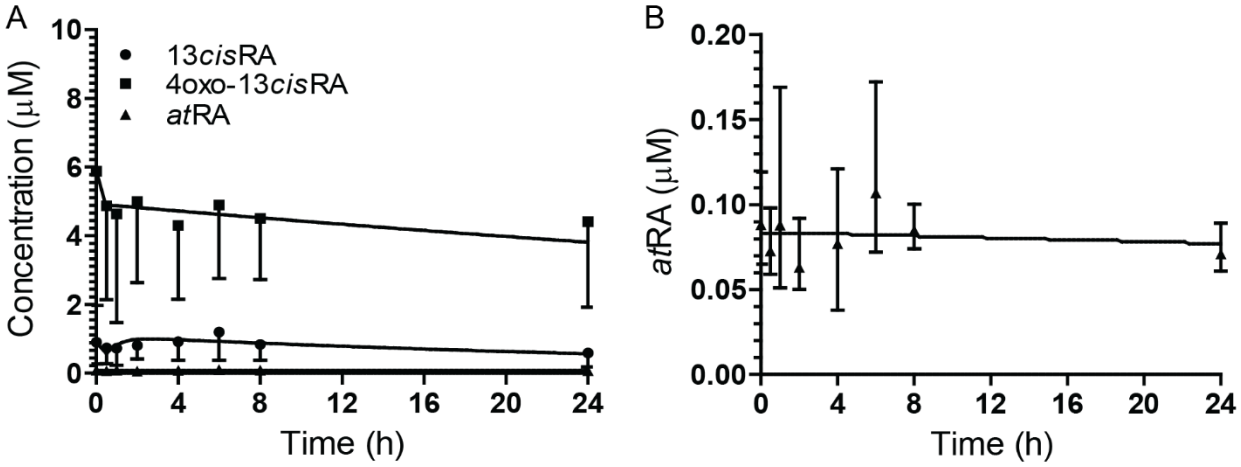

Figure 3.1. Concentrations of 13*cis*RA, 4-oxo-13*cis*RA, and *at*RA after 13 days of 40 mg bid 13*cis*RA dosing. Concentrations versus time profiles for 13*cis*RA, 4-oxo-13*cis*RA, and *at*RA (A) and concentrations of *at*RA alone (B) in serum following the final 40 mg dose of 13*cis*RA on study day 15. Data are presented as mean and range (N = 8). The line represents the best fit of the data.

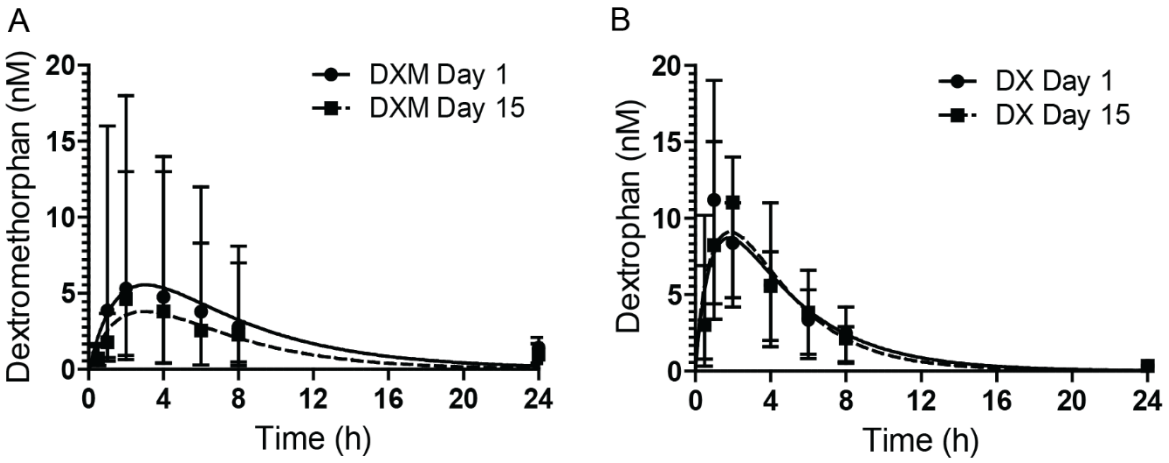

Figure 3.2. Concentrations of dextromethorphan (DXM) and dextrorphan (DX) before and after dosing with 13*cis*RA. Serum concentrations of DXM (A) or DX (B) on study day 1 prior to 13*cis*RA dosing and on study day 15 after 13*cis*RA dosing. Data are presented as mean and range of individual values (N = 8). The line represents the best fit of the data. Day 1: circle with solid line; Day 15: square with dashed line.

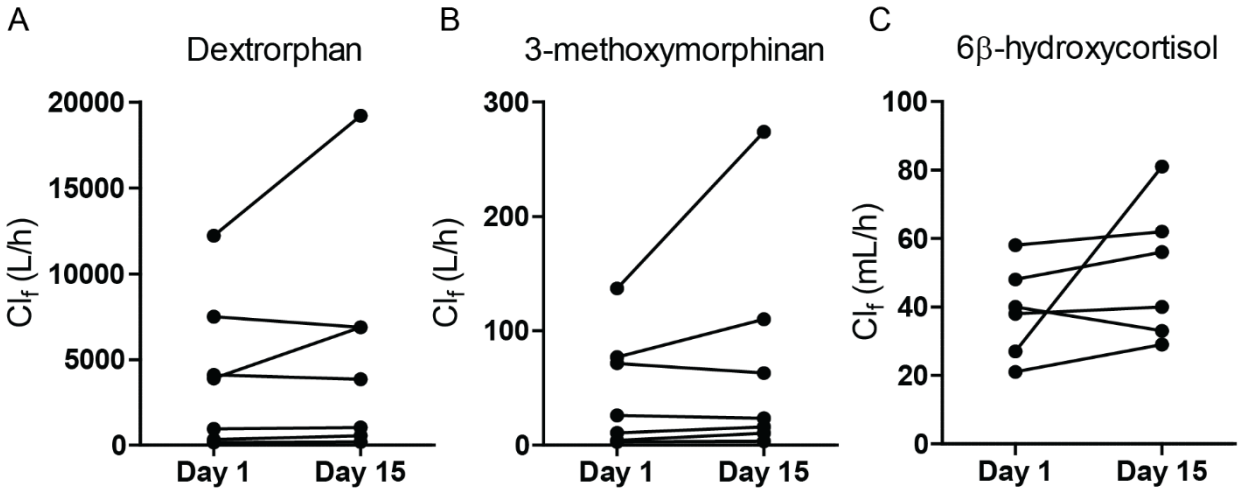

Figure 3.3. Formation clearance (Cl_f) values for dextrorphan, 3-methoxymorphinan, and 6β-hydroxycortisol in individual subjects before and after dosing with 13*cis*RA. The formation clearance (Cl_f) of the CYP2D6-specific metabolite of dextromethorphan, dextrorphan (A, N = 7), the CYP3A4-specific metabolite of dextromethorphan, 3-methoxymorphinan (B, N = 7), and an endogenous marker of CYP3A4 activity, 6β-hydroxycortisol (C, N = 6), were measured for each subject on study day 1 before 13*cis*RA dosing and on study day 15 after 13*cis*RA dosing. One subject was identified as an outlier and removed from all analyses involving urine and an additional subject had no measureable 6β-hydroxycortisol in urine collected from study day 15.

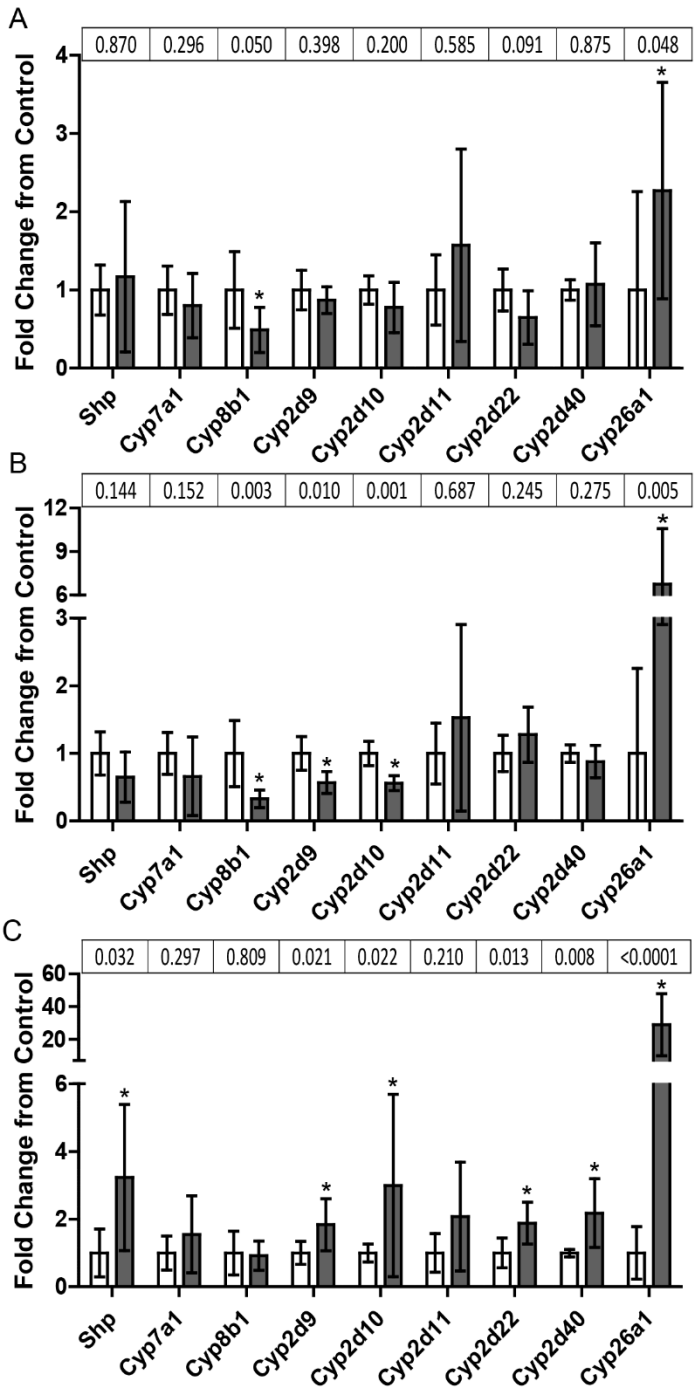

Figure 3.4. Effects of retinoids on mRNA expression in livers of mice. Fold-change compared to control of liver mRNA in mice (n=6) treated for four days with 5 mg/kg IP of 13*cis*RA (A), *at*RA (B), or 4-oxo-13*cis*RA (C). Inset tables provide p-values calculated from t-tests for each gene compared to control. *p<0.05

Table 3.1. Pharmacokinetic parameters for dextromethorphan and dextrorphan and formation clearance of the two CYP3A4 markers 3-methoxymorphinan and 6β-hydroxycortisol before (control) and after 13*cis*RA dosing (treatment).

	Control Mean (CV%)	Treatment Mean (CV%)	Treatment/Control GMR (90% CI)
Dextromethorphan			
C_{max} (nM)	3.59 (109)	3.00 (104)	0.829 (0.698 – 0.985)
$AUC_{0-\infty}$ (h*nM)	28.4 (127)	23.3 (119)	0.822 (0.677 – 0.998)
Cl/F (L/h)	3870 (94)	4750 (102)	1.23 (1.02 – 1.48)
$t_{1/2}$ (h)	5.07 (30)	5.03 (34)	0.991 (0.831 – 1.18)
Dextrorphan			
C_{max} (nM)	11.1 (44)	10.8 (29)	0.971 (0.747 – 1.26)
$AUC_{0-\infty}$ (h*nM)	51.3 (43)	52.9 (29)	1.03 (0.851 – 1.25)
Cl_f (L/h)[a]	1840 (106)	2360 (121)	1.29 (1.05 – 1.58)
AUC_m/AUC_p	1.81 (78)	2.28 (69)	1.25 (0.998 – 1.57)
U_m/U_p[a]	153 (70)	173 (72)	1.13 (0.817 – 1.56)
3-methoxymorphinan			
Cl_f (L/h)[a]	22.1 (107)	30.7 (135)	1.39 (1.05 – 1.84)
6β-hydroxycortisol			
Cl_f (mL/h)[a]	35.6 (48)	52.8 (29)	1.49 (0.993 – 2.24)

a) N=7. The urinary recovery of two analytes from one subject in the 0-8 h collection on study day 1 were determined to be outliers thus, all data from this subject was excluded from any analysis involving measurements from urine.

All parameters are shown as geometric means with a % CV

GMR, geometric mean ratio

Table 3.2. The fraction of dextromethorphan or each of its metabolites recovered in urine compared to total urinary recovery for dextromethorphan before (control) and after 13*cis*RA dosing (treatment).

Analyte	Control Mean (CV%)	Treatment Mean (CV%)
Dextromethorphan	0.02 (150)	0.02 (150)
Dextrorphan	0.04 (60)	0.04 (62)
Dextrorphan-*O*-glucuronide	0.93 (5.5)	0.93 (5.0)
3-methoxymorphinan	0.0004 (100)	0.0003 (89)
3-hydroxymorphinan	0.01 (36)	0.01 (31)

a) N=7. The urinary recovery of two analytes from one subject in the 0-8 h collection on study day 1 were determined to be outliers thus, all data from this subject was excluded from any analysis involving measurements from urine.

Fraction of urinary recovery determined as the molar amount of a given analyte divided by the sum of all analytes measured in urine. Data are shown as means with a % CV.

Chapter 4. IN VITRO TO IN VIVO PREDICTION OF TRANSCRIPTIONAL REGULATION OF CYTOCHROME P450S BY 13-*CIS* RETINOIC ACID AND ITS METABOLITES *ALL-TRANS* RETINOIC ACID AND 4-OXO-13-*CIS* RETINOIC ACID

4.1 INTRODUCTION

All-trans-retinoic acid (*at*RA), the active metabolite of vitamin A, has been shown to regulate expression of several cytochrome P450s (CYPs), including CYP2D6, in vitro and in mice (Mamoon *et al.*, 2008; Cai *et al.*, 2010; Koh *et al.*, 2014; Yang *et al.*, 2014). The proposed mechanism for regulation of CYP2D6 by *at*RA is via *at*RA-mediated regulation of the small heterodimer partner (SHP), which is a co-repressor that prevents hepatocyte nuclear factor 4α (HNF4α)-mediated transcription of CYP2D6 (Koh *et al.*, 2014). Both *at*RA and its stereoisomer, 13*cis*RA, are used clinically to treat a variety of conditions including acute promyelocytic leukemia, neuroblastoma, acne, and psoriasis. Interconversion occurs between *at*RA and 13*cis*RA and favors 13*cis*RA isomerization to *at*RA (Sass *et al.*, 1994; Chen and Juchau, 1997; Tsukada *et al.*, 2000). Because the half-life of 13*cis*RA (~20 hours) is longer than the half-life of *at*RA (~1 hour), following 13*cis*RA dosing, *at*RA exhibits formation rate-limited kinetics, and average exposure to *at*RA is similar following administration of either 13*cis*RA or *at*RA (Khoo *et al.*, 1992; Ozpolat *et al.*, 2003b; Muindi *et al.*, 2008a; Jing *et al.*, 2017). Thus, *at*RA is an important active metabolite of 13*cis*RA. Additionally, the major metabolite of 13*cis*RA, 4-oxo-13*cis*RA, has also been shown to be active in vitro (Baron *et al.*, 2005; Sonawane *et al.*, 2014).

A clinical study was conducted to test the hypothesis that 13*cis*RA and its metabolites, *at*RA and 4-oxo-13*cis*RA, would precipitate a drug-drug interaction (DDI) involving CYP2D6 down-regulation (Chapter 3). Surprisingly, no down-regulation of CYP2D6 was observed in the clinical study. These results were unexpected given the substantial evidence for *at*RA-mediated regulation of SHP (Mamoon *et al.*, 2008; Cai *et al.*, 2010; Yang *et al.*, 2014), in addition to findings by several groups for the involvement of HNF4α in transcriptional regulation of CYP2D6 (Lee *et*

al., 2008; Koh *et al.*, 2014). There is a lack of characterization of the concentration-dependent effects of *at*RA, 13*cis*RA, or 4-oxo-13*cis*RA on CYP2D6 expression in vitro. Therefore, it is not possible to fully assess whether the clinical study results represent a disconnect between CYP2D6 down-regulation in vitro and in vivo.

Methods to characterize CYP induction have been well established (Fahmi *et al.*, 2008, 2009, 2010; Fahmi and Ripp, 2010; Einolf *et al.*, 2014), and regulatory agencies provide guidance on how to conduct and interpret induction studies to predict the risk of clinical DDIs (EMA, 2012; Food and Drug Administration, 2017b). However, these methods may not be adequate to appropriately design experiments to study down-regulation. One challenge in predicting in vivo down-regulation from in vitro assessment is the limited dynamic range to study CYP down-regulation. Strong inducers can cause over 10-fold (>1000%) increases in CYP expression, but the magnitude of effect for down-regulation is limited to a maximum of 100% decrease, though assessment may be confounded by detection limits of mRNA or protein expression or activity. Similar to the response to CYP inducers, the magnitude of effect of down-regulation is also dependent on basal expression of the enzyme (Dickmann *et al.*, 2008). Studies have been conducted with CYP inducers in hepatocyte incubation media to increase baseline CYP expression (Dickmann *et al.*, 2011). However, kinetic results from cells treated simultaneously with inducers and down-regulators of CYPs can be altered. For example, IL-6 was shown to suppress expression of CYP1A2 and CYP3A4 with an EC_{50} of 730 and 83 pg/mL, respectively, in a selected hepatocyte donor. When hepatocytes from this same donor were first treated with inducers of CYP1A2 (omeprazole) or CYP3A4 (rifampin), the EC_{50} for IL-6 down-regulation were increased by 1.5- and 19-fold, respectively (Dickmann *et al.*, 2011). Thus, although low basal CYP expression limits

the range for detecting CYP down-regulation, including inducers in hepatocyte incubations likely confounds interpretation of study results.

To date, little attention has been paid to DDIs perpetrated by metabolites as inducing agents, although several recent publications have identified metabolites as inducers of CYPs (Sugiyama *et al.*, 2016; Ho *et al.*, 2018; Johänning *et al.*, 2018). Tamoxifen and several of its metabolites were found to induce the expression of CYP3A4 in hepatocytes with an EC_{50} between 200 – 300 nM (Johänning *et al.*, 2018). Additionally, ketamine and two of its pharmacologically active metabolites as estrogen receptor α (ERα) ligands, induced CYP2A6 and CYP2B6 in primary human astrocytes and HepaRG cells (Ho *et al.*, 2018). CYP2A6 and CYP2B6 can be transcriptionally regulated by ERα and are important in the formation of the active ketamine metabolites. These examples illustrate the importance of considering the role of metabolites in CYP induction and the potential effects of decreased parent drug exposure or increased exposure of pharmacologically active metabolites. However, methods to predict the magnitude of DDIs resulting from induction by a parent drug and its metabolites are lacking.

The aim of this study was to characterize the effects of 13*cis*RA, *at*RA, and 4-oxo-13*cis*RA on the expression of CYP2D6 and CYP3A4 in human hepatocytes and to determine whether a more comprehensive evaluation of the in vitro effects of 13*cis*RA, *at*RA and 4-oxo-13*cis*RA would explain the in vivo observations of CYP2D6 and CYP3A4 induction.

4.2 MATERIALS AND METHODS

4.2.1 Chemicals and reagents

Dimethyl sulfoxide (DMSO), rifampin, 13*cis*RA, and *at*RA were purchased from Sigma-Aldrich (St. Louis, MO). Dextorphan-d_3, 13*cis*RA-d_5 and *at*RA-d_5 were obtained from Toronto Research Chemicals (North York, Ontario, Canada). 4-oxo-13*cis*RA and 4-oxo-*at*RA-d_3 were

obtained from Santa Cruz Biotechnology (Dallas, TX). Testosterone and 6β-hydroxytestosterone-d_3 were purchased from Cerilliant (Round Rock, Texas). GW4064 was obtained from Genentech, Inc. Compound Management Group (South San Francisco, CA). Optima LC/MS grade water, acetonitrile, methanol, and formic acid, QuantiGene Plex 2.0 Assay Kits (Panel #13130), Geltrex®, and RNA*later* were purchased from Thermo Fisher Scientific (Waltham, MA). Universal Cryopreservation Recovery Media (UCRM™) was purchased from In Vitro ADMET Laboratories, Inc. (Columbia MD). InvitroGRO™ CP and HI culture media (without hydrocortisone) and Torpedo™ antibiotic mix were purchased from BioreaclamationIVT (Baltimore, MD). BD BioCoat™ 96-well Collagen I coated plates were purchased from Corning (Oneonta, NY).

4.2.2 Cell culture and in vitro assessment of CYP mRNA and activity

Cell culture. Cryopreserved human hepatocytes from Hu1558 (84-year-old Caucasian male) and Hu1765 (37-year-old Caucasian female) were purchased from Thermo Fisher Scientific (Waltham, MA), and hepatocytes from FOS (34-year-old Arabic male) were purchased from BioreaclamationIVT (Baltimore, MD). All donors were CYP2D6 extensive metabolizers. For all experiments, cryopreserved human hepatocytes were thawed at 37°C, resuspended in pre-warmed UCRM™ Medium, and centrifuged at 100 x *g* at room temperature for 10 minutes. The supernatants were discarded, and cells were resuspended in InVitroGRO CP medium with Torpedo™ for a final concentration of 1.0 x 10^6 cells/mL. Then 65 µL of the cell suspension was added to each well of 96-well, collagen-coated plates. Plates were incubated at 37°C in 5% CO_2 for 4-6 hours to allow cells to adhere to the plate. After the 4-6 hour incubation, the plating media was aspirated and replaced with 0.35 mg/mL Geltrex® in cold HI medium without hydrocortisone containing Torpedo™ as an overlay. The cells were incubated at 37°C in 5% CO_2 for 24 hours. On

day two, the cells were dosed with 100 µL/well of incubation media (HI media without hydrocortisone containing Torpedo^{TM}) with test material (13*cis*RA, *at*RA, 4-oxo-13*cis*RA, rifampin, or GW4064 depending on the experimental design) or vehicle control (0.1% DMSO). Experiments were conducted for 48 hours, and media and test materials were refreshed after 24 hours. All experiments were conducted in triplicate unless otherwise noted. In all experiments, cell viability was assessed using the lactate dehydrogenase assay as described previously (Halladay *et al.*, 2012), and cell morphology was monitored with the IncuCyte® Zoom System from Essen BioScience Inc. (Ann Arbor, MI).

Two time-course experiments were conducted to determine the optimal time to characterize changes in expression of *SHP*, *CYP2D6*, and *CYP3A4* and for assessment of retinoid depletion and interindividual variability in donor response to retinoids. In the first experiment, cells from the FOS donor were plated and cultured then treated with 0.1, 0.3, 1, 3, 10, 30, and 100 µM *at*RA or vehicle control in duplicate for 1, 2, 24, and 48 hours. Levels of *SHP*, *CYP2D6*, and *CYP3A4* mRNA and activity were assessed at each time point as described below. In the second time-course experiment, cells from the three hepatocyte donors were plated and cultured then treated with 1 µM of 13*cis*RA, *at*RA, or 4-oxo-13*cis*RA or vehicle control for 48 hours with media replenished at 24 h. Aliquots of media were taken at 2, 17, and 24 h after dosing on both treatment days for determination of 13*cis*RA, *at*RA, 4-oxo-13*cis*RA, and 4-oxo-*at*RA concentrations. Retinoid concentrations in media prior to addition to cells were also measured. Media samples were prepared for analysis of retinoid concentrations by precipitating 30 µL of sample plus 30 µL water with 60 µL acetonitrile plus internal standards (200 nM each of 13*cis*RA-d_5, *at*RA-d_5, or 4-oxo-*at*RA-d_3). Samples were centrifuged at 18,000 x *g* at 4°C for 30 min and supernantant was taken for analysis by liquid chromatography-tandem mass spectrometry (LC-MS/MS) as described

below for quantification of retinoids. At the end of the experiment, all media was removed and replaced with RNA*later* and cells were stored at -80˚C for analysis of *CYP26A1* and *RARβ* mRNA as described below.

To determine the concentration-dependent effects of retinoids on SHP, CYP2D6, and CYP3A4, cells from the three hepatocyte donors were plated and cultured then treated with rifampin (0.1, 1, 10, 25 µM), GW4064 (0.1, 0.5, 1 µM), 13*cis*RA, *at*RA, 4-oxo-13*cis*RA (0.005, 0.01, 0.04, 0.12, 0.37, 1.11, 3.33, 10, 30 µM), or vehicle control (0.1 % DMSO). Plates were incubated for 2 or 48 hours at 37°C in 5% CO_2 prior to assessment of *SHP* mRNA (2 hours) and CYP mRNA and activity (48 hours). To determine retinoid concentrations in media at 2 and 48 hours, 25 µL of media were transferred to a 96-well plate, quenched with 50 µL of acetonitrile, and stored at -80˚C until analysis by LC-MS/MS as described below for quantification of retinoids.

Determination of retinoid concentrations in incubations. From the time-course experiment, a noncompartmental analysis of concentration-time data was performed in Phoenix WinNonlin v6.3 (Pharsight, St. Louis, MO) to determine the area under the hepatocyte media concentration-time curve from zero to 24 h ($AUC_{0\text{-}24h}$). The AUC was calculated using the linear up, log down trapezoidal rule and the concentration at time zero was set as the concentration measured in the media prior to addition to cells. The average media concentration (C_{avg}) in each 24-hour treatment for the treated retinoid was determined by dividing the $AUC_{0\text{-}24h}$ by 24 hours. Data are presented as the geometric mean of the C_{avg} determined on the two treatment days. Data from the time-course experiment was used to confirm that the average concentration of retinoid measured between 2 and 48 hours in the concentration-effect experiments could be used as a surrogate for the actual concentration of retinoid at each nominal treatment level in order to quantify the concentration-dependent effects of retinoids on SHP, CYP2D6, and CYP3A4.

Quantitation of mRNA. Expression of *CYP26A1* and *RARβ* mRNA was quantified as previously described (Stevison *et al.*, 2017). Quantitative reverse-transcriptase polymerase chain reaction was used to measure mRNA with TaqMan gene expression assays Hs00175627_m1 for *CYP26A1*, Hs00977140_m1 for *RARβ*, and Hs99999905_m1 for *GAPDH*. *GAPDH* was used as the housekeeping gene to normalize expression of *CYP26A1* and *RARβ* in each sample. All samples were analyzed in triplicate, and data presented here are the mean of the triplicate analyses. For purposes of estimating a maximum possible induction of *CYP26A1*, any undetermined cycle threshold (C_T) values were assigned a C_T value of 39. The fold-change in *CYP26A1* and *RARβ* mRNA in retinoid-treated versus control-treated cells was determined with the $\Delta\Delta C_T$ method. A QuantiGene Plex 2.0 Assay Kit (Panel #13130) from Affymetrix (Santa Clara, CA) was used to quantitate mRNA levels of *SHP*, *CYP2D6*, and *CYP3A4* using a previously detailed method (Halladay *et al.*, 2012). The PXR reporter gene assay was performed and analyzed at Puracyp, Inc. (Carlsbad, CA)

Activity determination. To determine CYP activity, each well was washed three times with 100 µL of incubation medium (without hydrocortisone) followed by the addition of 100 µL incubation media containing cocktailed CYP substrates: dextromethorphan (5 µM; CYP2D6 probe substrate) and testosterone (200 µM; CYP3A4/5 probe substrate). The plates were incubated at 37°C in 5% CO_2 for 30 minutes. After a 30 minute incubation, 80 µL of each sample was removed and transferred to wells that contained 160 µL of acetonitrile with internal standards (dextrorphan-d_3 and 6β-hydroxytestosterone-d_3). The plates were centrifuged for 10 minutes at 2,000 x *g*, supernatant (60 µL) was removed and added to wells containing 180 µL water. The samples were analyzed by LC-MS/MS as previously described (Halladay *et al.*, 2012) to quantify the CYP-

specific metabolites (dextrorphan and 6β-hydroxytestosterone) to determine the activities of CYP2D6 and CYP3A4/5, respectively.

4.2.3 Protein binding

The unbound fraction of 13*cis*RA, *at*RA, and 4-oxo-13*cis*RA in human plasma and in the hepatocyte media was determined by rapid equilibrium dialysis (RED) and cross-validated using ultracentrifugation. Due to the high protein binding of the retinoids, human plasma and the hepatocyte incubation media were diluted (1:10 or 1:20 for plasma and 1:20 for media) in 100 mM potassium phosphate buffer, pH 7.4, then spiked with 1 μM (final concentration) 13*cis*RA, *at*RA, or 4-oxo-13*cis*RA. All experiments were conducted in triplicate. For each retinoid, 200 μL of spiked diluted plasma or diluted hepatocyte incubation media was aliquoted into the matrix chamber of a Thermo Scientific RED Device (Waltham, MA) insert and 400 μL of potassium phosphate buffer was added to the respective buffer chamber. The RED device was incubated at 37°C for 24 hours. An initial time-course experiment determined that the time needed to reach equilibrium was ~24 hours (data not shown). After 24 hours, 75 μL of diluted matrix or buffer sample was precipitated with 75 μL of acetonitrile plus internal standards (200 nM each of 13*cis*RA-d_5, *at*RA-d_5, or 4-oxo-*at*RA-d_3) and centrifuged at 18,000 x *g* at 4°C for 30 min. The supernatant was transferred for quantification of 13*cis*RA, *at*RA, or 4-oxo-13*cis*RA by LC-MS/MS as described below. The fraction unbound in the diluted matrix ($f_{u,dil}$) was calculated as the ratio between the concentration measured in the buffer chamber divided by the concentration measured in the matrix chamber. The fraction unbound (f_u) for each retinoid in undiluted plasma or hepatocyte incubation media was calculated from the data obtained with diluted matrices based on the known dilution factor of the plasma protein concentration and the known relationship between plasma protein concentration ([P]), the binding constant (K_a) and f_u (equation 4.1):

$$f_u = \frac{1}{1 + K_a[P]} \tag{4.1}$$

Equation 4.1 can be rearranged to yield equation 4.2,

$$f_u = \frac{1/D}{\left(\left(\frac{1}{f_{u,dil}}\right) - 1\right) + \frac{1}{D}} \tag{4.2}$$

in which $f_{u,dil}$ is the unbound faction in diluted matrix, f_u is the unbound fraction in undiluted matrix and D is the dilution factor. The f_u was determined from each $f_{u,dil}$ and D (1:10 or 1:20 for plasma and 1:20 for media). Two experiments were performed with 1:10 dilution in plasma and one experiment each was performed with 1:20 dilution in plasma or hepatocyte media, and the final f_u reported for plasma or hepatocyte media is the mean from the separate experiments.

To validate determination of f_u with diluted matrix by RED, binding of retinoids in hepatocyte incubation media was also determined by ultracentrifugation as previously described (Shirasaka *et al.*, 2013). 13*cis*RA, *at*RA, or 4-oxo-13*cis*RA were added to hepatocyte incubation media (1 μM final concentration), aliquoted into ultracentrifuge tubes, and either centrifuged in a Sorvall Discovery M150 SE ultracentrifuge (Thermo Fisher Scientific, Waltham, MA) at 435,000 x *g* for 90 minutes at 37°C (n=6 per retinoid) or incubated for 90 minutes at 37°C (n=6 per retinoid). Samples were prepared for LC-MS/MS analysis as described below and the f_u was determined as the ratio of retinoid concentration measured in centrifuged samples divided by the concentration measured in incubated samples. Values of f_u are presented as the mean from the single ultracentrifugation experiment.

4.2.4 Quantification of retinoids

Concentrations of retinoids in hepatocyte media and protein binding experiments were measured on an AB Sciex (Framingham, MA) qTrap 5500 mass spectrometer coupled to an Agilent Technologies (Santa Clara, CA) 1290 Infinity ultrahigh-pressure liquid chromatography system using a previously validated method (Arnold *et al.*, 2012) with some modifications. In brief, analytes were separated using a Kinetex® 100 x 2.1 mM, 1.7 µM C18 column (Phenomenex, Torrance, CA) and a mobile phase of A) 60:40 water:methanol and 0.1% formic acid and B) 60:40 acetonitrile:methanol and 0.1% formic acid. The gradient was from initial conditions of 50% B for 0.5 min to 95% B for 4 min, then held at 95% B for 2 min before re-equilibration for 1.5 min. The flow rate was 400 µL/min. Analyte detection was performed as previously described with the addition of *m/z* transition of 318→137 for 4-oxo-*at*RA-d_3 (Arnold *et al.*, 2012). The declustering potential, collision energy, and collision exit potential were 62, 18, and 14 for 13*cis*RA and *at*RA, 66, 23, and 16 for 4-oxo-13*cis*RA, 97, 97, and 6 for 13*cis*RA-d_5 and *at*RA-d_5, and 71, 35, and 10 for 4-oxo-13*cis*RA-d_3, respectively. Data were quantified using MultiQuant (AB Sciex, Foster City, CA). The lower limit of quantitation was 5.6 nM in hepatocyte incubation media and 2.8 nM in plasma for all analytes, and a minimum of six quality control samples were included in each analytical run with %CV < 10 for all analytes.

4.2.5 Prediction of drug-drug interactions

Prior to fitting, the nominal retinoid concentration was adjusted for the average depletion during the 48-hour incubation, which was determined from average concentration of each retinoid measured in media at 2 and 48 hours. To quantify the concentration-effect relationship of 13*cis*RA, *at*RA, or 4-oxo-13*cis*RA on CYP2D6 in human hepatocytes, estimates of the maximum fold-change relative to control (E_{max}) and the retinoid concentration at 50% of the maximum fold-

change (EC_{50}) were determined by fitting the observed concentration-effect data with three-parameter nonlinear regression in GraphPad Prism version 5.03 for Windows (GraphPad Software, San Diego, CA). The E_{max} and EC_{50} values are presented as the mean (90% confidence interval) for each donor. For use in predictions, the total EC_{50} were converted to a free EC_{50} ($EC_{50,u}$) using the fraction unbound in hepatocyte media ($f_{u,media}$) measured for each retinoid.

The change in CYP2D6 expression in vivo following 13*cis*RA dosing was predicted based on the magnitude of *CYP2D6* mRNA down-regulation in human hepatocytes and steady state concentrations of 13*cis*RA (0.88 µM) and its metabolites, *at*RA (0.069 µM) and 4-oxo-13*cis*RA (4.2 µM), determined following dosing of 40 mg 13*cis*RA BID to eight healthy volunteers as reported in Chapter 3. Total precipitant concentrations were converted to free precipitant concentrations ($[I_u]$) using the fraction unbound in plasma ($f_{u,plasma}$) measured for each retinoid. The overall effect of the three compounds on in vivo CYP expression was predicted assuming that all three precipitants (13*cis*RA, *at*RA, and 4-oxo-13*cis*RA) bind to the same receptor to result in altered CYP expression via a competitive mechanism as described previously (Sager *et al.*, 2017). The prediction for the change in exposure of dextromethorphan, a CYP2D6 probe substrate, following dosing of 13*cis*RA to steady state was performed as previously described (Fahmi *et al.*, 2008) with an adaptation to account for the presence of *m* number of retinoids *k* each competing for binding to the receptor of interest (equation 4.3). The f_m is the fraction of substrate metabolized by the CYP of interest. For dextromethorphan, the f_m by CYP2D6 in CYP2D6 extensive metabolizers was set to 0.98 (Lutz and Isoherranen, 2011).

$$\frac{AUC_{po}^{'}}{AUC_{po}} = \frac{Cl}{Cl^{'}} = \frac{1}{\left(\frac{1+\sum_{k=1}^{m}\frac{E_{\max,k}\times[I_u]_k}{EC_{50,adj,u,k}}}{1+\sum_{k=1}^{m}\frac{[I_u]_k}{EC_{50,adj,u,k}}}\right)\times f_m + (1-f_m)} \qquad (4.3)$$

4.2.6 Simulation of in vitro CYP2D6 mRNA and protein degradation

To explore the difference in the time-course of change in CYP2D6 mRNA and activity (as a surrogate for CYP2D6 protein levels), the effects from incubation of hepatocytes from the FOS donor with 1 µM *at*RA for 1, 2, 24, and 48 hours were plotted for the two endpoints. The first-order rate constant (k) determined for the decrease in mRNA over time was 0.04 h^{-1} and for activity over time was 0.015 h^{-1}. A model was constructed in MATLAB and SimBiology Toolbox Release 2018b (The MathWorks, Inc., Natick, MA) to simulate the decline of CYP2D6 mRNA and protein with differing inhibition of mRNA synthesis (100, 75, 50, and 25% inhibition). The rate of mRNA synthesis was assumed to be zero-order and set at 0.04 pmol/h as the input for the mRNA species. The first-order rate constant for mRNA degradation (k = 0.04 h^{-1}) was set as the input into the protein species, and the first-order degradation rate constant for CYP2D6 was applied to the protein species. The simulation was run until all species reached steady state, and then the rate of mRNA synthesis was decreased by 25, 50, 75, or 100% and the concentrations of the decline in mRNA or protein species as a function of time was followed.

4.3 RESULTS

4.3.1 CYP2D6 regulation by retinoids in human hepatocytes

Significant depletion of retinoids was observed in hepatocyte incubations in all donors (Figure 4.1) and the calculated C_{avg} of 13*cis*RA, *at*RA, and 4-oxo-13*cis*RA following 1 µM treatment are presented in Figure 4.1. Relative to nominal concentrations, the average depletion of the retinoids in the three donors was similar. The mean C_{avg} (Figure 4.1) over the treatment interval at 1 µM was 13% of the nominal for 13*cis*RA, 22% of the nominal for *at*RA, and 35% of the nominal for 4-oxo-13*cis*RA. In the concentration-effect experiments, the depletion of the retinoids

at 1 μM (average between 2 and 48 hours) was similar (within 5%) as observed in the time-course experiment. Thus, the average concentration measured from 2 and 48 hours at each treatment concentration was used to adjust each nominal concentration tested for estimation of EC_{50}. In Hu1558 hepatocytes, the calculated C_{avg} was 7 - 14% of nominal for 13*cis*RA, 7 - 18% of nominal for *at*RA, and 9 - 23% of nominal for 4-oxo-13*cis*RA across the concentration range tested. In Hu1765 hepatocytes a range of 11 - 26% of 13*cis*RA, 16 - 40% of *at*RA, and 28 - 50% of 4-oxo-13*cis*RA nominal concentrations were measured, and in the FOS donor 17 - 56% of 13*cis*RA, 20 - 77% of *at*RA, and 36 - 67% of 4-oxo-13*cis*RA nominal concentrations were measured.

Concentration-dependent decreases in *CYP2D6* mRNA were observed in response to treatment with 13*cis*RA, *at*RA, and 4-oxo-13*cis*RA, but large interindividual variability was observed among the three donors (Figure 4.2). The E_{max} (fraction of *CYP2D6* mRNA remaining) and EC_{50} (μM) for down-regulation of *CYP2D6* mRNA by retinoids in each donor are shown in Figure 4.2. No cytotoxicity or change in lactate dehydrogenase assay was observed in hepatocytes in response to retinoid treatments. For each hepatocyte donor the maximum down-regulation of *CYP2D6* mRNA and EC_{50} were comparable when treated with 13*cis*RA, *at*RA, or 4-oxo-13*cis*RA (Figure 4.2). Hu1765 was least responsive, whereas FOS was the most responsive to *CYP2D6* mRNA down-regulation. For the three donors, the average maximum *CYP2D6* mRNA remaining was 42% (range: 5 – 80%) after 13*cis*RA, 47% (range: 7 – 100%) after *at*RA, and 41% (range: 5 – 78%) after 4-oxo-13*cis*RA. The mean EC_{50} from the three hepatocyte lots were 34 nM (range: 2.9 – 82 nM) for 13*cis*RA, 22 nM (47 nM – >30μM) for *at*RA, and 60 nM (2.0 – 137 nM) for 4-oxo-13*cis*RA. The $EC_{50,u}$ was determined by multiplying EC_{50} by the $f_{u,media}$ and the value was used in predictions of the effects of 13*cis*RA, *at*RA, and 4-oxo-13*cis*RA on CYP2D6 (Table 4.1). The final $f_{u,media}$ measured by RED correlated well with ultracentrifugation values of unbound

fractions of 0.017 for 13*cis*RA, 0.028 for *at*RA, and 0.154 for 4-oxo-13*cis*RA. While all three retinoids down-regulated *CYP2D6* mRNA, down-regulation of CYP2D6 activity was inconsistent between the three donors (Figure 4.3). Up to 1.5-fold increase in CYP2D6 activity was observed at the highest concentrations of retinoids tested in Hu1765 donor, and the changes were significant at nominal concentrations greater than 0.04 µM for 13*cis*RA, greater than 0.123 µM for *at*RA, and at all treated concentrations of 4-oxo-13*cis*RA when analyzed by ANOVA with a Dunnet's post-hoc analysis. For FOS, both *CYP2D6* mRNA and CYP2D6 activity were decreased, however the magnitude of change was different (greater than 90% decrease in *CYP2D6* mRNA versus less than 50% decrease in CYP2D6 activity). In contrast, no decrease in CYP2D6 activity was observed in hepatocytes from Hu1558.

To investigate the disconnect between the magnitude of decrease in CYP2D6 mRNA and enzyme activity in the hepatocytes, simulations of mRNA and enzyme degradation were conducted. As illustrated in the simulation (Figure 4.4), if the half-life of mRNA is approximately 17 hours ($k = 0.04\ h^{-1}$), only ~15% of mRNA remained 48 hours after complete inhibition of mRNA synthesis. With 75% inhibition of mRNA synthesis, a ~50% decrease in mRNA could be expected. When mRNA synthesis was inhibited by 25 or 50%, less than a 50% decrease in mRNA at 48 hours could be expected. In contrast, regardless of the magnitude of inhibition of mRNA synthesis, at 48 hours, CYP2D6 enzyme expression would decrease by less than 50%. This difference in the magnitude of depletion of mRNA and enzyme are driven by the differences in degradation rate (or half-life) between mRNA and enzyme. For an enzyme with a half-life of ~48 hours ($k = 0.015\ h^{-1}$), hepatocytes would need to be treated for at least 72 hours to observe 50% enzyme down-regulation following complete inhibition of mRNA synthesis and absence of any lag time in effect on mRNA and protein synthesis.

4.3.2 Prediction of CYP2D6 down-regulation and a potential clinical DDI

The magnitude of CYP2D6 down-regulation in vivo was predicted for each retinoid individually and in combination (Table 4.1). Steady state concentrations of 13*cis*RA (0.88 µM), *at*RA (0.069 µM), and 4-oxo-13*cis*RA (4.2 µM) reported in Chapter 3 and $f_{u,plasma}$ were used to predict the potential for a clinical DDI with dextromethorphan. An average of 72% (range: 62 – 82%) of CYP2D6 remaining was predicted in response to the effects 13*cis*RA alone. Despite preclinical evidence for *at*RA down-regulation of CYP2D6, we predicted that CYP2D6 expression would decrease by only ~1% based on steady state *at*RA concentrations and in vitro concentration-response data for *CYP2D6* mRNA in the three hepatocyte lots. In contrast, across all donors, the average percent of CYP2D6 remaining based on circulating 4-oxo-13*cis*RA concentrations achieved after steady-state dosing with 13*cis*RA was 49% (range: 29 – 78%). Based on the predictions, CYP2D6 down-regulation in vivo is predicted to be mediated predominantly by the 4-oxo-13*cis*RA metabolite. When predictions were made with the combination of parent drug (13*cis*RA) and metabolites (*at*RA and 4-oxo-13*cis*RA) using in vitro data from Hu1558, Hu1765, and FOS, the predicted percent decreases in CYP2D6 were 35, 22, and 72%, respectively. The corresponding predictions for the increase in dextromethorphan AUC following dosing of 13*cis*RA were 1.5-, 1.3-, and 3.4-fold with an average of 2.0-fold increase predicted using the mean E_{max} and $EC_{50,u}$ from all donors. Thus, despite the large interindividual variability between the three donors, using a cut-off of ≥1.25 for the dextromethorphan AUC ratio, a DDI involving down-regulation of CYP2D6 would be predicted with all three hepatocyte lots.

Predictions for the change in dextromethorphan exposure were also made with concentration data from each subject enrolled in the clinical study described in Chapter 3 (Figure 4.5). The concentrations of 13*cis*RA, *at*RA, and 4-oxo-13*cis*RA are shown for each subject, and

the range of predicted and observed AUC ratios (AUCRs) for dextromethorphan after and before 13*cis*RA dosing are presented. The average total steady state concentration of 4-oxo-13*cis*RA in the clinical study subjects was 4.2 μM (range: 2.6 to 10 μM). These values correspond to free 4-oxo-13*cis*RA concentrations of 50 nM (range: 31 – 120 nM), which are higher than the average $EC_{50,u}$ for 4-oxo-13*cis*RA of 7.3 nM determined in this study (Table 4.1). Dextromethorphan exposure was predicted to increase by 2-fold with a wide confidence interval (1.3 – 4.9-fold) due to the variability in *CYP2D6* mRNA down-regulation in the three hepatocyte donor lots and the variability in retinoid exposures. In contrast to the predicted dextromethorphan AUCR, the observed geometric mean AUCR was 0.82 (90% confidence interval: 0.677 – 0.998).

Based on previous data supporting a role for SHP in regulation of CYP2D6 by *at*RA (Koh *et al.*, 2014), changes in *SHP* mRNA were explored in hepatocyte incubations. An initial time course experiment demonstrated that maximum responses in *SHP* mRNA occurred at 1 – 2 hours (Figure 4.4). Thus, changes in *SHP* mRNA in human hepatocytes in response to treatment with 13*cis*RA, *at*RA, and 4-oxo-13*cis*RA were assessed at 2 hours. *at*RA induced expression of *SHP* mRNA between 2- to 4-fold at the highest concentrations of *at*RA tested (Figure 4.6). Similarly, both 13*cis*RA and 4-oxo-13*cis*RA also induced *SHP* mRNA in a dose-dependent manner with a maximum 2- to 3-fold increase.

4.3.3 CYP induction by retinoids in human hepatocytes

The dose-response relationships for 13*cis*RA, *at*RA, or 4-oxo-13*cis*RA and CYP3A4 mRNA and activity in the three tested hepatocyte lots are shown in Figure 4.7 and Figure 4.8. Treatment of Hu1765 and FOS hepatocytes with 13*cis*RA, *at*RA, or 4-oxo-13*cis*RA resulted in a 1.5- to 3-fold increase in CYP3A4 expression, but no change in CYP3A4 mRNA or activity were observed with incubation of hepatocytes from donor Hu1558. As was the case for *CYP2D6* mRNA

down-regulation, the effects of each retinoid on CYP3A4 mRNA or activity were similar within a given donor, but variability was observed between the donors. Overall, the greatest induction of CYP3A4 mRNA and activity was observed for each retinoid in hepatocytes from the FOS donor.

The regulation of CYP3A4 by the nuclear receptor PXR and the induction of CYP3A4 by PXR ligands is well established. To investigate whether 13*cis*RA, *at*RA or 4-oxo-13*cis*RA are PXR ligands, a ligand binding assay was conducted (Figure 4.9). All three retinoids demonstrated concentration-dependent increases in receptor binding but were less potent binders than rifampin. For 13*cis*RA, *at*RA, and 4-oxo-13*cis*RA, the E_{max} values were 15, 29, and 9.5-fold increase in luciferase activity relative to control, and the EC_{50} values were estimated to be 20, 140, and 16 μM, respectively, compared to the rifampin E_{max} of 22-fold and EC_{50} of 4.7 μM. These data suggest that the increased CYP3A4 mRNA and activity observed in hepatocytes in response to treatment with retinoids may be mediated by retinoid activation of PXR.

4.3.4 Assessment of interindividual variability in response to retinoids

Endogenous *at*RA exerts many of its physiological effects by binding to and activating retinoic acid receptors (RARs) (Aström *et al.*, 1990; Idres *et al.*, 2002). *CYP26A1* is an RAR-target gene and the CYP primarily responsible for elimination of endogenous and dosed *at*RA (Thatcher *et al.*, 2010). Based on current knowledge, induction of *CYP26A1* is expected in cells treated with *at*RA (Topletz *et al.*, 2015). Therefore, to investigate whether the variable response of CYP2D6 and CYP3A4 in the three hepatocyte lots correlated to variability in the magnitude of induction of known retinoid-responsive genes, changes in expression of *CYP26A1* and *RARβ* were assessed. Vehicle control-treated cells from the FOS donor had low (C_T = 38) or undetectable levels (C_T > 40) of *CYP26A1*, but C_T values ranged from 22 – 25 in cells after treatment with 13*cis*RA, *at*RA, or 4-oxo-13*cis*RA. Although the fold-change in *CYP26A1* expression (normalized to the

housekeeping gene) in retinoid- versus control-treated cells could not be accurately quantified due to the undetectable levels of *CYP26A1* in control-treated cells, *CYP26A1* was estimated to increase by 1,000 – 10,000-fold in the FOS hepatocytes. In contrast, for Hu1765 hepatocytes, *CYP26A1* C_T values were ~31 in vehicle-treated cells and increased ~100-fold (to C_T 23 – 27) in response to all three retinoids. A similar pattern was seen in that FOS was more responsive in terms of *RARβ* induction (20- to 44-fold) compared to the Hu1765 (3- to 7-fold). Thus, for all the target genes tested in this study, the effect of retinoid treatment was greatest in FOS hepatocytes.

4.4 DISCUSSION

Based on numerous reports of retinoic acid inducing SHP (Mamoon *et al.*, 2008; Cai *et al.*, 2010; Koh *et al.*, 2014; Yang *et al.*, 2014), and a study in mice demonstrating *at*RA down-regulation of CYP2D6 via SHP (Koh *et al.*, 2014), we studied the potential for a DDI involving CYP2D6 down-regulation by 13*cis*RA in the clinic, and the data are presented in Chapter 3. No down-regulation was observed in the study, and the data supported apparent CYP2D6 induction after 13*cis*RA dosing. One limitation to available data from HepG2 cells and hepatocytes is that concentrations of *at*RA studied for their effects on SHP induction were high (1 – 10 μM) relative to pharmacologically relevant *at*RA concentrations (Mamoon *et al.*, 2008; Cai *et al.*, 2010; Yang *et al.*, 2014) and no assessment of *at*RA effects on CYP2D6 were reported. Indeed, evidence for direct effects of *at*RA on CYP2D6 expression is limited to one study in CYP2D6-humanized mice (Koh *et al.*, 2014). Thus, a thorough evaluation of the effects of *at*RA on CYP2D6 expression in human hepatocytes was necessary to determine whether the results of the clinical study represent a true disconnect between in vitro-and-in vivo CYP down-regulation. Additionally, 13*cis*RA rather than *at*RA was used to probe the potential clinical interaction. However, no data are available for the effect of 13*cis*RA or its major circulating metabolite, 4-oxo-13*cis*RA, on CYP2D6 expression.

In fact, we found that 4-oxo-13*cis*RA induced expression of several *Cyp2d* isoforms in mice (Chapter 3), thus induction may potentially oppose *at*RA down-regulation of CYP2D6 in human liver. Therefore, this study aimed to assess the dose-dependent effects of 13*cis*RA, *at*RA and 4-oxo-13*cis*RA on CYP2D6 expression in hepatocytes and determine whether those effects would predict CYP2D6 down-regulation in the clinic.

All three retinoids decreased expression of *CYP2D6* mRNA to a similar extent and with similar EC_{50}s within each of the three hepatocyte donor lots, although variability was observed between the donors. Using our prediction model and free concentrations, 4-oxo-13*cis*RA was predicted to have the largest effect on CYP2D6 followed by 13*cis*RA, and no change in CYP2D6 was predicted with *at*RA. The average unbound concentration of 4-oxo-13*cis*RA in the clinical study was ~50 nM, which is 3 – 200-fold greater than the estimated $EC_{50,u}$ of 0.24 – 17 nM. In contrast, the unbound concentration of *at*RA (~0.01 nM) after 13*cis*RA dosing is lower than $EC_{50,u}$ of 0.16 – 1.3 nM, and no DDI would be expected from *at*RA exposure. It was assumed that the three retinoids exert effects on CYP2D6 regulation via the same receptor-binding pathway. Thus, an equation accounting for competitive binding to the same receptor was used to determine the fraction of CYP2D6 expression remaining following the combined exposure of 13*cis*RA, *at*RA, and 4-oxo-13*cis*RA (Sager *et al.*, 2017). Predictions of the combined effect of 13*cis*RA and its metabolites on CYP2D6 were similar to that of 4-oxo-13*cis*RA alone. Based on predictions made with the average E_{max} and $EC_{50,u}$ from the three hepatocyte donors and $C_{ss,u}$ for each retinoid, an average 2-fold increase in dextromethorphan exposure was predicted after dosing with 13*cis*RA, and the DDI prediction was driven by exposure to 4-oxo-13*cis*RA.

Current regulatory guidance documents recommend investigating new chemical entities as perpetrators of induction-mediated DDIs, but do not address potential effects of metabolites on

CYP induction (EMA, 2012; Food and Drug Administration, 2017b). However, several recent reports have identified metabolites with greater or equal effects on CYP induction as their respective parent molecules (Schneider, 2017; Ho *et al.*, 2018; Johänning *et al.*, 2018). This study illustrates another example in which parent molecule (13*cis*RA) and metabolites (*at*RA and 4-oxo-13*cis*RA) all transcriptionally regulate CYP2D6 in vitro. Because 4-oxo-13*cis*RA circulates at higher concentrations than 13*cis*RA or *at*RA, effects of this metabolite drive the prediction for a clinical DDI. Although no down-regulation of CYP2D6 was observed clinically, the induction of CYP2D6 that was observed was hypothesized to be related to effects of 4-oxo-13*cis*RA based on evidence of induction of *Cyp2d* isoforms in the mouse (Chapter 3). Therefore, data from 13*cis*RA effects on CYP2D6 demonstrate the need to consider metabolites as perpetrators of DDIs resulting from transcriptional regulation of CYPs.

This study clearly demonstrates a lack of in vitro to in vivo correlation for CYP2D6 down-regulation by retinoids. To investigate the in vitro to in vivo disconnect, the effects of retinoids on *SHP* were determined. As expected from previous reports (Cai *et al.*, 2010; Yang *et al.*, 2014), we observed ~2-fold induction of *SHP* mRNA in a donor-dependent manner following treatment with 10 μM *at*RA. Further, the timing of *SHP* mRNA induction in this study is consistent with previous studies showing rapid induction of *SHP* within two hours of *at*RA treatment in HepG2 cells with mRNA levels returning to baseline by 24 – 48 hours (Cai *et al.*, 2010). Induction of *SHP* mRNA was also observed with 13*cis*RA and 4-oxo-13*cis*RA, which has not been previously reported. If retinoid-mediated induction of *SHP* is the cause for *CYP2D6* down-regulation observed in vitro, what accounts for the in vitro-to-in vivo disconnect? *SHP* is a classic farsenoid X receptor (FXR)-target gene and is induced by excess bile acids in the liver as a negative feedback mechanism for maintenance of bile acid homeostasis (Goodwin *et al.*, 2000). Retinoic acid induction of *SHP* has

been shown to be FXR-independent and likely occurs via retinoid binding to the retinoid X receptor (RXR), though *at*RA and 13*cis*RA are weak RXR ligands (Heyman *et al.*, 1992; Allenby *et al.*, 1993; Cai *et al.*, 2010). Thus, it is possible that the in vitro-to-in vivo disconnect occurs because treatment of 13*cis*RA in vitro recapitulates the activation of the FXR/RXR heterodimer that occurs with endogenous bile acids or retinoids in vivo, and that administration of 13*cis*RA does not cause further signaling through this pathway in vivo.

One limitation to this study was that effects of retinoids on CYP2D6 activity were inconsistent between hepatocyte donors. Additionally, in the FOS donor where >90% of CYP2D6 mRNA was depleted, only minor changes in CYP2D6 activity were observed. The half-life of CYP2D6 has been estimated to be ~48 hours (Venkatakrishnan and Obach, 2005). Thus, the maximum decrease in CYP2D6 expression expected in a 48-hour incubation would be 50% assuming no lag time in response for mRNA or protein down-regulation. With complete inhibition of *CYP2D6* mRNA synthesis, the 48-hour simulations showed a 90% decrease in *CYP2D6* mRNA, but ~70% of CYP2D6 protein would remain. To observe a 50% decrease in CYP2D6 protein, simulations indicated that mRNA synthesis would need to be fully inhibited for 72 hours. Simulations also showed that with less than complete inhibition of *CYP2D6* mRNA synthesis, the magnitude of mRNA and protein degradation decreased. This suggests that down-regulators of CYP2D6 must drastically alter mRNA synthesis in order for down-regulation of CYP2D6 activity or protein levels to be observed. Increases in CYP2D6 activity, as seen in vivo following dosing of 13*cis*RA, were observed for one of three hepatocyte donor lots (Hu1765), though it is unclear whether these results are significant due to the low effect size and lack of clear concentration-effect relationship.

The effects of 13*cis*RA, *at*RA, and 4-oxo-13*cis*RA on CYP3A4 were also assessed to determine whether the weak induction of CYP3A4 observed after dosing of 13*cis*RA could be predicted from hepatocyte data. Up to 3-fold induction of CYP3A4 mRNA and activity was observed in response to treatment with retinoids. Although no kinetic determination of retinoid effects on CYP3A4 was performed due to the weak induction of CYP3A4 mRNA and activity, these data from hepatocytes support the clinical observation. Previous studies have demonstrated that retinoids can induce CYP3A4 via activation of constitutive androstane receptor (CAR)/RXR or vitamin D receptor (VDR)/RXR heterodimers (Wang *et al.*, 2008; Chen *et al.*, 2010). In this study, 13*cis*RA, *at*RA, and 4-oxo-13*cis*RA were shown to be ligands for the pregnane X receptor (PXR). It is well documented that CYP3A4 is inducible by PXR ligands (Stanley *et al.*, 2006; Sinz, 2013). Furthermore, PXR-activating ligands can also activate CAR, and activation of either of these nuclear receptors can induce expression of CYP3A4 or CYP2B6 (Stanley *et al.*, 2006; Fahmi *et al.*, 2010). Additionally, retinoids also bind to RXR which is the heterodimer partner for PXR, CAR, and VDR (Heyman *et al.*, 1992; Allenby *et al.*, 1993). Thus, 13*cis*RA, *at*RA, and 4-oxo-13*cis*RA likely induce CYP3A4 as ligands of PXR/RXR and possibly CAR/RXR or VDR/RXR. The well-defined mechanisms for transcriptional activation of CYP3A4 permit in vitro-to-in vivo prediction of induction. In contrast, the mechanisms for CYP down-regulation observed in vitro, in particular CYP2D6 as evidenced by this study, are generally unknown and the potential impact of these findings in vivo cannot be predicted at present.

In conclusion, this study showed that 13*cis*RA, *at*RA, and 4-oxo-13*cis*RA all down-regulate *CYP2D6* mRNA in human hepatocytes. A DDI involving CYP2D6 down-regulation following administration of 13*cis*RA was predicted from in vitro data, and the 13*cis*RA metabolite, 4-oxo-13*cis*RA, was predicted to drive the interaction. These results support other in vitro

observations of CYP down-regulation by retinoids but are inconsistent with clinical findings. This study also highlights the role metabolites can play as precipitants of DDIs and suggests that future studies should include metabolites in assessment of potential DDIs involving transcriptional regulation.

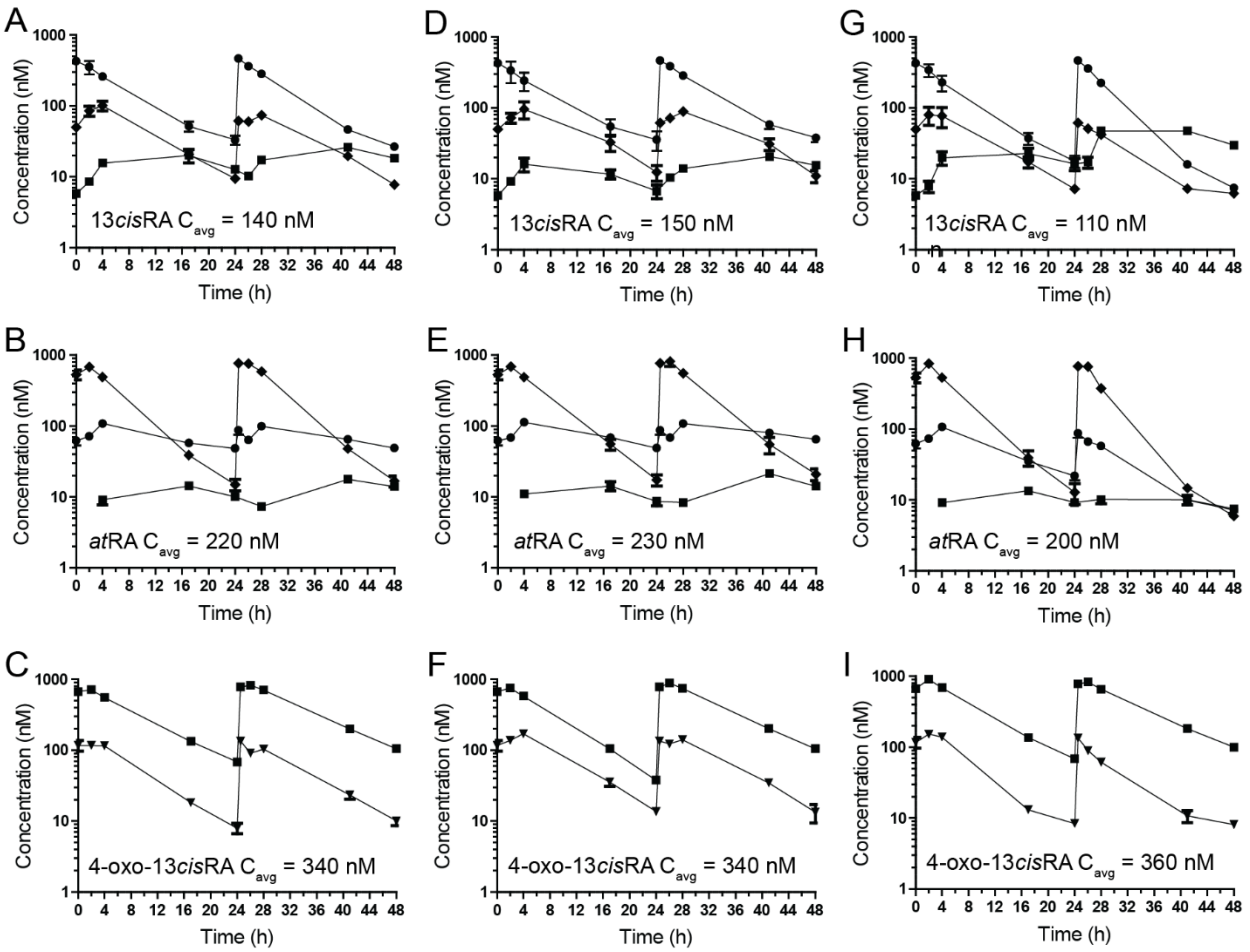

Figure 4.1. Concentration versus time profiles for retinoids after treatment of Hu1558 (A, B, C), Hu1765 (D, E, F), and FOS (G, H, I) hepatocytes following treatment with 1 µM 13*cis*RA (top row), *at*RA (middle row), or 4-oxo-13*cis*RA (bottom row). Hepatocytes were treated for 48 hours and retinoid concentrations in media were measured at 2, 17, and 24 hours on each treatment day. Concentrations of the treated retinoid and metabolites are presented as mean and standard deviation. Inset shows the C_{avg} (geometric mean) of the treated retinoid determined on the two treatment days. 13*cis*RA (circles), *at*RA (diamonds), 4-oxo-13*cis*RA (squares), 4-oxo-*at*RA (inverted triangles)

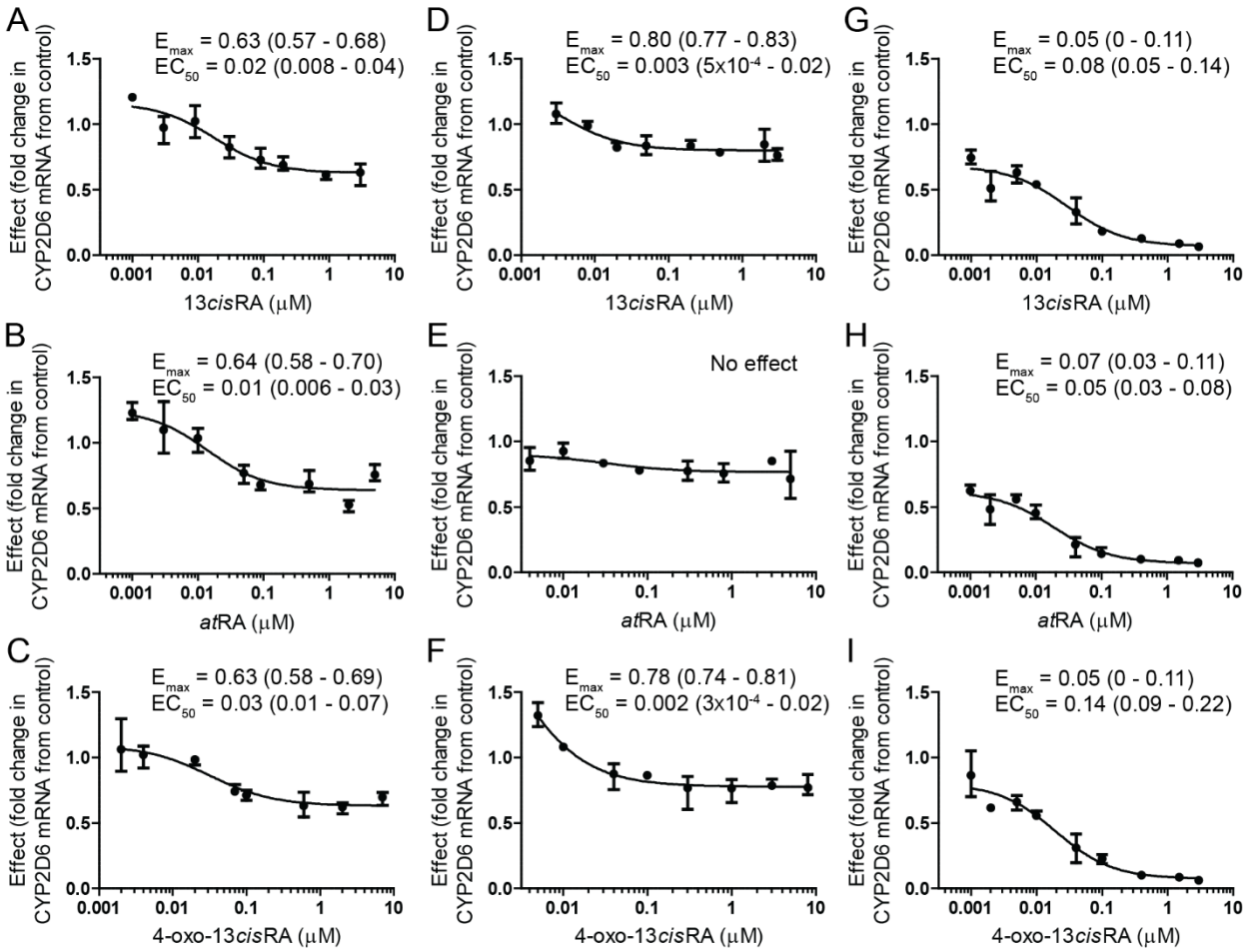

Figure 4.2. The effects on *CYP2D6* mRNA following treatment with 13*cis*RA (top row), *at*RA (middle row), and 4-oxo-13*cis*RA (bottom row) compared to control in Hu1558 (A, B, C), Hu1765 (D, E, F), and FOS (G, H, I) hepatocytes. The points show the mean and range of the measured effect and the line shows the fit of the data. E_{max} and EC_{50} (μM) are presented as mean (90% CI).

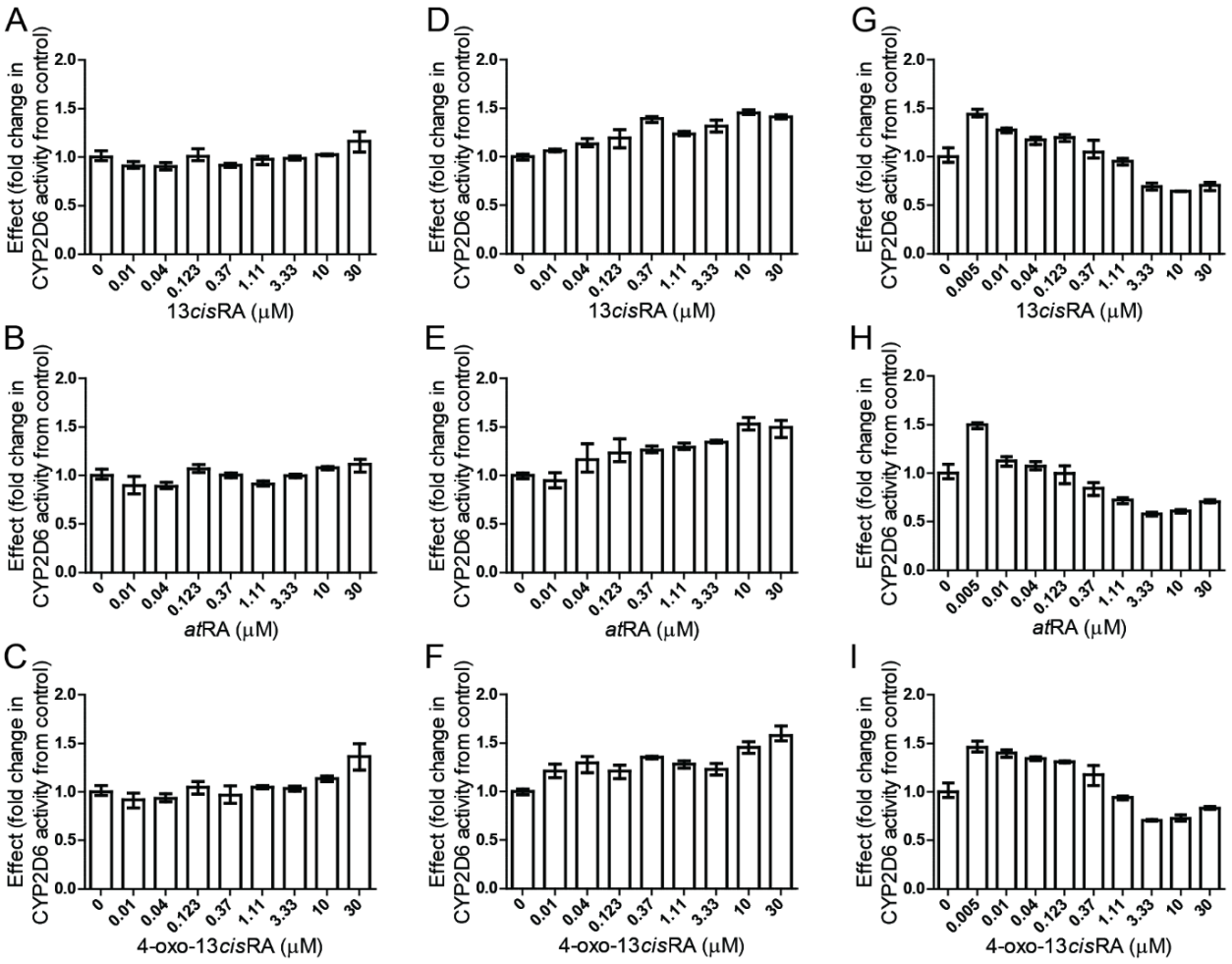

Figure 4.3. The effects of 13*cis*RA (top row), *at*RA (middle row), and 4-oxo-13*cis*RA (bottom row) on CYP2D6 activity in Hu1558 (A, B, C), Hu1765 (D, E, F), and FOS (G, H, I) hepatocytes. Data are presented as mean and range of the measured effect (formation of dextrorphan from dextromethorphan in a 90 min incubation following 48 h retinoid treatments).

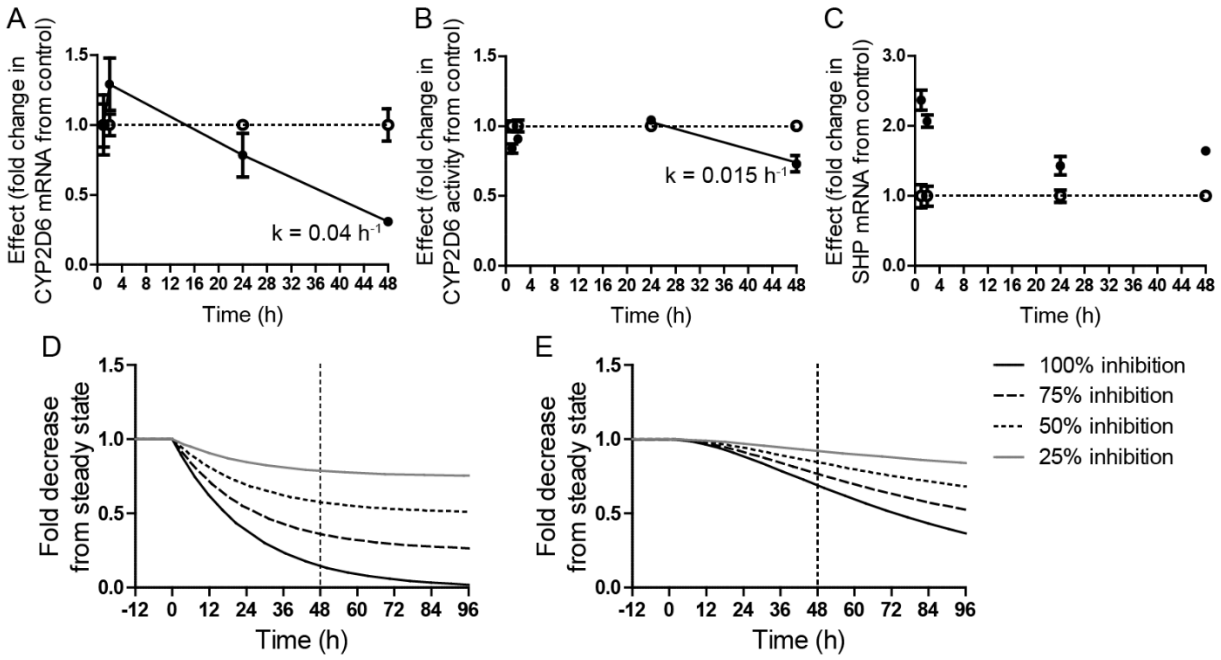

Figure 4.4. Depletion over time of (A) *CYP2D6* mRNA, (B) CYP2D6 activity, and (C) *SHP* mRNA after treatment of FOS hepatocytes with 1 µM atRA (solid circles) or vehicle (open circles). The degradation rate for mRNA was 0.04 h^{-1} (17 h half-life) and for activity was 0.015 h^{-1} (48 h half-life). Simulations of (D) *CYP2D6* mRNA and (E) protein were conducted with a zero-order synthesis rate of 0.04 pmol/h set as the input of mRNA and mRNA and protein elimination rate constants set to 0.04 h^{-1} and 0.015 h^{-1}, respectively. Simulations were run until steady state of mRNA and protein were achieved and then the synthesis rate was inhibited by 100% (solid black line), 75% (dashed line), 50% (dotted line), or 25% (solid gray line) for panels D and E.

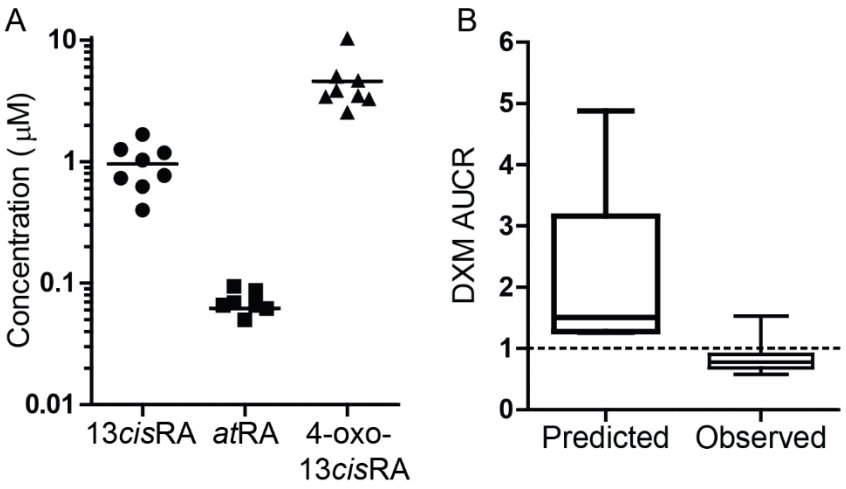

Figure 4.5. Predicted change in dextromethorphan exposure after and before 13*cis*RA dosing to individual clinical study subjects. A) Individual concentrations of 13*cis*RA, *at*RA, and 4-oxo-13*cis*RA for the eight subjects enrolled in the clinical study (mean shown by line). B) Predicted versus observed changes in the area under the curve ratio (AUCR) of dextromethorphan (DXM) after and before dosing of 40 mg 13cisRA BID to steady state for each subject. Data are presented as a box representing the 25th, median, and 75th percentiles and whiskers show the minimum and maximum AUCR. The mean predicted AUCR was 2.0.

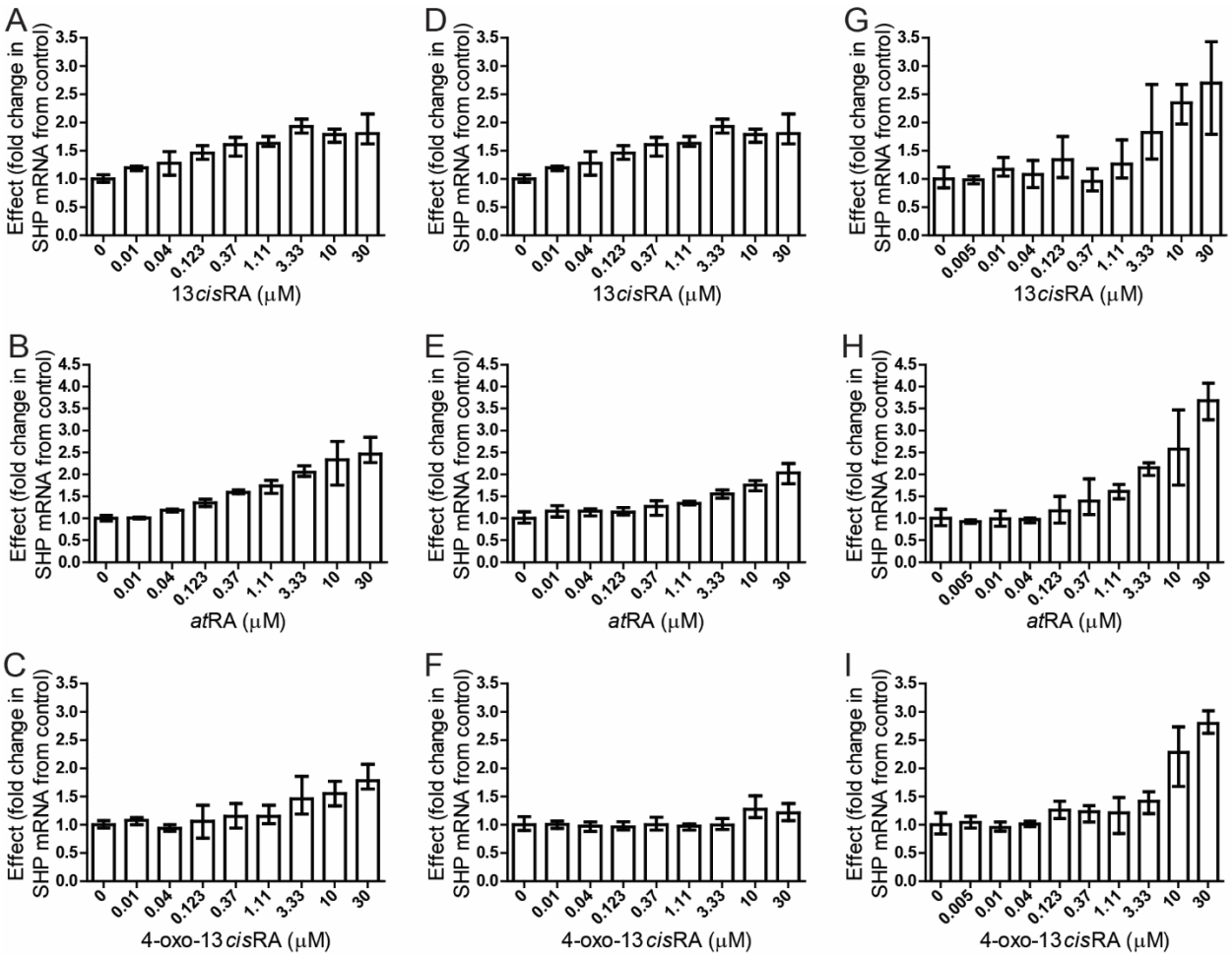

Figure 4.6. The effects of 13*cis*RA (top row), *at*RA (middle row), and 4-oxo-13*cis*RA (bottom row) on *SHP* mRNA in Hu1558 (A, B, C), Hu1765 (D, E, F), and FOS (G, H, I) hepatocytes. Data are presented as mean and range of SHP response.

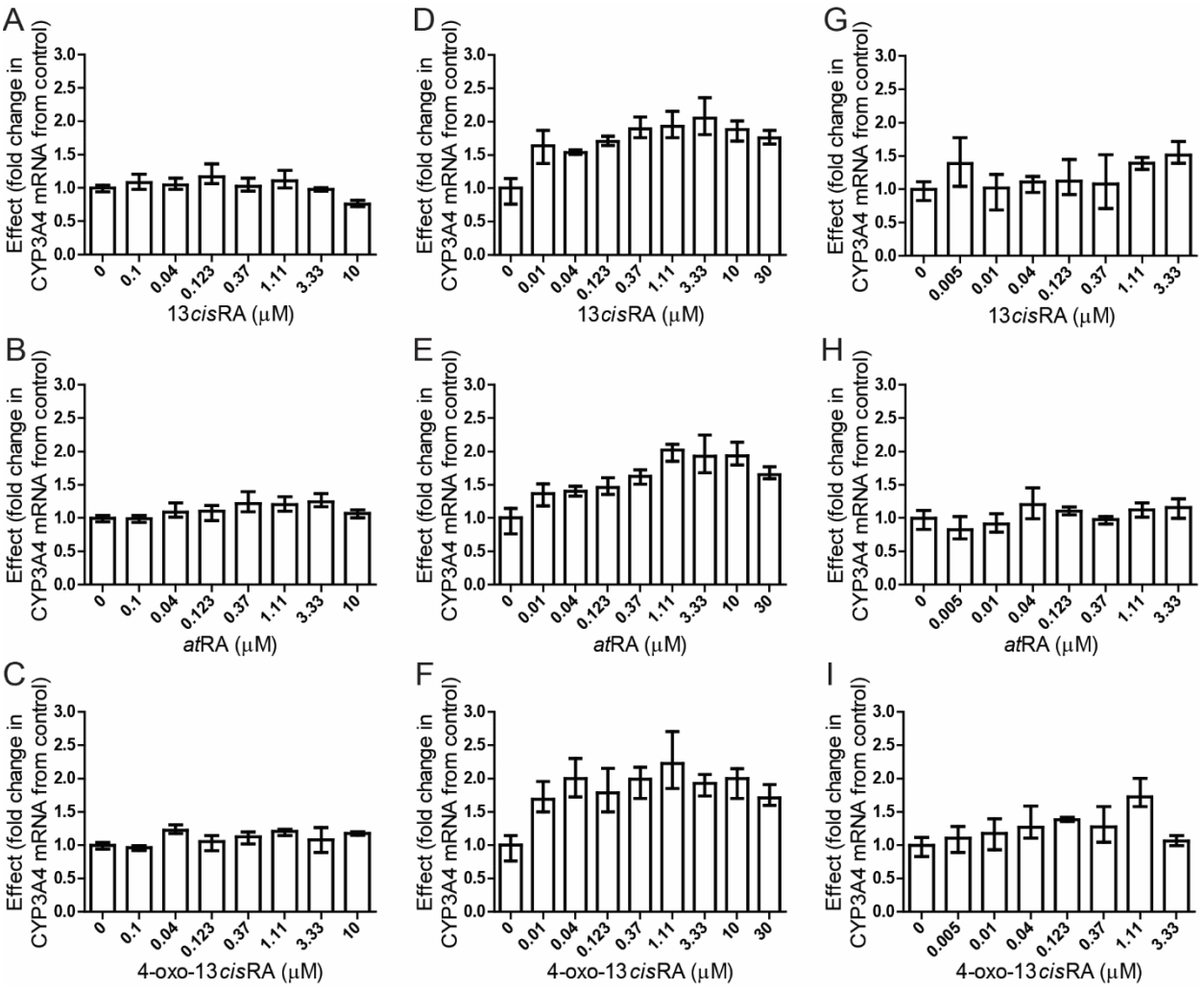

Figure 4.7. The effects of 13*cis*RA, *at*RA, and 4-oxo-13*cis*RA on *CYP3A4* mRNA in Hu1558 (A - D), Hu1765 (E - H), and FOS (I – L) hepatocytes. Data are presented as the mean and range of the effect on *CYP3A4* mRNA.

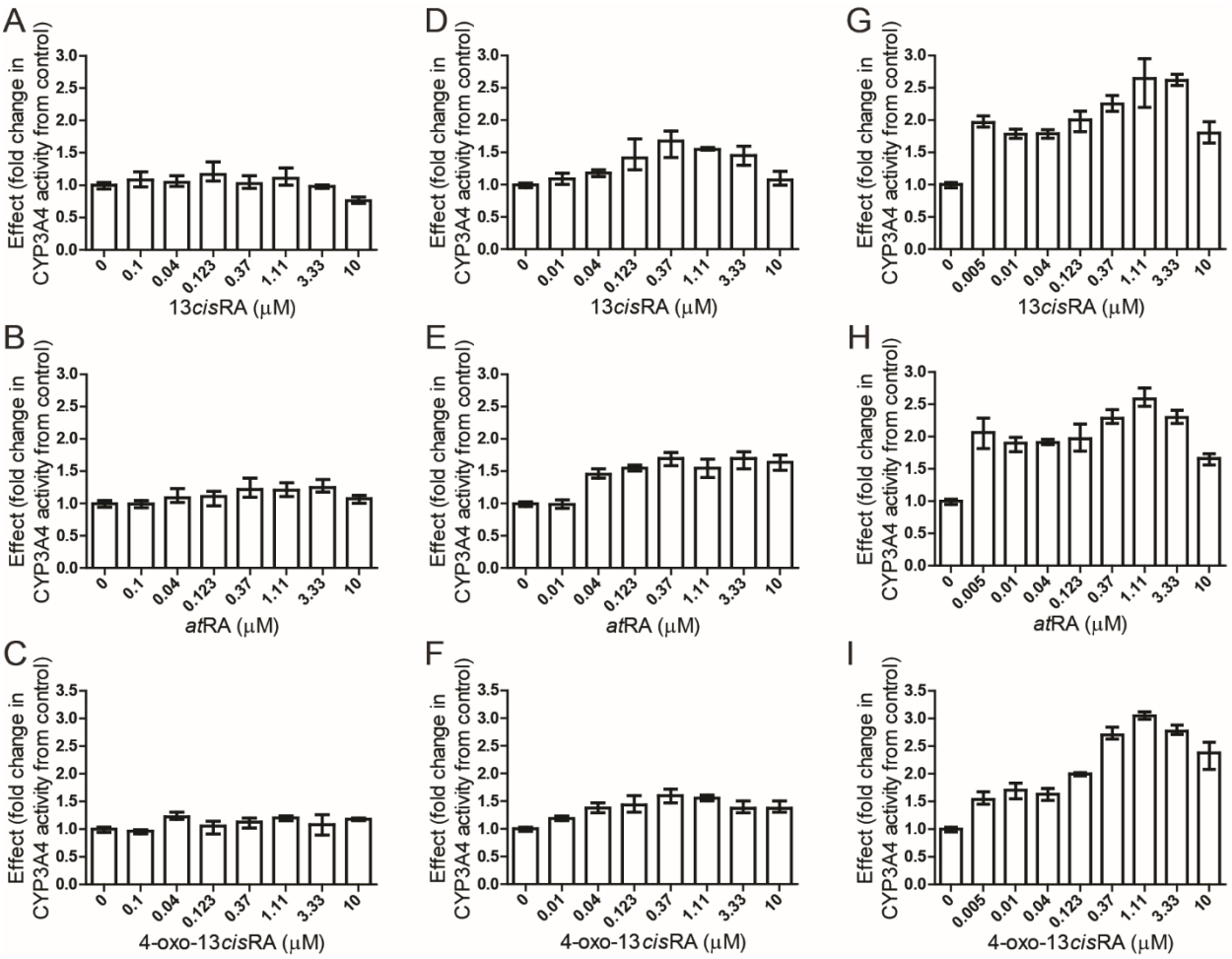

Figure 4.8. The effects of 13cisRA, atRA, and 4-oxo-13cisRA on CYP3A4 activity in Hu1558 (A - C), Hu1765 (D - F), and FOS (G – I) hepatocytes. Data are presented as the mean and range of the measured effect (formation of 6β-OH-testosterone from testosterone in a 90 min incubation following 48 h retinoid treatments).

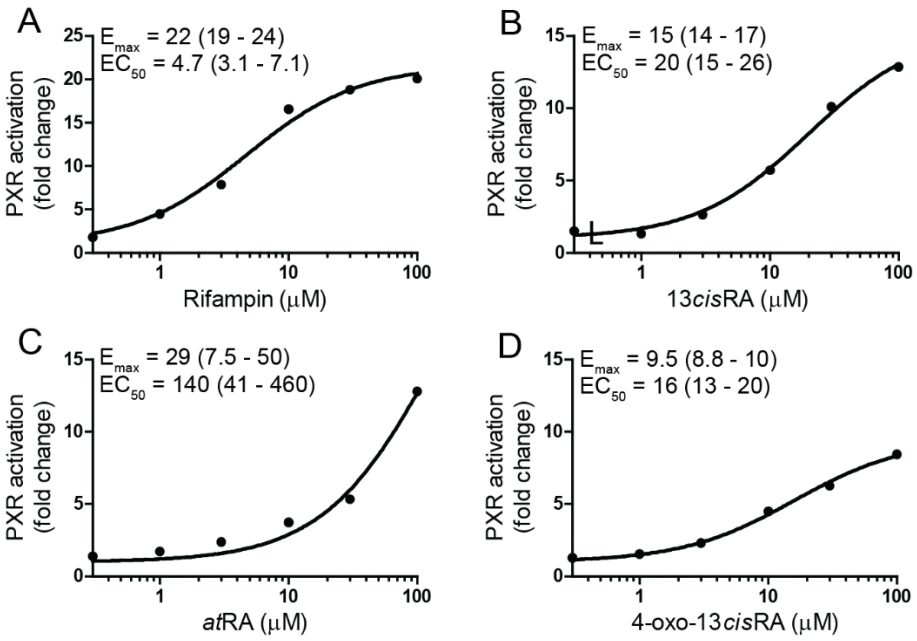

Figure 4.9. The effects of increasing concentrations of (A) rifampin (positive control), (B) 13cisRA, (C) atRA, and (D) 4-oxo-13cisRA on PXR activation. The points show the mean of the measured effect (n=2) and the line shows the fit of the data. E_{max} and EC_{50} (μM) are presented as mean (90% CI).

Table 4.1. Average unbound concentration in plasma and hepatocyte media for retinoids and the predicted in vivo change in CYP2D6 from 13*cis*RA, *at*RA, and 4-oxo-13*cis*RA individually or in combination.

		Precipitant			
Donor	Endpoint	13*cis*RA	*at*RA	4-oxo-13*cis*RA	Combined parent and metabolites
	$f_{u,plasma}$	0.0004	0.0002	0.012	
	$f_{u,media}$	0.011	0.027	0.121	
Hu1558	$EC_{50,u}$ (nM)	0.18	0.37	3.8	
	Predicted % CYP2D6 remaining	0.76	0.99	0.66	0.65
Hu1765	$EC_{50,u}$ (nM)	0.03	NA	0.24	
	Predicted % CYP2D6 remaining	0.82	NA	0.78	0.78
FOS[a] Rep. 1	$EC_{50,u}$ (nM)	0.91	1.3	17	
	Predicted % CYP2D6 remaining	0.74	0.99	0.29	0.27
FOS[a] Rep. 2	$EC_{50,u}$ (nM)	0.40	0.16	8.4	
	Predicted % CYP2D6 remaining	0.62	0.93	0.31	0.29
Mean	$EC_{50,u}$ (nM)	0.38	0.60	7.3	
	Predicted % CYP2D6 remaining	0.72	0.99	0.49	0.48

a) The concentration-dependent effects of retinoids in FOS donor hepatocytes were assessed in two replicate experiments

NA = not applicable

Chapter 5. CONCLUSIONS

The goal of this thesis was to demonstrate that in vitro characterization of precipitants of drug-drug interactions (DDIs) can be used to predict the magnitude of in vivo DDIs. Retinoic acid was used as a model compound to investigate in vitro to in vivo translation of complex DDIs.

To quantify the increase in endogenous *all-trans* retinoic acid (*at*RA) concentrations following inhibition of CYP26, the enzyme primarily responsible for *at*RA elimination, single and multiple dose studies of the panCYP26 inhibitor, talarozole, were conducted in mice. The change in CYP26A1 and CYP26B1 activity after a single dose of talarozole was predicted based on in vitro inhibition characteristics for CYP26A1 and CYP26B1 and the pharmacokinetic profile of talarozole. The observed increases in *at*RA concentrations in serum, liver, and testis agreed well with the predicted change in CYP26A1 and CYP26B1 activity over time in response to a single dose of talarozole. However, after multiple doses of talarozole, increases in endogenous *at*RA were observed only in serum and not in liver and testis. Induction of *Cyp26a1* was observed in liver and testis after multiple doses of talarozole suggesting that inhibition of this isoform by talarozole was insufficient to overcome induction in response to increased endogenous *at*RA in vivo. Further, the increased *at*RA concentrations in serum without a change in liver suggest that CYP26B1 in extrahepatic sites plays a key role in regulating systemic *at*RA exposure.

To test whether *at*RA down-regulation of CYP2D6 in mice translates to CYP2D6 down-regulation in humans, a clinical study with the *at*RA isomer, 13*cis*RA, and the CYP2D6 substrate, dextromethorphan, was conducted in eight healthy male volunteers. In response to exposure to 13*cis*RA and its metabolites *at*RA or 4-oxo-13*cis*RA, no down-regulation of CYP2D6 was observed. In fact, the increased oral clearance of dextromethorphan, increased dextrorphan-to-dextromethorphan AUC ratio, and increased formation clearance of dextrorphan

following dosing of 13*cis*RA all suggest induction, rather than down-regulation, of CYP2D6 in vivo. Data in mice indicate that CYP2D6 induction is likely driven by the activity of the primary circulating metabolite of 13*cis*RA, 4-oxo-13*cis*RA. To our knowledge this is the first report of a clinical study designed specifically to assess the potential for a DDI involving CYP down-regulation by a small molecule drug.

To determine whether induction of CYP2D6 observed in the clinic would be predicted from in vitro assessment, a thorough characterization of the effects of 13*cis*RA, *at*RA, and 4-oxo-13*cis*RA on CYP2D6 expression and activity in human hepatocytes was conducted. All retinoids were shown to down-regulate *CYP2D6* mRNA in vitro to a similar extent. A 2-fold increase in dextromethorphan AUC was predicted from in vitro data using steady state concentrations of 13*cis*RA, *at*RA, and 4-oxo-13*cis*RA from the clinical study. Interestingly, predictions for the increase in dextromethorphan following dosing of 13*cis*RA were driven by concentrations of 4-oxo-13*cis*RA, highlighting the fact that metabolites may be important precipitants of DDIs involving transcriptional regulation. This study clearly demonstrated a disconnect between down-regulation of CYP enzymes observed in vitro and in vivo. In contrast, induction of CYP3A4, likely mediated by activation of PXR/RXR by retinoids, was observed in hepatocytes and in the clinical study. The data generated here highlight the lack of understanding for the mechanisms involved in CYP down-regulation in vitro and the importance of mechanistic understanding to translate DDIs to the clinic.

In conclusion, the results from this thesis demonstrate that in vitro characterization of precipitants of DDIs must be coupled with a thorough understanding of transcriptional regulation of CYPs in vivo in order to correctly predict clinical DDIs.

BIBLIOGRAPHY

Adamson PC, Bailey J, Pluda J, Poplack DG, Bauza S, Murphy RF, Yarchoan R, and Balis FM (1995) Pharmacokinetics of all-trans-retinoic acid administered on an intermittent schedule. *J Clin Oncol* **13**:1238–1241.

Ahluwalia B, Gambhir K, and Sekhon H (1975) Distribution of labeled retinyl acetate and retinoic acid in rat and human testes. A possible site of retinyl acetate incorporation in rat testes. *J Nutr* **105**:467–474.

Allenby G, Bocquel MT, Saunders M, Kazmer S, Speck J, Rosenberger M, Lovey A, Kastner P, Grippo JF, and Chambon P (1993) Retinoic acid receptors and retinoid X receptors: interactions with endogenous retinoic acids. *Proc Natl Acad Sci U S A* **90**:30–4, National Academy of Sciences.

Altucci L, Leibowitz MD, Ogilvie KM, de Lera AR, and Gronemeyer H (2007) RAR and RXR modulation in cancer and metabolic disease. *Nat Rev Drug Discov* **6**:793–810.

Amory JKK, Ostrowski KAA, Gannon JRR, Berkseth K, Stevison F, Isoherranen N, Muller CHH, and Walsh T (2017) Isotretinoin administration improves sperm production in men with infertility from oligoasthenozoospermia: a pilot study. *Andrology* **5**:1115–1123.

Armstrong JL, Redfern CPF, and Veal GJ (2005) 13-cis Retinoic acid and isomerisation in paediatric oncology—is changing shape the key to success? *Biochem Pharmacol* **69**:1299–1306.

Armstrong JL, Taylor GA, Thomas HD, Boddy A V., Redfern CPF, and Veal GJ (2007) Molecular targeting of retinoic acid metabolism in neuroblastoma: the role of the CYP26 inhibitor R116010 in vitro and in vivo. *Br J Cancer* **96**:1675–1683.

Arnold SLM, Amory JK, Walsh TJ, and Isoherranen N (2012) A sensitive and specific method for measurement of multiple retinoids in human serum with UHPLC-MS/MS. *J Lipid Res* **53**:587–598.

Arnold SLM, Kent T, Hogarth CA, Griswold MD, Amory JK, and Isoherranen N (2015a) Pharmacological inhibition of ALDH1A in mice decreases all-trans retinoic acid concentrations in a tissue specific manner. *Biochem Pharmacol* **95**:177–192.

Arnold SLM, Kent T, Hogarth CA, Schlatt S, Prasad B, Haenisch M, Walsh T, Muller CH, Griswold MD, Amory JK, and Isoherranen N (2015b) Importance of ALDH1A enzymes in determining human testicular retinoic acid concentrations. *J Lipid Res* **56**:342–357.

Aström A, Pettersson U, Krust A, Chambon P, Voorhees JJ, Astrom A, Pettersson U, Krust A, Chambon P, and Voorhees JJ (1990) Retinoic acid and synthetic analogs differentially activate retinoic acid receptor dependent transcription. *Biochem Biophys Res Commun* **173**:339–345.

Baron JM, Heise R, Blaner WS, Neis M, Joussen S, Dreuw A, Marquardt Y, Saurat J-H, Merk HF, Bickers DR, and Jugert FK (2005) Retinoic Acid and its 4-Oxo Metabolites are Functionally Active in Human Skin Cells In Vitro. *J Invest Dermatol* **125**:143–153, Elsevier.

Berry DC, and Noy N (2009) All-trans-retinoic acid represses obesity and insulin resistance by activating both Peroxisome Proliferation-Activated Receptor &beta/&delta and Retinoic Acid Receptor. *Mol Cell Biol* **29**:3286–3296.

Bonet ML, Ribot J, and Palou A (2012) Lipid metabolism in mammalian tissues and its control by retinoic acid. *Biochim Biophys Acta* **1821**:177–189.

Borges S, Li L, Hamman MA, Jones DR, Hall SD, and Gorski JC (2005) Dextromethorphan to dextrorphan urinary metabolis ratio does not reflect dextromethorphan oral clearance. *Drug Metab Dispos* **33**:1052–55.

Boulias K, Katrakili N, Bamberg K, Underhill P, Greenfield A, and Talianidis I (2005) Regulation of hepatic metabolic pathways by the orphan nuclear receptor SHP. *EMBO J* **24**:2624–33, EMBO Press.

Brazzell RK, and Colburn WA (1982) Pharmacokinetics of the retinoids isotretinoin and etretinate. A comparative review. *J Am Acad Dermatol* **6**:643–51.

Brazzell RK, Vane FM, Ehmann CW, and Colburn W a (1983) Pharmacokinetics of isotretinoin during repetitive dosing to patients. *Eur J Clin Pharmacol* **24**:695–702.

Brown GT, Cash BG, Blihoghe D, Johansson P, Alnabulsi A, and Murray GI (2014) The expression and prognostic significance of retinoic acid metabolising enzymes in colorectal cancer. *PLoS One* **9**:e90776.

Busada JT, Kaye EP, Renegar RH, and Geyer CB (2014) Retinoic Acid Induces Multiple Hallmarks of the Prospermatogonia-to-Spermatogonia Transition in the Neonatal Mouse1. *Biol Reprod* **90**, Oxford University Press.

Cai S-Y, He H, Nguyen T, Mennone A, and Boyer JL (2010) Retinoic acid represses CYP7A1 expression in human hepatocytes and HepG2 cells by FXR/RXR-dependent and independent mechanisms. *J Lipid Res* **51**:2265–74, American Society for Biochemistry and Molecular Biology.

Cantorna MT, Nashold FE, and Hayes CE (1995) Vitamin A deficiency results in a priming environment conducive for Th1 cell development. *Eur J Immunol* **25**:1673–1679.

Chang C-L, Hong E, Lao-Sirieix P, and Fitzgerald RC (2008) A novel role for the retinoic acid-catabolizing enzyme CYP26A1 in Barrett's associated adenocarcinoma. *Oncogene* **27**:2951–2960.

Chen H, and Juchau MR (1997) Glutathione S-transferases act as isomerases in isomerization of 13-cis-retinoic acid to all-trans-retinoic acid in vitro. *Biochem J* **327**:721–726.

Chen S, Wang K, and Wan Y-JY (2010) Retinoids activate RXR/CAR-mediated pathway and induce CYP3A. *Biochem Pharmacol* **79**:270–276, NIH Public Access.

Chung SSW, and Wolgemuth DJ (2004) Role of retinoid signaling in the regulation of spermatogenesis. *Cytogenet Genome Res* **105**:189–202.

Colburn WA, Vane FM, and Shorter HJ (1983) Pharmacokinetics of isotretinoin and its major blood metabolite following a single oral dose to man. *Eur J Clin Pharmacol* **24**:689–694, Springer-Verlag.

Collins S (2002) The role of retinoids and retinoic acid receptors in normal hematopoiesis. *Leukemia* **16**:1896–1905.

D'Ambrosio DN, Clugston RD, and Blaner WS (2011) Vitamin A Metabolism: An Update. *Nutrients* **3**:63–103.

Davis JC, Snyder EM, Hogarth CA, Small C, and Griswold MD (2013) Induction of spermatogenic synchrony by retinoic acid in neonatal mice. *Spermatogenesis* **3**:e23180.

Diaz P, Huang W, Keyari CM, Buttrick B, Price L, Guilloteau N, Tripathy S, Sperandio VG, Fronczek FR, Astruc-Diaz F, and Isoherranen N (2016) Development and characterization of novel and selective inhibitors of cytochrome P450 CYP26A1, the human liver retinoic acid hydroxylase. *J Med Chem* **59**:2579–2595.

Dickmann LJ, Patel SK, Rock DA, Wienkers LC, and Slatter JG (2011) Effects of Interleukin-6 (IL-6) and an Anti-IL-6 Monoclonal Antibody on Drug-Metabolizing Enzymes in Human Hepatocyte Culture. *Drug Metab Dispos* **39**:1415–1422.

Dickmann LJ, Tay S, Senn TD, Zhang H, Visone A, Unadkat JD, Hebert MF, and Isoherranen N (2008) Changes in maternal liver Cyp2c and Cyp2d expression and activity during rat pregnancy. *Biochem Pharmacol* **75**:1677–1687, Elsevier.

Duester G (2008) Retinoic Acid Synthesis and Signaling during Early Organogenesis. *Cell* **134**:921–931.

Einolf HJ, Chen L, Fahmi OA, Gibson CR, Obach RS, Shebley M, Silva J, Sinz MW, Unadkat JD, Zhang L, and Zhao P (2014) Evaluation of Various Static and Dynamic Modeling Methods to Predict Clinical CYP3A Induction Using In Vitro CYP3A4 mRNA Induction Data. *Clin Pharmacol Ther* **95**:179–188, Wiley-Blackwell.

EMA (2012) *Guideline on the investigation of drug interactions*.

Evers R, Dallas S, Dickmann LJ, Fahmi OA, Kenny JR, Kraynov E, Nguyen T, Patel AH, Slatter JG, and Zhang L (2013) Critical Review of Preclinical Approaches to Investigate Cytochrome P450-Mediated Therapeutic Protein Drug-Drug Interactions and Recommendations for Best Practices: A White Paper. *Drug Metab Dispos* **41**:1598–1609.

Fahmi OA, Hurst S, Plowchalk D, Cook J, Guo F, Youdim K, Dickins M, Phipps A, Darekar A,

Hyland R, and Obach RS (2009) Comparison of different algorithms for predicting clinical drug-drug interactions, based on the use of CYP3A4 in vitro data: predictions of compounds as precipitants of interaction. *Drug Metab Dispos* **37**:1658–66, American Society for Pharmacology and Experimental Therapeutics.

Fahmi OA, Kish M, Boldt S, and Scott Obach R (2010) Cytochrome P450 3A4 mRNA is a more reliable marker than CYP3A4 activity for detecting pregnane X receptor-activated induction of drug-metabolizing enzymes. *Drug Metab Dispos* **38**:1605–1611.

Fahmi OA, Maurer TS, Kish M, Cardenas E, Boldt S, and Nettleton D (2008) A combined model for predicting CYP3A4 clinical net drug-drug interaction based on CYP3a4 inhibition, inactivation, and induction determined in vitro. *Drug Metab Dispos* **36**:1698–1708.

Fahmi OA, and Ripp SL (2010) Evaluation of models for predicting drug-drug interactions due to induction. *Expert Opin Drug Metab Toxicol* **6**:1399–1416, Taylor & Francis.

Fenaux P, Wang ZZ, and Degos L (2007) Treatment of acute promyelocytic leukemia by retinoids. *Curr Top Microbiol Immunol* **313**:101–128.

Food and Drug Administration (2017a) *Clinical Drug Interaction Studies — Study Design, Data Analysis, and Clinical Implications Guidance for Industry*.

Food and Drug Administration (2017b) *In Vitro Metabolism- and Transporter-Mediated Drug-Drug Interaction Studies Guidance for Industry*.

Fransén K, Franzén P, Magnuson A, Elmabsout AA, Nyhlin N, Wickbom A, Curman B, Törkvist L, D'Amato M, Bohr J, Tysk C, Sirsjö A, Halfvarson J, Fransen K, Franzén P, Magnuson A, Elmabsout AA, Nyhlin N, Wickbom A, Curman B, Törkvist L, D'Amato M, Bohr J, Tysk C, Sirsjö A, and Halfvarson J (2013) Polymorphism in the retinoic acid metabolizing enzyme CYP26B1 and the development of Crohn's disease. *PLoS One* **8**:1–5.

Gaedigk A, Sangkuhl K, Whirl-Carrillo M, Klein T, and Steven Leeder J (2017) Prediction of CYP2D6 phenotype from genotype across world populations. *Genet Med* **19**:69–76.

Gibson CR, Lin C, Singh R, Brown CM, Richards K, Brunner J, Michel K, Adelsberger J, Carlini E, Boothe-Genthe C, Raab C, Luu M, Michael A, Parikh M, Ciecko P, Subramanian R, Krolikowski P, Rodrigues AD, Baillie TA, and Rushmore TH (2005) Induction of CYP1A in the beagle dog by an inhibitor of kinase insert domain-containing receptor: Differential effects in vitro and in vivo on mRNA and functional activity. *Drug Metab Dispos* **33**:1044–1051.

Goodwin B, Jones SA, Price RR, Watson MA, McKee DD, Moore LB, Galardi C, Wilson JG, Lewis MC, Roth ME, Maloney PR, Willson TM, and Kliewer SA (2000) A Regulatory Cascade of the Nuclear Receptors FXR, SHP-1, and LRH-1 Represses Bile Acid Biosynthesis. *Mol Cell* **6**:517–526, Cell Press.

Griswold MD (2016) Spermatogenesis: The commitment to meiosis. *Physiol Rev* **96**:1–17.

Gudas LJ (2012) Emerging roles for retinoids in regeneration and differentiation in normal and disease states. *Biochim Biophys Acta* **1821**:213–221, Elsevier B.V.

Gudas LJ, and Wagner JA (2011) Retinoids regulate stem cell differentiation. *J Cell Physiol* **226**:322–330.

Guidez F, Ivins S, Zhu J, Söderström M, Waxman S, and Zelent A (1998) Reduced Retinoic Acid-Sensitivities of Nuclear Receptor Corepressor Binding to PML- and PLZF-RARα Underlie Molecular Pathogenesis and Treatment of Acute Promyelocytic Leukemia. *Blood* **91**:2634–2642.

Halladay JS, Wong S, Khojasteh SC, and Grepper S (2012) An 'all-inclusive' 96-well cytochrome P450 induction method: Measuring enzyme activity, mRNA levels, protein levels, and cytotoxicity from one well using cryopreserved human hepatocytes. *J Pharmacol Toxicol Methods* **66**:270–275, Elsevier.

Hariparsad N, Ramsden D, Palamanda J, Dekeyser JG, Fahmi OA, Kenny JR, Einolf H, Mohutsky M, Pardon M, Siu YA, Chen L, Sinz M, Jones B, Walsky R, Dallas S, Balani SK, Zhang G, Buckley D, and Tweedie D (2017) Considerations from the IQ Induction Working Group in Response to Drug-Drug Interaction Guidance from Regulatory Agencies: Focus on Downregulation, CYP2C Induction, and CYP2B6 Positive Control. *Drug Metab Dispos* **45**:1049–1059, American Society for Pharmacology and Experimental Therapeutics.

Heise R, Mey J, Neis MM, Marquardt Y, Joussen S, Ott H, Wiederholt T, Kurschat P, Megahed M, Bickers DR, Merk HF, and Baron JM (2006) Skin retinoid concentrations are modulated by CYP26AI expression restricted to basal keratinocytes in normal human skin and differentiated 3D skin models. *J Invest Dermatol* **126**:2473–2480.

Heyman RA, Mangelsdorf DJ, Dyck JA, Stein RB, Eichele G, Evans RM, and Thaller C (1992) 9-cis retinoic acid is a high affinity ligand for the retinoid X receptor. *Cell* **68**:397–406, Cell Press.

Ho M-F, Correia C, Ingle JN, Kaddurah-Daouk R, Wang L, Kaufmann SH, and Weinshilboum RM (2018) Ketamine and ketamine metabolites as novel estrogen receptor ligands: Induction of cytochrome P450 and AMPA glutamate receptor gene expression. *Biochem Pharmacol* **152**:279–292, Elsevier.

Hogarth CA, Arnold S, Kent T, Mitchell D, Isoherranen N, and Griswold MD (2015) Processive pulses of retinoic acid propel asynchronous and continuous murine sperm production. *Biol Reprod* **92**:37.

Hogarth CA, Evans E, Onken J, Kent T, Mitchell D, Petkovich M, and Griswold MD (2015) CYP26 enzymes are necessary within the postnatal seminiferous epithelium for normal murine spermatogenesis. *Biol Reprod* **93**:19, Oxford University Press.

Hogarth CA, and Griswold MD (2013a) Immunohistochemical approaches for the study of spermatogenesis. *Methods Mol Biol* **927**:309–320.

Hogarth CA, and Griswold MD (2013b) Retinoic acid regulation of male meiosis. *Curr Opin Endocrinol Diabetes Obes* **20**:217–223.

Idres N, Marill J, Flexor MA, and Chabot GG (2002) Activation of retinoic acid receptor-dependent transcription by all-trans-retinoic acid metabolites and isomers. *J Biol Chem* **277**:31491–31498.

J. Dickmann L, K. Patel S, C. Wienkers L, and Greg Slatter J (2012) Effects of Interleukin 1β (IL-1β) and IL-1β/Interleukin 6 (IL-6) Combinations on Drug Metabolizing Enzymes in Human Hepatocyte Culture. *Curr Drug Metab* **13**:930–937.

Jiang X, Zhuang Y, Xu Z, Wang W, and Zhou H (2016) Development of a Physiologically Based Pharmacokinetic Model to Predict Disease-Mediated Therapeutic Protein–Drug Interactions: Modulation of Multiple Cytochrome P450 Enzymes by Interleukin-6. *AAPS J* **18**:767–776.

Jing J, Nelson C, Paik J, Shirasaka Y, Amory JK, and Isoherranen N (2017) Physiologically Based Pharmacokinetic Model of All-trans-Retinoic Acid with Application to Cancer Populations and Drug Interactions. *J Pharmacol Exp Ther* **361**:246–258.

Johänning J, Kröner P, Thomas M, Zanger UM, Nörenberg A, Eichelbaum M, Schwab M, Brauch H, Schroth W, and Mürdter TE (2018) The formation of estrogen-like tamoxifen metabolites and their influence on enzyme activity and gene expression of ADME genes. *Arch Toxicol* **92**:1099–1112, Springer Berlin Heidelberg.

Kakizuka A, Miller Jr. WH, Umesono K, Warrell Jr. RP, Frankel SR, Murty VVVS, Dmitrovsky E, and Evans RM (1991) Chromosomal translocation t(15;17) in human acute promyelocytic leukemia fuses RARα with a novel putative transcription factor, PML. *Cell* **66**:663–674.

Kane MA, Folias AE, Pingitore A, Perri M, Obrochta KM, Krois CR, Cione E, Ryu JY, and Napoli JL (2010) Identification of 9-cis-retinoic acid as a pancreas-specific autacoid that attenuates glucose-stimulated insulin secretion. *Proc Natl Acad Sci U S A* **107**:21884–9.

Kane MA, Folias AE, Wang C, and Napoli JL (2008) Quantitative Profiling of Endogenous Retinoic Acid in Vivo and in Vitro by Tandem Mass Spectrometry. *Anal Chem* **80**:1702–1708.

Kedishvili NY (2013) Enzymology of retinoic acid biosynthesis and degradation. *J Lipid Res* **54**:1744–1760.

Khoo K-C, Reik D, and Colburn WA (1982) Pharmacokinetics of Isotretinoin Following a Single Oral Dose. *J Clin Pharmacol* **22**:395–402, Blackwell Publishing Ltd.

Khoo K-C, Reik D, and Colburn WA (1992) Pharmacokinetics of Isotretinoin Following a Single Oral Dose. *J Clin Pharmacol* **22**:395–402, Blackwell Publishing Ltd.

Kim I, Ahn S-H, Inagaki T, Choi M, Ito S, Guo GL, Kliewer SA, and Gonzalez FJ (2007)

Differential regulation of bile acid homeostasis by the farnesoid X receptor in liver and intestine. *J Lipid Res* **48**:2664–2672.

Koh KH, Pan X, Shen H-W, Arnold SLM, Yu A-M, Gonzalez FJ, Isoherranen N, and Jeong H (2014) Altered expression of small heterodimer partner governs cytochrome P450 (CYP) 2D6 induction during pregnancy in CYP2D6-humanized mice. *J Biol Chem* **289**:3105–3113.

Krivospitskaya O, Elmabsout AA, Sundman E, Söderström LA, Ovchinnikova O, Gidlöf AC, Scherbak N, Norata GD, Samnegård A, Törmä H, Abdel-Halim SM, Jansson J-H, Eriksson P, Sirsjö A, and Olofsson PS (2012) A CYP26B1 polymorphism enhances retinoic acid catabolism and may aggravate atherosclerosis. *Mol Med* **18**:712–718.

Kurlandsky SB, Gamble M V., Ramakrishnan R, and Blaner WS (1995) Plasma delivery of retinoic acid to tissues in the rat. *J Biol Chem* **270**:17850–17857.

Lee CM, Pohl J, and Morgan ET (2009) Dual mechanisms of CYP3A protein regulation by proinflammatory cytokine stimulation in primary hepatocyte cultures. *Drug Metab Dispos* **37**:865–872.

Lee SS, Cha E-Y, Jung H-J, Shon J-H, Kim E-Y, Yeo C-W, and Shin J-G (2008) Genetic polymorphism of hepatocyte nuclear factor-4alpha influences human cytochrome P450 2D6 activity. *Hepatology* **48**:635–645.

Li H, MacLean G, Cameron D, Clagett-Dame M, and Petkovich M (2009) Cyp26b1 expression in murine Sertoli cells is required to maintain male germ cells in an undifferentiated state during embryogenesis. *PLoS One* **4**:e7501.

Liu Y, Chen H, Wang J, Zhou W, Sun R, and Xia M (2015) Association of serum retinoic acid with hepatic steatosis and liver injury in nonalcoholic fatty liver disease. *Am J Clin Nutr* **102**:130–137.

Lucek RW, and Colburn WA (1985) Clinical Pharmacokinetics of the Retinoids. *Clin Pharmacokinet* **10**:38–62.

Lutz JD, Dixit V, Yeung CK, Dickmann LJ, Zelter A, Thatcher JE, Nelson WL, and Isoherranen N (2009) Expression and functional characterization of cytochrome P450 26A1, a retinoic acid hydroxylase. *Biochem Pharmacol* **77**:258–268.

Lutz JD, and Isoherranen N (2011) Prediction of Relative In Vivo Metabolite Exposure from In Vitro Data Using Two Model Drugs: Dextromethorphan and Omeprazole. *Drug Metab Dispos* **40**:159–168.

MacHavaram KK, Almond LM, Rostami-Hodjegan A, Gardner I, Jamei M, Tay S, Wong S, Joshi A, and Kenny JR (2013) A physiologically based pharmacokinetic modeling approach to predict disease-drug interactions: Suppression of CYP3A by IL-6. *Clin Pharmacol Ther* **94**:260–268.

Mamoon A, Subauste A, Subauste MC, and Subauste J (2014) Retinoic acid regulates several genes in bile acid and lipid metabolism via upregulation of small heterodimer partner in hepatocytes. *Gene* **550**:165–170.

Mamoon A, Ventura-Holman T, Maher JF, and Subauste JS (2008) Retinoic acid responsive genes in the murine hepatocyte cell line AML 12. *Gene* **408**:95–103.

Marill J, Capron CC, Idres N, and Chabot GG (2002) Human cytochrome P450s involved in the metabolism of 9-cis- and 13-cis-retinoic acids. *Biochem Pharmacol* **63**:933–943.

Marill J, Cresteil T, Lanotte M, and Chabot GG (2000) Identification of human cytochrome P450s involved in the formation of all-trans-retinoic acid principal metabolites. *Mol Pharmacol* **58**:1341–1348.

Martens JHA, Brinkman AB, Simmer F, Francoijs K-J, Nebbioso A, Ferrara F, Altucci L, and Stunnenberg HG (2010) PML-RARα/RXR Alters the Epigenetic Landscape in Acute Promyelocytic Leukemia. *Cancer Cell* **17**:173–185.

Matthay KK (2013) Targeted isotretinoin in neuroblastoma: kinetics, genetics, or absorption. *Clin Cancer Res* **19**:311–313.

McCormick AM, Kroll KD, and Napoli JL (1983) 13-cis-Retinoic acid metabolism in vivo. The major tissue metabolites in the rat have the all-trans configuration. *Biochemistry* **22**:3933–3940.

McSorley LC, and Daly AK (2000) Identification of human cytochrome P450 isoforms that contribute to all-trans-retinoic acid 4-hydroxylation. *Biochem Pharmacol* **60**:517–526.

Moulas AN, Gerogianni IC, Papadopoulos D, and Gourgoulianis KI (2006) Serum retinoic acid, retinol and retinyl palmitate levels in patients with lung cancer. *Respirology* **11**:169–174.

Muindi J, Frankel SR, Miller WHJ, Jakubowski A, Scheinberg DA, Young CW, Dmitrovsky E, and Warrell RJP (1992) Continuous treatment with all-trans retinoic acid causes a progressive reduction in plasma drug concentrations: implications for relapse and retinoid "resistance" in patients with acute promyelocytic leukemia. *Blood* **79**:299–303.

Muindi JR, Roth MD, Wise RA, Connett JE, O'Connor GT, Ramsdell JW, Schluger NW, Romkes M, Branch RA, and Sciurba FC (2008a) Pharmacokinetics and metabolism of all-trans- and 13-cis-retinoic acid in pulmonary emphysema patients. *J Clin Pharmacol* **48**:96–107, Blackwell Publishing Ltd.

Muindi JR, Roth MD, Wise RA, Connett JE, O'Connor GT, Ramsdell JW, Schluger NW, Romkes M, Branch RA, and Sciurba FC (2008b) Pharmacokinetics and metabolism of all-trans- and 13-cis-retinoic acid in pulmonary emphysema patients. *J Clin Pharmacol* **48**:96–107, Blackwell Publishing Ltd.

Nadin L, and Murray M (1999) Participation of CYP2C8 in retinoic acid 4-hydroxylation in human hepatic microsomes. *Biochem Pharmacol* **58**:1201–1208.

Napoli JL (2012) Physiological insights into all-trans-retinoic acid biosynthesis. *Biochim Biophys Acta* **1821**:152–167.

Nau H (2001) Teratogenicity of isotretinoin revisited: species variation and the role of all-trans-retinoic acid. *J Am Acad Dermatol* **45**:S183-7.

Nelson CH, Buttrick BR, and Isoherranen N (2013) Therapeutic potential of the inhibition of the retinoic acid hydroxylases CYP26A1 and CYP26B1 by xenobiotics. *Curr Top Med Chem* **13**:1402–1428.

Njar VCO, Gediya L, Purushottamachar P, Chopra P, Vasaitis TS, Khandelwal A, Mehta J, Huynh C, Belosay A, and Patel J (2006) Retinoic acid metabolism blocking agents (RAMBAs) for treatment of cancer and dermatological diseases. *Bioorg Med Chem* **14**:4323–4340.

Noy N (2010) Between death and survival: retinoic acid in regulation of apoptosis. *Annu Rev Nutr* **30**:201–217.

Nya-Ngatchou JJ, Arnold SLM, Walsh TJ, Muller CH, Page ST, Isoherranen N, and Amory JK (2013) Intratesticular 13-cis retinoic acid is lower in men with abnormal semen analyses: a pilot study. *Andrology* **1**:325–331.

Özdemir M, Crewe KH, Tucker GT, and Rostami-Hodjegan A (2004) Assessment of In Vivo CYP2D6 Activity: Differential Sensitivity of Commonly Used Probes to Urine pH. *J Clin Pharmacol* **44**:1398–1404, Wiley-Blackwell.

Ozpolat B, Lopez-Berestein G, Adamson P, Fu CJ, and Williams AH (2003a) Pharmacokinetics of intravenously administered liposomal all-trans-retinoic acid (ATRA) and orally administered ATRA in healthy volunteers. *J Pharm Pharm Sci* **6**:292–301.

Ozpolat B, Lopez-Berestein G, Adamson P, Fu CJ, and Williams AH (2003b) Pharmacokinetics of intravenously administered liposomal all-trans-retinoic acid (ATRA) and orally administered ATRA in healthy volunteers. *J Pharm Pharm Sci* **6**:292–301.

Ozpolat B, Mehta K, Tari AM, and Lopez-Berestein G (2002) All-trans-retinoic acid-induced expression and regulation of retinoic acid 4-hydroxylase (CYP26) in human promyelocytic leukemia. *Am J Hematol* **70**:39–47.

Pan X, and Jeong H (2015) Estrogen-Induced Cholestasis Leads to Repressed CYP2D6 Expression in CYP2D6-Humanized Mice s. *Mol Pharmacol* **88**:106–112.

Pan X, Kent R, Won K-J, and Jeong H (2017a) Cholic Acid Feeding Leads to Increased CYP2D6 Expression in CYP2D6-Humanized Mice s. *Drug Metab Dispos* **45**:346–352.

Pan X, Lee Y-K, and Jeong H (2015) Farnesoid X Receptor Angonist Represses Cytochrome P450 2D6 Expression by Upregulating Small Heterodimer Partner. *Drug Metab Dispos* **43**:1002–7.

Pan X, Ning M, and Jeong H (2017b) Transcriptional regulation of CYP2D6 expression. *Drug Metab Dispos* **45**:42–48.

Pandolfi PP, Grignani F, Alcalay M, Mencarelli A, Biondi A, LoCoco F, Grignani F, and Pelicci PG (1991) Structure and origin of the acute promyelocytic leukemia myl/RAR alpha cDNA and characterization of its retinoid-binding and transactivation properties. *Oncogene* **6**:1285–1292.

Peng C-C, Templeton I, Thummel KE, Davis C, Kunze KL, and Isoherranen N (2011) Evaluation of 6β-hydroxycortisol, 6β-hydroxycortisone, and a combination of the two as endogenous probes for inhibition of CYP3A4 in vivo. *Clin Pharmacol Ther* **89**:888–895, Nature Publishing Group.

Peng L, Yoo B, Gunewardena SS, Lu H, Klaassen CD, and Zhong X -b. (2012) RNA sequencing reveals dynamic changes of mRNA abundance of cytochromes P450 and their alternative transcripts during mouse liver development. *Drug Metab Dispos* **40**:1198–1209.

Reynolds CP, Matthay KK, Villablanca JG, and Maurer BJ (2003) Retinoid therapy of high-risk neuroblastoma. *Cancer Lett* **197**:185–192.

Reynolds CP, Schindler PF, Jones DM, Gentile JL, Proffitt RT, and Einhorn PA (1994) Comparison of 13-cis-retinoic acid to trans-retinoic acid using human neuroblastoma cell lines. *Prog Clin Biol Res* **385**:237–244.

Rosenberger M, and Neukom C (1982) Retinoic acid metabolites. 3. Total synthesis of (2E,4E,6E,8E)-3,7-dimethyl-9-[6,6-dimethyl-2-(hydroxymethyl)-1-cyclohexen-1-yl]-2,4,6,8-nonatetraenoic acid. *J Org Chem* **47**:1782–1785.

Ross AC (2012) Vitamin A and retinoic acid in T cell-related immunity. *Am J Clin Nutr* **96**:1166S–1172S.

Ross AC, Cifelli CJ, Zolfaghari R, and Li N-Q (2011) Multiple cytochrome P-450 genes are concomitantly regulated by vitamin A under steady-state conditions and by retinoic acid during hepatic first-pass metabolism. *Physiol Genomics* **43**:57–67.

Rowbotham SE, Illingworth NA, Daly AK, Veal GJ, and Boddy A V (2010) Role of UDP-Glucuronosyltransferase Isoforms in 13 -cis Retinoic Acid Metabolism in Humans. *Drug Metab Dispos* **38**:1211–1217.

Russell LD, Ettlin RA, Hikim APS, and Clegg ED (1993) Histological and histopathological evaluation of the testis. *Int J Androl* **16**:83.

Ruzicka T, Larsen FG, Galewicz D, Horváth A, Coenraads PJ, Thestrup-Pedersen K, Ortonne JP, Zouboulis CC, Harsch M, Brown TC, and Zultak M (2004) Oral alitretinoin (9-cis-retinoic acid) therapy for chronic hand dermatitis in patients refractory to standard therapy: results of a randomized, double-blind, placebo-controlled, multicenter trial. *Arch Dermatol* **140**:1453–1459.

Sager JE, Lutz JD, Foti RS, Davis C, Kunze KL, and Isoherranen N (2014) Fluoxetine- and norfluoxetine-mediated complex drug-drug interactions: in vitro to in vivo correlation of effects on CYP2D6, CYP2C19, and CYP3A4. *Clin Pharmacol Ther* **95**:653–62, Nature Publishing Group.

Sager JE, Tripathy S, Price LSL, Nath A, Chang J, Stephenson-Famy A, and Isoherranen N (2017) In vitro to in vivo extrapolation of the complex drug-drug interaction of bupropion and its metabolites with CYP2D6; simultaneous reversible inhibition and CYP2D6 downregulation. *Biochem Pharmacol* **123**:85–96.

Samokyszyn VM, Gall WE, Zawada G, Freyaldenhoven MA, Chen G, Mackenzie PI, Tephly TR, and Radominska-Pandya A (2000) 4-hydroxyretinoic acid, a novel substrate for human liver microsomal UDP-glucuronosyltransferase(s) and recombinant UGT2B7. *J Biol Chem* **275**:6908–6914, American Society for Biochemistry and Molecular Biology.

Sass JO, Forster A, Bock KW, and Nau H (1994) Glucuronidation and isomerization of all-trans- and 13-CIS-retinoic acid by liver microsomes of phenobarbital- or 3-methylcholanthrene-treated rats. *Biochem Pharmacol* **47**:485–492.

Schmitt C, Kuhn B, Zhang X, Kivitz A, and Grange S (2011) Disease-drug-drug interaction involving tocilizumab and simvastatin in patients with rheumatoid arthritis. *Clin Pharmacol Ther* **89**:735–740, Nature Publishing Group.

Schneider EK (2017) Cytochrome P450 3A4 Induction: Lumacaftor versus Ivacaftor Potentially Resulting in Significantly Reduced Plasma Concentration of Ivacaftor. *Drug Metab Lett* **11**:1–4.

Schoeff L (1983) Vitamin A. *Am J Med Technol* **49**:447–452.

Schug TT, Berry DC, Shaw NS, Travis SN, and Noy N (2007) Opposing Effects of Retinoic Acid on Cell Growth Result from Alternate Activation of Two Different Nuclear Receptors. *Cell* **129**:723–733, Cell Press.

Shelton DN, Sandoval IT, Eisinger A, Chidester S, Ratnayake A, Ireland CM, and Jones DA (2006) Up-regulation of CYP26A1 in adenomatous polyposis coli-deficient vertebrates via a WNT-dependent mechanism: implications for intestinal cell differentiation and colon tumor development. *Cancer Res* **66**:7571–7577.

Shimamoto Y, Ishida J, Yamagata K, Saito T, Kato H, Matsuoka T, Hirota K, Daitoku H, Nangaku M, Yamagata K, Fujii H, Takeda J, and Fukamizu A (2004) Inhibitory effect of the small heterodimer partner on hepatocyte nuclear factor-4 mediates bile acid-induced repression of the human angiotensinogen gene. *J Biol Chem* **279**:7770–6, American Society for Biochemistry and Molecular Biology.

Shin K-H, Choi MH, Lim KS, Yu K-S, Jang I-J, and Cho J-Y (2013) Evaluation of Endogenous Metabolic Markers of Hepatic CYP3A Activity Using Metabolic Profiling and Midazolam Clearance. *Clin Pharmacol Ther* **94**:601–609.

Shirasaka Y, Sager JE, Lutz JD, Davis C, and Isoherranen N (2013) Inhibition of CYP2C19 and CYP3A4 by omeprazole metabolites and their contribution to drug-drug interactions. *Drug Metab Dispos* **41**:1414–1424.

Sinz MW (2013) Evaluation of pregnane X receptor (PXR)-mediated CYP3A4 drug-drug interactions in drug development. *Drug Metab Rev* **45**:3–14, Taylor & Francis.

Sklan D (1987) Vitamin A in human nutrition. *Prog Food Nutr Sci* **11**:39–55.

Smith JE, Milch PO, Muto Y, and Goodman DS (1973) The plasma transport and metabolism of retinoic acid in the rat. *Biochem J* **132**:821–827.

Snyder EM, Davis JC, Zhou Q, Evanoff R, and Griswold MD (2011) Exposure to Retinoic Acid in the Neonatal but Not Adult Mouse Results in Synchronous Spermatogenesis1. *Biol Reprod* **84**:886–893.

Sonawane P, Cho HE, Tagde A, Verlekar D, Yu AL, Reynolds CP, and Kang MH (2014) Metabolic characteristics of 13-cis-retinoic acid (isotretinoin) and anti-tumour activity of the 13-cis-retinoic acid metabolite 4-oxo-13-cis-retinoic acid in neuroblastoma. *Br J Pharmacol* **171**:5330–5344.

Stanley LA, Horsburgh BC, Ross J, Scheer N, and Roland Wolf C (2006) PXR and CAR: Nuclear Receptors which Play a Pivotal Role in Drug Disposition and Chemical Toxicity. *Drug Metab Rev* **38**:515–597, Taylor & Francis.

Stevison F, Hogarth C, Tripathy S, Kent T, and Isoherranen N (2017) Inhibition of the all-trans retinoic acid (atRA) hydroxylases CYP26A1 and CYP26B1 results in dynamic, tissue-specific changes in endogenous atRA signaling. *Drug Metab Dispos* **45**.

Stoppie P, Borgers M, Borghgraef P, Dillen L, Goossens J, Sanz G, Szel H, Van Hove C, Van Nyen G, Nobels G, Vanden Bossche H, Venet M, Willemsens G, and Van Wauwe J (2000) R115866 inhibits all-trans-retinoic acid metabolism and exerts retinoidal effects in rodents. *J Pharmacol Exp Ther* **293**:304–312.

Sugiyama I, Murayama N, Kuroki A, Kota J, Iwano S, Yamazaki H, and Hirota T (2016) Evaluation of cytochrome P450 inductions by anti-epileptic drug oxcarbazepine, 10-hydroxyoxcarbazepine, and carbamazepine using human hepatocytes and HepaRG cells. *Xenobiotica* **46**:765–774, Taylor & Francis.

Tang X-H, and Gudas LJ (2011) Retinoids, Retinoic Acid Receptors, and Cancer. *Annu Rev Pathol Mech Dis* **6**:345–364.

Tay S, Dickmann L, Dixit V, and Isoherranen N (2010) A comparison of the roles of peroxisome proliferator-activated receptor and retinoic acid receptor on CYP26 regulation. *Mol Pharmacol* **77**:218–227.

Thatcher JE, Buttrick B, Shaffer SA, Shimshoni JA, Goodlett DR, Nelson WL, and Isoherranen N (2011) Substrate specificity and ligand interactions of CYP26A1, the human liver retinoic

acid hydroxylase. *Mol Pharmacol* **80**:228–239.

Thatcher JE, and Isoherranen N (2009) The role of CYP26 enzymes in retinoic acid clearance. *Expert Opin Drug Metab Toxicol* **18**:1199–1216, Taylor & Francis.

Thatcher JE, Zelter A, and Isoherranen N (2010) The relative importance of CYP26A1 in hepatic clearance of all-trans retinoic acid. *Biochem Pharmacol* **80**:903–912.

Thudi NR, Shrivastav VK, Monif T, Khuroo A, Gurule S, Partani PO, Tandon M, and Mathur R (2011) Pharmacokinetic and bioequivalence study of endogenous compound tretinoin 10 mg capsules in healthy volunteers by base line correction approach. *Clin Res Regul Aff* **28**:68–73, Taylor & Francis.

Topletz AR, Le HN, Lee N, Chapman JD, Kelly EJ, Wang J, and Isoherranen N (2013) Hepatic Cyp2d and Cyp26a1 mRNAs and activities are increased during mouse pregnancy. *Drug Metab Dispos* **41**:312–319, American Society for Pharmacology and Experimental Therapeutics.

Topletz AR, Thatcher JE, Zelter A, Lutz JD, Tay S, Nelson WL, and Isoherranen N (2012) Comparison of the function and expression of CYP26A1 and CYP26B1, the two retinoic acid hydroxylases. *Biochem Pharmacol* **83**:149–163.

Topletz AR, Tripathy S, Foti RS, Shimshoni JA, Nelson WL, and Isoherranen N (2015) Induction of CYP26A1 by metabolites of retinoic acid: Evidence that CYP26A1 is an important enzyme in the elimination of active retinoids. *Mol Pharmacol* **87**:430–441, American Society for Pharmacology and Experimental Therapeutics.

Tripathy S, Chapman JD, Han CY, Hogarth CA, Arnold SLM, Onken J, Kent T, Goodlett DR, and Isoherranen N (2016) All-trans-retinoic acid enhances mitochondrial function in models of human liver. *Mol Pharmacol* **89**:560–574.

Tsukada M, Schröder M, Roos TC, Chandraratna RA, Reichert U, Merk HF, Orfanos CE, and Zouboulis CC (2000) 13-cis retinoic acid exerts its specific activity on human sebocytes through selective intracellular isomerization to all-trans retinoic acid and binding to retinoid acid receptors. *J Invest Dermatol* **115**:321–327.

Van Wauwe JP, Coene MC, Goossens J, Cools W, and Monbaliu J (1990) Effects of cytochrome P-450 inhibitors on the in vivo metabolism of all-trans-retinoic acid in rats. *J Pharmacol Exp Ther* **252**:365–369.

Vane FM, and Buggé CJ (1981) Identification of 4-Oxo-13-cis-Retinoic Acid As the Major Metabolite of 13-cis-Retinoic Acid in Human Blood. *Drug Metab Dispos* **9**:515–520.

Vane FM, Bugge CJ, Rodriguez LC, Rosenberger M, and Doran TI (1990) Human biliary metabolites of isotretinoin: identification, quantification, synthesis, and biological activity. *Xenobiotica* **20**:193–207.

Veal GJ, Cole M, Errington J, Pearson ADJ, Foot ABM, Whyman G, Boddy A V., and

UKCCSG Pharmacology Working Group (2007) Pharmacokinetics and metabolism of 13-cis-retinoic acid (isotretinoin) in children with high-risk neuroblastoma - a study of the United Kingdom Children's Cancer Study Group. *Br J Cancer* **96**:424–431.

Veal GJ, Errington J, Redfern CPF, Pearson ADJ, and Boddy A V. (2002) Influence of isomerisation on the growth inhibitory effects and cellular activity of 13-cis and all-trans retinoic acid in neuroblastoma cells. *Biochem Pharmacol* **63**:207–215.

Venkatakrishnan K, and Obach RS (2005) In vitro-in vivo extrapolation of CYP2D6 inactivation by paroxetine: Prediction of nonstationary pharmacokinetics and drug interaction magnitude. *Drug Metab Dispos* **33**.

Verfaille CJ, Coel M, Boersma IH, Mertens J, Borgers M, and Roseeuw D (2007) Oral R115866 in the treatment of moderate to severe facial acne vulgaris: an exploratory study. *Br J Dermatol* **157**:122–126.

Verfaille CJ, Thissen CACB, Bovenschen HJ, Mertens J, Steijlen PM, and van de Kerkhof PCM (2007) Oral R115866 in the treatment of moderate to severe plaque-type psoriasis. *J Eur Acad Dermatology Venereol* **21**:1038–1046.

Vernet N, Dennefeld C, Rochette-Egly C, Oulad-Abdelghani M, Chambon P, Ghyselinck NB, and Mark M (2006) Retinoic Acid Metabolism and Signaling Pathways in the Adult and Developing Mouse Testis. *Endocrinology* **147**:96–110.

Wang K, Chen S, Xie W, and Wan Y-JY (2008) Retinoids induce cytochrome P450 3A4 through RXR/VDR-mediated pathway. *Biochem Pharmacol* **75**:2204–2213, Elsevier.

Wolbach SB, and Howe PR (1925) Tissue changes following deprication of fat-soluble A vitamin. *J Exp Med* **42**:753–777.

Wu S-J, Chen Y-J, Shieh T-Y, Chen C-M, Wang Y-Y, Lee K-T, Lin Y-M, Chien P-H, and Chen P-H (2015) Association study between novel CYP26 polymorphisms and the risk of Betel Quid-related malignant oral disorders. *Sci World J* **2015**:1–9.

Xia H-F, Ma J-J, Sun J, Yang Y, and Peng J-P (2010) Retinoic acid metabolizing enzyme CYP26A1 is implicated in rat embryo implantation. *Hum Reprod* **25**:2985–2998.

Xu Y, Hijazi Y, Wolf A, Wu B, Sun Y-N, and Zhu M (2015) Physiologically Based Pharmacokinetic Model to Assess the Influence of Blinatumomab-Mediated Cytokine Elevations on Cytochrome P450 Enzyme Activity. *CPT Pharmacometrics Syst Pharmacol* **4**:507–515, Wiley-Blackwell.

Yang F, He Y, Liu H-XX, Tsuei J, Jiang X, Yang L, Wang Z-TT, and Wan Y-JJY (2014) All-trans retinoic acid regulates hepatic bile acid homeostasis. *Biochem Pharmacol* **91**:483–489, Elsevier Inc.

Zamek-Gliszczynski MJ, Mohutsky MA, Rehmel JLF, and Ke AB (2014) Investigational Small-Molecule Drug Selectively Suppresses Constitutive CYP2B6 Activity at the Gene

Transcription Level: Physiologically Based Pharmacokinetic Model Assessment of Clinical Drug Interaction Risk. *Drug Metab Dispos* **42**:1008–1015.

Zhong G, Ortiz D, Zelter A, Nath A, and Isoherranen N (2018) CYP26C1 Is a Hydroxylase of Multiple Active Retinoids and Interacts with Cellular Retinoic Acid Binding Proteins. *Mol Pharmacol* **93**:489–503, American Society for Pharmacology and Experimental Therapeutics.

Zhuang Y, de Vries DE, Xu Z, Marciniak SJ, Chen D, Leon F, Davis HM, and Zhou H (2015) Evaluation of disease-mediated therapeutic protein-drug interactions between an anti-interleukin-6 monoclonal antibody (sirukumab) and cytochrome P450 activities in a phase 1 study in patients with rheumatoid arthritis using a cocktail approach. *J Clin Pharmacol* **55**:1386–1394, Wiley-Blackwell.

VITA

Faith (Hartsfield) Stevison was born in Fayetteville, Arkansas. She earned her Bachelor of Science degree in Biochemistry from the University of Arkansas in 2002 and a Master of Science degree in Pharmaceutical Sciences at the University of Arkansas for Medical Sciences in 2006. After completing her Master of Science degree, Faith joined the department of Pharmacokinetics, Dynamics, and Metabolism at Pfizer, Inc., in St. Louis, Missouri where she worked until joining the Clinical Pharmacology department at Seattle Genetics, Inc., in Bothell, Washington in 2010. She then enrolled in the department of Pharmaceutics at the University of Washington in 2013 and joined the lab of Dr. Nina Isoherranen in 2014.